UNIVERSITY OF THE
WITWATERSRAND,
JOHANNESBURG

A Process Systems Analysis Towards Hydrogen Pathways Optimisation

Caroline Kaitano

(1141980)

Master of Science in Engineering by research:

"A dissertation submitted to the Faculty of Engineering and Built Environment, University of the Witwatersrand, Johannesburg, in fulfillment of the requirements for the degree of Master of Science in Engineering."

Supervised by Professor Thokozani Majozi

2024

Declaration

I declare that this dissertation is my own unaided work. It is being submitted for the Degree of Master of Science in Chemical Engineering to the University of the Witwatersrand, Johannesburg. It has not been submitted before for any degree or examination to any other University.

……..

(Signature of Candidate)

8th ……day of……August……..year…2024……..

Conference Presentations

The work detailed in this Masters dissertation has been presented at international conferences as follows:

1. Kaitano, C., Majozi, T., 'A process systems analysis towards hydrogen pathways optimisation.' International Conference on Cleaner Production and Sustainability (CPS2021). 12-13 December 2021, online.
2. Kaitano, C., Majozi, T., 'On Optimisation of Hydrogen Production Pathways through a Process Systems Analysis Approach. 25th Conference on Process Integration for Energy Saving and Pollution Reduction (PRES'22), 5-8 September 2022, Bol, Croatia.
3. Kaitano, C., Majozi, T., 'A Process Systems Analysis Towards Hydrogen Production Pathways Optimisation: A multi-criteria decision analysis. Process Systems Engineering Asia Conference (PSEAsia22), 10-14 December 2022, Chennai, India.

Synopsis

Hydrogen is garnering increasing attention as a promising and eco-friendly energy carrier, holding the potential to address global energy and environmental challenges. The emergence of the hydrogen economy is a pivotal technological leap forward in future energy systems. Its central objective is to generate hydrogen primarily from abundant energy sources, thus mitigating our dependence on fossil fuels across industries, businesses, residences, and transportation sectors. At its core, the hydrogen economy encompasses essential facets, including the generation, dissemination, transformation, and retention of hydrogen gas and its diverse applications. Establishing efficient hydrogen production processes represents a critical stride toward the overarching global objective of constructing an economy that revolves around hydrogen as a principal energy carrier, capable of providing a substantial portion of our energy needs and services.

The work in this dissertation comprehensively explores hydrogen production pathways by applying a superstructure approach, encompassing various options. A comprehensive database comprising 19 distinct hydrogen production pathways is established in this study. These pathways are subjected to a rigorous analysis, considering availability, environmental sustainability, and economic costs. The overarching goal is to discern the most feasible routes for hydrogen production. The framework devised in this research systematically narrows the initial 19 pathways to a final selection of three, achieving an impressive 84 % reduction in the search space. Among these, the pathway involving steam reforming with carbon capture at 1230 K and 10 bar emerges as the most promising option for hydrogen generation.

Having identified the optimal reaction pathway, the focus of the study shifts beyond the framework towards the process design and optimisation of this specific route. After a thorough post-optimisation analysis, it is concluded that the steam reformer operates most favorably under a temperature of 908 K and a pressure of 10 bar. This optimised pathway boasts a remarkable 48 % conversion of methane, underscoring its exceptional environmental and economic advantages.

This dissertation not only elucidates the systematic framework employed in synthesizing and evaluating the hydrogen pathways superstructure, leading to a significantly reduced search space, but also delves into the intricacies of process design and optimization for the most viable hydrogen production pathway. In doing so, it contributes valuable insights and a structured methodology to the field of hydrogen energy research, offering a blueprint for sustainable and efficient hydrogen production in the pursuit of a cleaner and more sustainable energy future.

In loving memory of my mother

Edeline Chiyangwa

Acknowledgments

First and foremost, I would like to express my profound gratitude to God for His guidance and boundless wisdom. Without His divine presence and blessings, I would never have embarked on this remarkable journey, let alone reached this significant milestone in my academic career.

I would like to extend my heartfelt appreciation to Professor Thokozani Majozi, my esteemed supervisor, for bestowing upon me the invaluable opportunity to pursue my studies further. His mentorship and support have been the cornerstone of my academic growth. His guidance, during the triumphs and the trials of my masters journey, has been a guiding light that I will forever cherish.

In addition, I am deeply grateful to my NRF/DST Chair in Sustainable Process Engineering (SPE) colleagues, whose support has been a constant source of motivation. Their camaraderie, both within and outside the office, has fostered an environment of encouragement and shared success.

My special, heartfelt appreciation to my dear Aunt Bertha and her husband, James Wardrobe. Their belief in my educational aspirations has been a pillar of support that I will always hold dear.

I cannot overlook the importance of acknowledging my sister, Cathrine, and my father, Maxwell Kaitano, whose support and encouragement have continuously inspired me.

I extend my heartfelt gratitude to the Glorious Church family for their support and prayers. Their spiritual support has been a source of comfort and strength, providing me with the resilience to overcome challenges.

Lastly, I would like to express my sincere appreciation for the National Research Foundation (NRF) funding. Their financial support has played a pivotal role in enabling me to pursue my studies and achieve my academic goals. Their investment in my education is deeply appreciated and has significantly impacted my academic journey.

Contents

List of figures

List of tables

CHAPTER 1

INTRODUCTION

1.1. Background

Energy is a critical component in all life forms, and it is becoming increasingly fundamental in ensuring survival. Due to the ever-increasing global population and industrialization, energy demand has risen to an all-time high. The excess strain has been imposed on the current energy sector. Meeting the energy demands to sustain living standards has become one of the most critical challenges for humanity (Department of Environmental Affairs, 2015). Currently, the bulk of energy demand is met through the utilisation of fossil fuels.

Two significant concerns arise when using fossil fuels for energy demands. The first concern is that fossil fuels are considered non-renewable resources, meaning they cannot be replaced once used. Fossil fuels cannot renew themselves at a sufficient rate for them to be extracted within meaningful human time frames; therefore, they do not promote sustainable development (UCS, 2016).

In addition, an inverse proportionality relationship exists between the cost of fossil fuel extraction and the amount of fossil fuels available. Fossil fuels become extremely difficult to extract as they decrease, resulting in more specialized equipment and increased labour to extract these resources (UCS, 2016). Therefore, as fossil fuel reserves run out, the cost of extraction increases, likely leading to a point whereby fossil fuels become too costly to harvest; thus, humanity will be forced to turn to alternative resources (UCS, 2016).

The second primary concern with fossil fuels is the emissions resulting from their combustion. These emissions can be sulphur dioxide (SO_2) and smoke, which result in

excessive pollution with a possibility of acid rain or carbon dioxide (CO_2) (Energy Envoys, n.d.). CO_2 is one of the significant contributors to greenhouse gases (GHG), and nearly all human activities, including chemical, biological, and industrial processes, produce this gas (Lim et al., 2012). Due to the excessive use of fossil fuels in the South African energy mix, South Africa has been ranked as the 1st biggest emitter of greenhouse gases in Africa and the top 15 % globally (Mashishi, 2021).

Currently, non-renewable energy sources are being utilized at an alarming rate. As a result, reducing dependence on fossil fuels and substituting them with renewable energy sources has become urgent worldwide. To that extent, nations are executing policy and research to appropriate alternatives in advance. It is, therefore, essential to develop reliable, clean, and affordable energy systems.

Discovering diverse renewable resources is one approach to addressing the expanding worldwide energy demand. However, handling them proficiently is fundamental to getting more yields from a similar measure of energy utilization. Scientific and technical improvements have permitted the replacement of conventional fuels with new fuels and energy sources (Dincer & Acar, 2017). These new alternative sources should perform as efficiently as the current conventional ones, and they should also emit less harmful environmental effects and be more affordable and reliable. However, substituting one energy source with another may require developing new technologies and infrastructure (Dincer & Acar, 2017).

The utilization of renewable energy sources, e.g., wind and solar, does not contribute to the emission of greenhouse gases. However, their full utilization is unreliable due to their intermittent and unpredictable nature, thus resulting in their limited use (Nikolaidis & Poullikkas, 2017a). The increase in the contribution of renewable energy by concurrently adapting its production to demand would not be achievable without using energy storage systems. The difficulty of the storage systems is maintaining the stored energy for as long as required and retrieving it when necessary. This has led to the hydrogen economy as a reliable alternative to current energy systems.

The hydrogen economy is an economy that relies on hydrogen as the primary energy carrier that would deliver a substantial fraction of energy and services. Hydrogen as an energy carrier means it can store and deliver electrical energy through chemical reactions rather than combustion (Faye et al., 2022). The utilization of hydrogen as an energy carrier has been a topic of discussion since the 1970s; however, it has not come to fruition due to the exorbitant investment costs, availability of cheaper alternatives, and high production costs (Riera et al., 2023). The need for countries to reduce greenhouse emissions has led to hydrogen re-emerging as a potential hydrogen carrier (Riera et al., 2023). According to "The Future of Hydrogen" report released by the IEA in 2019, hydrogen got the world's attention due to its potential role as an appealing elective fuel as it does not produce greenhouse gases (International Energy Agency, 2019). It is an energy carrier that is first produced by utilizing another fuel source and then transported for future utilization where its latent chemical energy can be fully recognized (Edwards et al., 2007).

The ability of hydrogen to supplant fossil fuels in the transportation sector could address one of the significant environmental issues in the world. Hydrogen can be produced from many primary sources and utilized as a fuel or feedstock to produce chemicals such as methanol and ammonia. Alternative to fossil fuels, it is regarded as a secondary form of renewable energy. Hydrogen will also boost the sustainability, reliability, and flexibility of energy systems (Riera et al., 2023). Hydrogen consumed in refining and treating metals is about 0.1 GT (Nikolaidis & Poullikkas, 2017a).

The major problem with hydrogen utilisation is the need for inexpensive production methods and end-use. Various hydrogen production methods are available, which, depending on their raw materials, still have their limitations. Around 96% of hydrogen is produced from fossil fuels worldwide, with 49% from natural gas, 29% from liquid hydrocarbons, and 18% from coal (Abdin et al., 2020; Quarton & Samsatli, 2020). There is no substantial production of hydrogen from renewable resources (Riera et al., 2023). According to Human et al. (2021), water electrolysis is the lone hydrogen production technology viable with intermittent renewable sources and appropriate for

disseminated on-site production. However, its costs remain high due to being energy intensive. Traditional fossil fuel methods like steam reforming are economical but produce high greenhouse gas emissions. Therefore, there is a need to optimize hydrogen production technologies to obtain affordable, available, and environmentally sustainable pathways.

1.2. Motivation

The motivation behind this research is drawn from the need for a more sustainable energy system as the population increases. Non-renewable energy sources are facing massive strain as the population increases. The current energy system relies on fossil fuels, which are rapidly getting exhausted. Furthermore, these fossil fuels produce GHG, like methane, nitrous oxide, fluorinated gases and mainly CO_2.

South Africa uses fossil fuels for its many processes to meet its energy demands. The continued use of fossil fuels does not promote sustainable development, with sustainable development being defined as development that meets the needs of the present without compromising the ability of future generations to meet their own needs (Uralovich et al., 2023). This could adversely affect meeting the energy requirements for future generations. Alternative energies need to be explored to reduce the direct use of fossil fuels. This could be in the form of renewable energy sources, which are derived from natural processes that are replenished constantly, such as solar, wind, hydro, and geothermal energy. However, renewable sources are unreliable due to their intermittent and unpredictable nature. Thus, it is currently impossible for the energy system to rely entirely on renewable energy as it does not guarantee energy availability at any given time.

As previously highlighted, fossil fuels emit greenhouse gases. Greenhouse gases absorb and emit radiant energy within the thermal infrared range. One such gas is CO_2, produced during fossil fuel combustion. Greenhouse gases contribute to global warming by trapping heat in the atmosphere. Such climate changes are catastrophic to biological systems and the environment in which they exist. If fossil fuel utilization

continues at the current rate, global temperatures could increase, causing sea levels to rise. This could potentially cause the displacement of many people due to the flooding of coastal areas, the erosion of shorelines, and the contamination of freshwater supplies by seawater.

An alternative energy system is required to meet energy demands while minimizing the impact of adverse environmental and non-renewable resources. Hydrogen has been identified as a suitable substitute. However, achieving a fully established hydrogen economy requires well-established hydrogen energy systems with better resources and production methods.

The current work, therefore, seeks to develop a mathematical framework that allows the synthesis and optimization of reaction pathways to produce hydrogen. The basis of optimization is affordability, availability, and environmental sustainability, which are to be optimized simultaneously. The main question to be addressed in this research is: What is the most optimum chemical reaction for hydrogen production in the South African economy/infrastructure, considering affordability, availability, and environmental sustainability?

1.3. Objectives

The objectives of this study can be summed up as follows:

- To develop a reaction pathway superstructure that contains all pathways for hydrogen production and conversion.
- To investigate the reaction pathways according to affordability, availability, and environmental sustainability.
- To determine the optimal production pathway for hydrogen.
- To determine the optimum flowsheet for hydrogen production.

The basis of this work is to demonstrate the simultaneous optimization of hydrogen production pathways according to sustainability metrics with a detailed framework against the commonly practiced single optimization.

The problem statement in this study can be stated as follows:

Given a reaction pathway database (RPD) containing the following information:

(i) Reaction pathway mechanism, i.e., sub-reactions involved in the reaction system
(ii) Reaction operating conditions, i.e., temperature and pressure
(iii) Catalyst required and its associated composition
(iv) Products produced in the system
(v) Conversions
(vi) Inlet feed ratios
(vii) Costs

Determine:

(i) A mathematical framework that can reduce the search space to a manageable region containing the most feasible reaction pathway.
(ii) The optimum pathway for hydrogen production in the search space.
(iii) The optimum flowsheet for hydrogen production using sustainability metrics.

1.4. Dissertation structure

The rest of the dissertation is divided into the following chapters:

(i) Chapter 2 provides a comprehensive review of the literature focusing on the various methods of hydrogen production, their advantages, and disadvantages. A literature review is also presented on the different multi-criteria decision-making methods that have been utilised in the selection of hydrogen production pathways.
(ii) Chapter 3 presents a detailed framework development of the study. This includes the developed superstructure and detailed models used in the analysis of different hydrogen production pathways.
(iii) Chapter 4 shows the application of the developed framework to a theoretical case study.

(iv) Chapter 5 shows the validation of the developed framework against literature studies.

(v) Chapter 6 presents the detailed design and optimization of the chosen hydrogen pathway and the results thereof.

1.5. References

Abdin, Z., Zafaranloo, A., Rafiee, A., Mérida, W., Lipiński, W., & Khalilpour, K. R. (2020). Hydrogen as an energy vector. Renewable and Sustainable Energy Reviews, 120 (December 2019). https://doi.org/10.1016/j.rser.2019.109620

Department of Environmental Affairs (DEA). (2015). Chapter 12-Energy. *In Environnment Outlook*, 238-276. Johannesburg

Dincer, I., & Acar, C. (2017). Innovation in hydrogen production. International Journal of Hydrogen Energy, 42(22), 14843–14864. https://doi.org/10.1016/j.ijhydene.2017.04.107

Edwards, P. P., Kuznetsov, V. L., & David, W. I. F. (2007). Hydrogen energy. Philosophical Transactions of the Royal Society A: Mathematical, Physical and Engineering Sciences, 365(1853), 1043–1056. https://doi.org/10.1098/rsta.2006.1965

Energy Envoys. (n.d.). *Energy Tutorial: Energy and Sustainability Non-renewable and renewable resources*. http://www.energyenvoys.org.uk/sites/default/files/Non-renewable and renewable resources_0.pdf

Faye, O., Szpunar, J., & Eduok, U. (2022). A critical review on the current technologies for the generation, storage, and transportation of hydrogen. International Journal of Hydrogen Energy, 47(29), 13771–13802. https://doi.org/10.1016/j.ijhydene.2022.02.112

Human, G., van Schoor, G., & Uren, K. R. (2021). Genetic fuzzy rule extraction for optimised sizing and control of hybrid renewable energy hydrogen systems. International Journal of Hydrogen Energy, 46(5), 3576–3594. https://doi.org/10.1016/j.ijhydene.2020.10.238

International Energy Agency. (2019). The Future of Hydrogen: Seizing today's opportunities. IEA Publications, June, 203.

Lim, Y., Lee, C. J., Jeong, Y. S., Song, I. H., Lee, C. J., & Han, C. (2012). Optimal design and decision for combined steam reforming process with dry methane reforming to reuse CO_2 as a raw material. Industrial and Engineering Chemistry Research, 51(13), 4982–4989. https://doi.org/10.1021/ie200870m

Mashishi, N. (2021). South Africa the 12th biggest source of greenhouse gases? Yes, but that's not the only measure that matters. Africa Check. https://www.polity.org.za/article/south-africa-the-12th-biggest-source-of-greenhouse-gases-yes-but-thats-not-the-only-measure-that-matters-2021-04-19

Nikolaidis, P., & Poullikkas, A. (2017). A comparative overview of hydrogen production processes. Renewable and Sustainable Energy Reviews, 67, 597–611. https://doi.org/10.1016/j.rser.2016.09.044

Quarton, C. J., & Samsatli, S. (2020). The value of hydrogen and carbon capture, storage and utilisation in decarbonising energy: Insights from integrated value chain optimisation. Applied Energy, 257(June 2019), 113936. https://doi.org/10.1016/j.apenergy.2019.113936

Riera, J. A., Lima, R. M., & Knio, O. M. (2023). A review of hydrogen production and supply chain modeling and optimization. International Journal of Hydrogen Energy, 48(37), 13731–13755. https://doi.org/10.1016/j.ijhydene.2022.12.242

UCS. (2016). The Hidden Costs of Fossil Fuels. Union of Concerned Scientists. https://www.ucsusa.org/resources/hidden-costs-fossil-fuels

Uralovich, K. S., Toshmamatovich, T. U., Kubayevich, K. F., Sapaev, I. B., Saylaubaevna, S. S., Beknazarova, Z. F., & Khurramov, A. (2023). A primary factor in sustainable development and environmental sustainability is environmental education. *Caspian Journal of Environmental Sciences*, *21*(4), 965–975. https://doi.org/10.22124/cjes.2023.7155

CHAPTER 2

LITERATURE REVIEW

2.1. Introduction

This section gives a detailed literature review of the previous work that has been conducted on the hydrogen economy. The section starts with a general and comprehensive review of the state of energy systems worldwide and narrows down to South Africa. This is followed by an extensive review of the hydrogen economy and its recognition challenges. In addition, a comprehensive review of considerations in selecting a production pathway is presented. The chapter concludes with a discussion of the different multi-criteria decision-making (MCDM) techniques that have been implemented and outlines the advantages and disadvantages of each technique.

2.2. World energy systems

Energy plays a vital role in the existence and social well-being of humans (Seker & Aydin, 2022). It is the primary fuel for social and economic development (Clerici & Alimonti, 2015). Its demand has increased as the population increases, the global economy grows, and technology advances. Energy demand is directly proportional to population growth, economic growth, and technological advances.

As a result of global economic growth, an increasing global population of 7.7 billion in 2019 (El Hajj Chehade et al., 2020), and technological advancements, global energy demand is predicted to increase by about 1.3 % yearly until 2040, with an increase in demand for energy services (Megia et al., 2021). World energy consumption is anticipated to increase by nearly 50 % by 2050, prompting world economic and political stability into an uncertain position (El Hajj Chehade et al., 2020; Durán et al., 2020). In this regard, fossil fuels like oil, natural gas, and coal have been intensely used

for energy production to meet global energy demand (Ishaq et al., 2022). The utilization of fossil fuels is expected to remain dominant until at least 2050 (Megia et al., 2021). Using fossil fuels emits greenhouse gases such as carbon dioxide and nitrogen oxides, which contribute to global climate change as they trap heat in the earth's atmosphere. By 2050, it is essential to generate a minimum of 10 TW (terawatt) of energy without carbon emissions in order to fulfil the growing global demand for electricity and maintain a clean environment (Qureshi et al., 2023).

About 85 % of global energy demand is met through carbon-based fuels (Megia et al., 2021). Due to this, tons of CO_2 are emitted into the atmosphere every year to meet the energy demand. Of the emitted CO_2, over 90 % results from fossil fuels, and these emissions are expected to increase further as the demand increases (Megia et al., 2021). During the COP27 conference held in Egypt, scientists asserted that global CO_2 emissions from fossil fuels are projected to increase by 1% in 2022, setting a new record of 37.5 billion tonnes (Qureshi et al., 2023). Global average temperatures have increased by 1.1 ℃ and are expected to rise to 2.6 ℃ by 2100 due to these emissions since the pre-industrial age, with visible impacts on weather and climate extremes (IEA, 2021).

The current energy system is facing significant strain from rapid but uneven economic recovery from the COVID-19-induced recession, causing an increase in natural gas, coal, and electricity prices (IEA, 2021). According to Megia et al. (2021), the COVID-19 pandemic affected the energy system by causing a 5 % fall in global energy demand, a 7 % decrease in energy-related CO_2 emissions, and an 18 % decline in energy investment. Renewable energies have been less affected by the pandemic when compared to other fuels. According to the International Energy Agency (IEA), pressure on the energy system is not abating soon.

Many prominent energy, transport, and industrial firms have begun initiatives to develop the energy transition with hydrogen. Nevertheless, to fulfill the progressively more requirements for it, large-scale industrial processes must be established for producing it.

2.3. Energy systems in South Africa

Power production plays a crucial role in the industrial revolution of any country (Ishaq et al., 2022). The energy sector is at the heart of South Africa's economy and social development because of the country's high energy intensity (DOE, 2019). The South African energy sector is governed by abundant and low-cost coal and is graded among the lowest energy costs in the world (Ratshomo, 2021). Besides coal, contributing about 69 % to the total primary energy costs in 2016, South Africa gets energy locally from biomass, natural gas, hydro-power, nuclear power, solar power, and wind (DOE, 2019).

In 2018, coal made up 65 % of South Africa's primary energy supply, followed by crude oil with 18 %, renewables with 11 %, 3 % from natural gas, 2 % nuclear, and 1 % geothermal (Ratshomo, 2021). Figure 2.1 shows South Africa's primary energy supply in 2020. Given that crude oil reserves are scarce, the country imports more than 90% of its crude oil from Saudi Arabia, Nigeria, and Angola. During the transformation stage, the country met approximately 6.6% of its fuel needs with gas, 46.8% with coal, and 46.6% with crude oil (DOE, 2019).

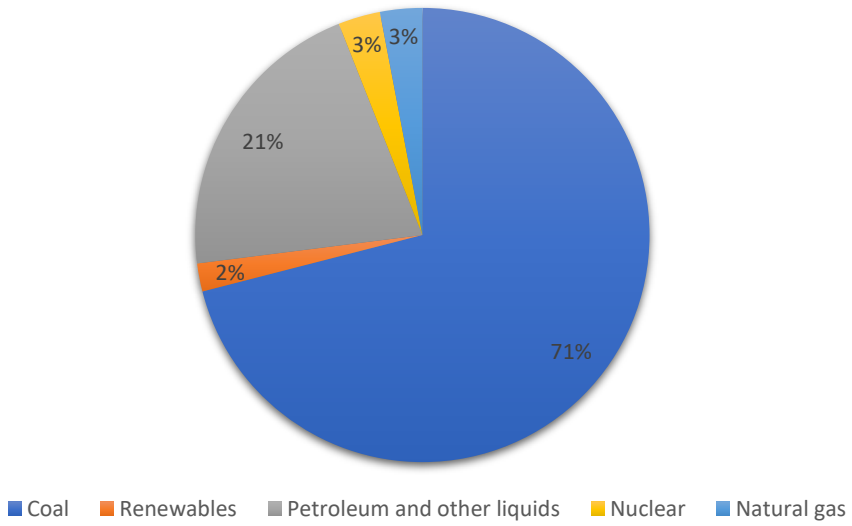

Figure 2.1: South Africa's primary energy supply in 2020 (U.S Energy Information Administration, 2021)

According to DOE (2019), South Africa's reliance on coal-centred energy is not likely to change much in the next two decades due to the relative scarcity of appropriate substitutes for coal. However, with its abundant natural sun and wind resources, South Africa is viewed as a prime candidate for increased utilization of renewable energy. The country's power generation relies heavily on coal, but it has several small-scale hydroelectric plants and only one nuclear power station (DOE, 2019). At the same time, South Africa has an abundance of sunlight, which is ideal for solar water heating and electricity generation.

Despite driving rapid economic growth in advanced industrial societies, the widespread use of fossil fuels has resulted in increasing climate change due to the emissions of combustion pollutants and a rise in carbon dioxide levels in the atmosphere. The consequences are climate change, rising sea levels, and escalating international conflicts (Norouzi, 2022). In contrast, the impending depletion of fossil resources and the prediction of rising prices make replacing the current energy system more important than ever. As a result, using new energy sources instead of fossil fuels is unavoidable. Future energy systems must rely on structural and fundamental changes that include using non-carbon energy sources such as solar, wind, geothermal, and biomass.

The utilisation of renewable energy sources does not contribute to the net emissions of greenhouse gases. However, their full utilization is currently limited due to the unreliability of the sources stemming from intermittency and unpredictability (Nikolaidis & Poullikkas, 2017a). The increase in the contribution of renewable energy with the concurrent adaptation of its production to demand would not be achievable without using energy storage systems. The difficulty of the storage systems is maintaining the stored energy for as long as required and retrieving it when necessary. As a result, this has led to the hydrogen economy as a reliable alternative to the current energy systems. Hydrogen is gaining extensive acknowledgment worldwide as a complete solution and a prospective fuel as it extends carbon-free solutions (Ishaq et al., 2022).

2.4. The hydrogen economy

The hydrogen economy concept was first introduced by a renowned scientist, John Bockris, in the 20th century (Tetteh & Salehi, 2023). It represents one of the most significant technological advancements for future energy systems. Its primary aim is to produce hydrogen predominantly from readily available energy sources, replacing reliance on fossil-based fuels in industries, commercial sectors, households, and transportation. The critical components of the hydrogen economy encompass the production, distribution, conversion, and storage of hydrogen gas, along with its various applications. Establishing efficient hydrogen production is a crucial step in building and realizing the global goal of an economy centred around hydrogen as an energy vector that would deliver a substantial fraction of energy and services (Nikolaidis & Poullikkas, 2017a).

As a clean fuel, hydrogen has been identified as a potential and viable alternative to fossil fuels and, in the future, an energy carrier, not only because of its environmental sustainability but also its high energy density of 120 MJ.kg^{-1} (Chih et al., 2023). Clean fuels have physical and chemical properties that make them cleaner than gasoline in combustion with the current structure and composition (Norouzi, 2022). These fuels emit fewer pollutants during combustion, and their use slows the increase and accumulation of carbon dioxide, which causes global warming. Hydrogen is reliable mainly as a future energy carrier because of its clean combustion pathways and high gravimetric energy density (Bahari et al., 2019).

Electrochemical science serves as the foundation for the so-called hydrogen economy, which entails the production of molecular hydrogen from non-fossil sources, its distribution and storage, and its cold combustion in a fuel cell to generate electricity, as shown in Figure 2.2 (Rebouillat et al., 2011). The ease of production from water, nearly unique consumption, and inherent environmental utility of hydrogen set it apart from other alternative fuel options. Hydrogen offers several significant advantages, such as efficient energy conversion, carbon-free production through water splitting, creation of diverse intermediate fuels like synthetic fuels and ammonia, ample storage

options, compatibility with existing infrastructure for long-distance transportation, and a superior lower heating value (LHV) compared to alternative fuels (Dash et al., 2023).

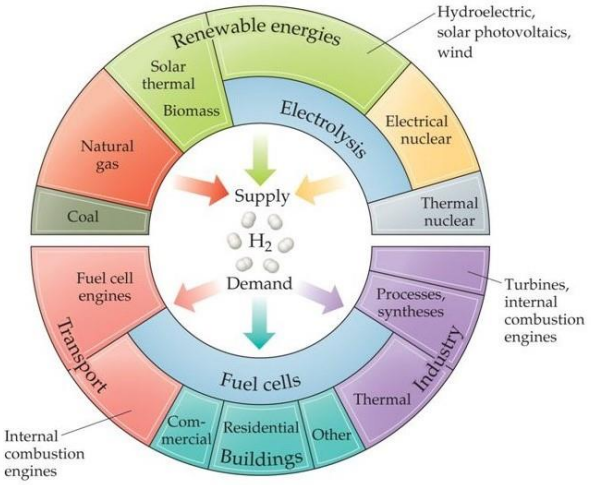

Figure 2.2: The hydrogen economy (Rebouillat et al., 2011)

In 1671, Robert Boyle discovered hydrogen by dipping different metals in acid to investigate their properties while observing a single-displacement reaction (Ishaq et al., 2022). Later, with Boyle, Henry Cavendish established hydrogen as a distinct element and declared hydrogen to be a flammable gas. In the early nineteenth century, giant airships used hydrogen for buoyancy, and it was later used in the detonation of the first H-bomb in 1954 (Ishaq et al., 2022).

Hydrogen can be used in all fossil fuel applications, and it, in particular, complements renewable energy sources and makes them accessible to consumers anytime and from any location. Almost all renewable energy sources are unavailable regularly, are not portable or storable on their own, and cannot be used as fuel, particularly in transportation. Hydrogen as an energy carrier has the potential to create and improve flexibility in global energy consumption patterns. However, it should be noted that there is currently no large commercial market for hydrogen as an energy carrier, with its primary applications being in the oil industry (Norouzi, 2022).

While hydrogen is not widely used in commercial energy applications worldwide, it is time to find its place in the global energy market. The limitation of fully utilizing

hydrogen lies in the need for economic and sustainable production methods. Presently, existing hydrogen generation technologies result in carbon dioxide emissions, making it essential to shift towards carbon-free methods of producing hydrogen gas for the hydrogen economy's long-term viability (Qureshi et al., 2023). Therefore, the main objective is to transition towards carbon dioxide emission-free hydrogen production, utilizing various methods. Despite numerous advantages, significant scientific, technological, and economic challenges have impeded the transition from fossil fuels to hydrogen-based energy systems. Hydrogen can be generated from either primary or secondary sources. Primary sources directly extract hydrogen from natural sources, while secondary sources use energy, usually electricity, to decompose water into oxygen and hydrogen. In both industries, renewable and non-renewable energy sources can provide propulsion energy. The chosen method for hydrogen production will differ depending on the amount of access to various sources, the required technological needs, and the volume of gas required for each geographical location.

2.5. Hydrogen production

Hydrogen can be generated from various primary energy sources, given the appropriate chemical reaction schemes. The most common sources are natural gas, biomass, coal, water, and electricity (Riera et al., 2023). The availability of hydrogen production energy sources is elementary to hydrogen-related problems. Hydrogen costs and related emissions vary depending on the technique and energy used. This is why hydrogen production technologies are categorized based on different colors.

Four years ago, the terms "green" and "grey" hydrogen started gaining recognition and acceptance within the scientific, industrial, and political communities. These terms have often been used interchangeably with "green," "clean," or "environmentally friendly" hydrogen (Incer-Valverde et al., 2023). Green hydrogen is commonly used to describe hydrogen produced without emitting CO_2, while grey hydrogen is derived from natural gas. However, the emergence of Carbon Capture, Utilization, and Storage (CCUS) technologies has enabled hydrogen production with minimal or virtually no CO_2 emissions, even when produced from fossil fuels. A few years ago, the term blue

hydrogen was coined to describe hydrogen produced from fossil fuels with the integration of CCUS (Incer-Valverde et al., 2023). More recently, the concept of blending green hydrogen with natural gas gained prominence as a pathway to transition to a fully hydrogen-based economy, similar to the concept of blue hydrogen (Olaniyi et al., 2023). This new option has opened up previously overlooked opportunities in research, especially in the context of de-carbonization efforts.

The production of hydrogen can be accomplished through various methods, such as electrolysis, steam methane reforming, gasification, thermochemical processes, photochemical processes, biochemical processes, and biological processes. Simultaneously, numerous energy sources are available for generating the electrical energy needed for electrolysis without relying on fossil fuels and avoiding CO_2 emissions. These sources include Renewable Energy Sources (RES) and nuclear energy.

Furthermore, hydrogen can be sourced from different materials, including water, biomass, natural gas, and various types of coal. Therefore, it has become necessary to categorize hydrogen with different colors based on the source of hydrogen molecules, the extraction process, and the energy source used for production as well as the amount of CO_2 produced in its production. This categorization is commonly referred to as the hydrogen rainbow; however, Incer-Valverde et al. (2023) contrasted this and suggested a peacock explained it better since other colors are not found on the rainbow. It is important to note that hydrogen itself remains colorless, but assigning colors provides a straightforward and transparent way to indicate the specific method of hydrogen production under consideration without delving into the technical details of the process.

The production of hydrogen can be classified into 5 main significant categories as follows:

i. Brown – coal gasification-based hydrogen production,
ii. Grey – production based on natural gas reforming techniques,

iii. Blue – coal gasification and natural gas-based hydrogen integrated with carbon capture and storage,

iv. Green – renewable energy-based hydrogen production

v. Purple – nuclear energy-based hydrogen production

More colors have been defined in the literature and are summarized in Figure 2.3 (Ajanovic et al., 2022).

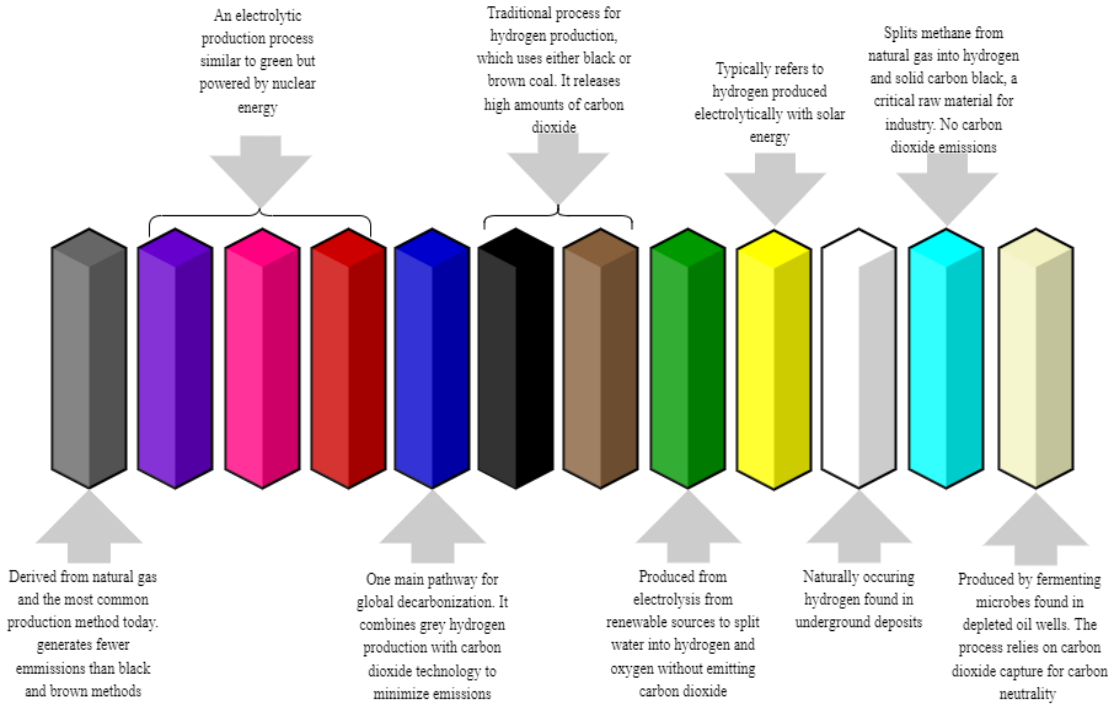

Figure 2.3: Colours of hydrogen

Hydrogen in molecular form can be obtained from various feedstocks using technologies with varying economic, environmental, and social performance. These sources include fossil fuels, biomass, and water. Energy is required to extract hydrogen from these sources, and the energy should be in continuous supply. Around 95 % of hydrogen is produced from fossil fuels, with 49 % from natural gas and 29 % from liquid hydrocarbons (Quarton & Samsatli, 2020). Coal gasification, methane steam reforming, water electrolysis, and biomass gasification are used to extract hydrogen. Currently, 48 % of global hydrogen demand is met by generating synthesis gas via

steam reforming of natural gas, 30 % by petroleum reforming, 18 % by coal gasification, and 4 % by water electrolysis (Faheem et al., 2021). Figure 2.4 summarises the leading hydrogen production technologies from energy sources.

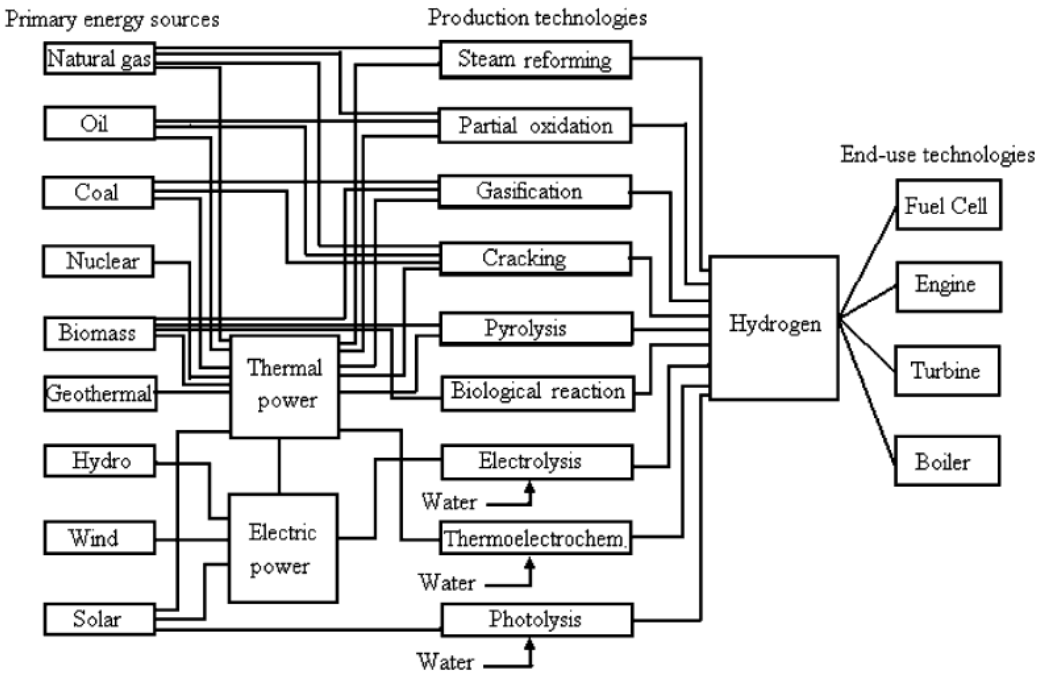

Figure 2.4: Main alternative techniques of hydrogen production from energy sources (Palma et al., 2012)

2.5.1. Hydrogen production from fossil fuels

Fossil fuels remain dominant in the global hydrogen supply because production costs remain acceptable. Hydrocarbon reforming and pyrolysis are the leading mature technologies used to produce hydrogen from fossil fuels, with hydrocarbon reforming being the most advanced technique. Apart from hydrocarbon as a reactant for hydrocarbon reforming, oxygen or steam are other reactants required for this process, and these give partial oxidation and steam reforming, respectively (Megia et al., 2021). These can be combined with carbon capture and storage or utilization methods to capture carbon dioxide emissions, thus obtaining a carbon-neutral process and generating blue hydrogen (Ishaq et al., 2022).

2.5.1.1. Steam reforming

The steam reforming process is currently state-of-the-art technology for producing over 50 % of the world's hydrogen (Durán et al., 2020; Giwa & Giwa, 2013; Tetteh & Salehi, 2023). It is a process in which methane from natural gas is heated with steam in the presence of a catalyst to produce a mixture of carbon monoxide and hydrogen (Durán et al., 2020). The mixture is referred to as synthesis gas. The overall reaction is endothermic, and the total number of molecules increases as the reaction progresses. It is carried out at high temperatures of 1000-1200 K (Faheem et al., 2021) and pressures of 10-40 bar (De Souza et al., 2014). Heat is supplied to the reforming reactor by combusting part of the natural gas or the purge gas from the pressure-swing adsorber (PSA) in a furnace to sustain the steam reforming process. Carbon monoxide is first produced with hydrogen, giving rise to synthesis gas, according to equation 2.1. The water gas shift mechanism in equation 2.2 is then used to enrich hydrogen and reduce carbon monoxide concentrations. The overall steam reforming is represented by equation 2.3.

$$CH_{4(g)} + 2\,H_2O_{(g)} \rightleftarrows 3\,H_{2(g)} + CO_{(g)} \qquad 2.1$$

$$H_2O_{(g)} + CO_{(g)} \rightleftarrows H_{2(g)} + CO_{2(g)} \qquad 2.2$$

$$CH_{4(g)} + 2H_2O_{(g)} \rightleftarrows 4\,H_{2(g)} + CO_{2(g)} \qquad 2.3$$

Due to the high temperatures in the steam reforming process, expensive construction materials are required to withstand thermal stresses. The emergence of temperature profiles in the catalyst bed and coke formation is also considered one of the limitations of this process. High-performance catalysts are required to maximize the amount of hydrogen produced. Nickel catalysts supported on ceramic or oxides are commonly used for steam reforming. Noble metals are also available but are too economically demanding for commercial use.

Apart from the drawbacks of steam reforming, this process produces hydrogen-rich synthesis gas. Compared to other reforming processes, steam reforming produces synthesis gas with the highest hydrogen-to-carbon ratios, as high as 3:1. Since hydrogen is mixed with other by-products, separation is required. In most hydrogen plants, the PSA process is utilized, which can produce hydrogen with up to 99.999 % purity. The recovery of the PSA is between 70-95 % (Megia et al., 2021).

The steam reforming process was first recorded in 1924 and attracted tremendous interest from researchers, leading to its first industrialization in 1930 (Zhang et al., 2021). This process remains an important research topic in the scientific field, and efforts to improve steam reforming have advanced over the years. A series of advanced technologies have been established to improve steam reforming energy efficiency. These technologies include sorbent-enhanced steam reforming (Chanburanasiri et al., 2011), chemical looping process (Luo et al., 2018), photocatalytic steam reforming (Shimura et al., 2010), plasma steam reforming (Hrabovsky et al., 2018), and electro-catalytic steam reforming (Lu et al., 2019).

2.5.1.2. Partial oxidation of methane

Partial oxidation, also known as oxy-reforming, is another attractive method to produce hydrogen. This process is accomplished by feeding methane and sub-stoichiometric oxygen into the reactor without water (De Souza et al., 2014). It can operate with various feedstocks, including methane, heavy fuel oil, and coal. The partial oxidation process is exothermic; therefore, it can reduce the energy demand for the reforming process (Hrabovsky et al., 2018). The primary reaction for partial oxidation involves highly exothermic incomplete combustion of methane, which converts the fuel into hydrogen and carbon monoxide. The reaction mechanism for this process can be represented by equation 2.4 :

$$CH_{4(g)} + 0.5\ O_{(g)} \rightleftarrows 2\ H_{2(g)} + CO_{(g)} \qquad 2.4$$

While this reaction and the formation of hydrogen and carbon monoxide are thermodynamically favored above 550 °C (Megia et al., 2021), the selectivity is affected by the formation of water in oxidation reactions (equation 2.5 and 2.6), which

are more exothermic (Bharadwaj & Schmidt, 1994). Carbon monoxide is a coke precursor, which can be removed by its oxidation toward carbon dioxide or by the water−gas shift reaction, increasing the hydrogen yield.

$$CH_{4(g)} + 1.5\ O_{2(g)} \rightleftarrows 2\ H_2O_{(g)} + CO_{2(g)} \qquad 2.5$$

$$CH_{4(g)} + 2\ O_{2(g)} \rightleftarrows 2\ H_2O_{(g)} + CO_{(g)} \qquad 2.6$$

The partial oxidation process harbors several advantages. Its main advantage is that it does not need external energy provision, and this is due to the immense heat production owing to its exothermic nature. Other advantages include simple operation, lower energy consumption, and flexible feedstock. However, this process is only used on a microscopic scale due to the increased soot formation caused by high temperatures and a low hydrogen-to-carbon monoxide ratio of less than 2:1 in partial oxidation. Furthermore, the short useful life of the unit due to the high reaction exothermicity leads to hot spots and, subsequently, catalyst deactivation by sintering (Megia et al., 2021).

The initial papers describing the partial oxidation of methane to hydrogen were published in 1929 by Liander, in 1933 by Padovani and Franchetti, and in 1946 by Prettre and his colleagues (York et al., 2003).

2.5.1.3. Autothermal reforming

Autothermal reforming is a process of combining the steam reforming reaction with the partial oxidation process. It is assumed that the heat required by the endothermic steam reforming is supplied by the exothermic partial oxidation, which makes this process self-sustaining (Ã et al., 2008). Both steam and oxygen are introduced into the reformer, leading to oxidation and steam reforming co-occurring, giving a net reaction enthalpy of zero (Megia et al., 2021). According to Nnabuife et al. (2022), autothermal reforming is mainly used for large conversion units.

Generally, autothermal reforming is operated adiabatically. Operating conditions vary between temperatures of 900°C - 1500°C and pressures of 1-80 bar (Voitic et al.,

2018). A sharp temperature increase in the exothermic regions and a steady decrease in the subsequent endothermic section is evident in the autothermal reforming process. The total heat balance and the product ratio are adjusted by varying the feed ratios. The overall reaction to this process can be represented by equation 2.7:

$$CH_{4(g)} + 0.25\,O_{2(g)} + 0.5\,H_2O_{(g)} \rightleftarrows 2.5\,H_{2(g)} + CO_{(g)} \qquad 2.7$$

Autothermal reforming is deemed more advantageous than steam reforming and partial oxidation. This advantage is considering the increased energy efficiencies, faster start-up times, faster response times to transient operation, easier to operate with a minor system, better temperature control, lower operational temperature, and less coking. Furthermore, it renders higher hydrogen production efficiencies than partial oxidation but lower than steam reforming (Megia et al., 2021). As the process is independent of an external heat source, autothermal reforming has the ability to boost the thermal conversion efficiency of hydrogen production and minimize its operational cost (Carapellucci & Giordano, 2020). Nevertheless, a significant shortcoming of autothermal reforming is the large investment required for an oxygen producing plant, which becomes cost-effective only at high production capacities. Though air can be directly utilized as an alternative to pure oxygen, the existence of inert nitrogen triggers large gas volumes, leading to the system requiring larger equipment.

2.5.1.4. Dry reforming

Dry reforming is also known as carbon dioxide reforming. It has gained substantial attention by reducing and utilizing two types of greenhouse gases: methane and carbon dioxide. This technique is attractive mainly due to the possibility of capturing and reusing the carbon dioxide from exhaust flue gases of power and industrial plants (Carapellucci & Giordano, 2020). Dry reforming is an alternative to producing hydrogen using methane and waste carbon dioxide, according to equation 2.8. Generally, temperatures as high as 700 - 900 ℃ are required for this process, given its endothermic nature (Taherian et al., 2022). Dry reforming is highly endothermic and is favourable at high temperatures and low pressure.

$$CH_{4(g)} + CO_{2(g)} \rightarrow 2\,H_{2(g)} + 2\,CO_{(g)} \qquad 2.8$$

This process has significant advantages: (i) it is an attractive route toward carbon dioxide extenuation, (ii) methane conversion, and (iii) hydrogen to carbon monoxide ratio of approximate unity due to the simultaneous occurrence of the reverse water gas reaction. Although dry reforming has many environmental and economic advantages, it is not commercialized, and industrial application of the dry reforming process is also limited. Indeed, two processes of this kind produce synthesis gas, called Calcor and Sparg (Arora & Prasad, 2016).

The thermodynamics for the dry reforming method is not as favorable as the autothermal reforming or the steam reforming process. Nevertheless, the proportional consumption of methane and carbon dioxide, fed in a 1:1 ratio, could reduce carbon impact, leading to greener methane consumption. According to Lavoie (2014), the thermodynamic barrier is an immense challenge and detrimental to processes that depend simply on heat to convert the two molecules at high conversion levels. Moreover, dry reforming also requires a pure and continuous carbon dioxide source, which may not be accessible in all industrial facilities.

The major drawback to the commercialization of dry reforming is coking (equation 2.9) and sintering, which quickly causes the deactivation of the catalyst. Carbon deposition depends on temperature, catalyst, and the existence of oxygen and steam in the process. However, carbon deposition could be significantly reduced by adjusting parameters and utilizing a suitable catalyst (Abbasi et al., 2020).

$$2CO_{(g)} \rightarrow C_{(s)} + CO_{2(g)} \qquad 2.9$$

2.5.1.5. Tri-reforming

Tri-reforming of methane has been designed to produce synthesis gas by synergistically combining steam reforming, dry reforming of methane, and partial methane oxidation in a single reactor. With this process concept, carbon dioxide, steam, and oxygen in the flue gas from fossil-fuel-based power plants can be used as co-reactants for the tri-reforming of methane for hydrogen production (Song & Pan, 2004).

The combination of dry reforming with steam reforming can accomplish two critical missions. Firstly, to produce syngas with the desired hydrogen to carbon monoxide ratios. Secondly, to mitigate the significant carbon formation problem for dry reforming. Integrating steam reforming and partial oxidation with dry reforming could dramatically reduce or eliminate coking on catalysts, thus increasing catalyst life and process efficiency.

The tri-reforming process is more energy efficient than steam reforming or dry reforming for hydrogen production, with the hydrogen to carbon monoxide molar ratio in the range of 1:1.5-1:2 (Majewski & Wood, 2014). Modifying the molar ratio of compounds during tri-reforming permits control of the hydrogen-to-carbon monoxide ratio in the produced gases to the requisite level. This process can transform low-quality, carbon dioxide-rich natural gas into helpful synthesis gas.

Methane tri-reforming has been studied at a laboratory scale, and mathematical models of tri-reforming reactors have been analyzed. Using thermal efficiency calculations, Minutillo & Perna (2010) proposed optimal operating parameters for tri-reforming of 850 ℃ and a molar ratio between the flue gas and methane of 1:2-1:3.

2.5.1.6. Coal Gasification

Coal gasification is another process used to produce hydrogen, and it is a thermochemical conversion process in which coal is converted into gaseous products, including hydrogen and carbon monoxide. Coal gasification aims to be alternative to coal combustion to reduce harmful emissions and increase the energy density of the fuel (Megia et al., 2021). Coal is converted to synthesis gas in the presence of steam, oxygen, or air at high temperatures and pressures. Besides the primary reactions, there may be other secondary reactions in which coal reacts with other reaction products, such as carbon dioxide, through the Boudouard reaction, further producing carbon monoxide.

The gasification process generally uses four different types of coal. These are lignite (low rank), sub-bituminous coal (low rank), bituminous coals (medium rank), and

anthracites (high rank) (Midilli et al., 2021). The techniques usually applied include fixed bed gasification, moving bed gasification, fluidized bed gasification, entrained flow gasification, and plasma gasification. Among these gasification processes, entrained coal and plasma gasification may generally be carried out at higher temperatures between 1200 and 1700 ℃. However, the others may require lower operating temperatures than 1200 ℃ (Midilli et al., 2021).

The gasification process has three stages (Matamba et al., 2022). The first step is auto-thermal heating of the feedstock mixture via oxidation and exothermic reactions. The second stage is the pyrolysis stage, in which the feed is heated to high temperatures and converted to light hydrocarbons. The pyrolysis stage is endothermic and results in the formation of tar and char. The third step entails converting carbon dioxide and water into carbon monoxide, hydrogen, and methane, the main products of gasification. This step determines the heating value of the produced syngas.

Coal gasification seems to be a substantial process for cleaner and more cost-effective energy production and other chemical products. It converts coal's high moisture and ash content into useful outputs more efficiently, providing synthesis gas production with a high calorific value. As a result of coal gasification, electricity can be produced more efficiently by using hydrogen-rich gas. Furthermore, carbon emissions are considerably decreased.

The main issue with producing hydrogen through coal gasification rather than other technologies that use different feedstocks is higher carbon dioxide emissions due to the high carbon content. As a result, benefits are being developed by combining coal gasification with carbon-capture-based technologies (Megia et al., 2021). Coal gasification differs from other technologies that use fossil fuels in terms of economics due to lower feedstock costs; however, the unit capital costs are higher.

According to Nnabuife et al. (2022), coal gasification is not as advanced as the coal combustion approach and various hydrogen production techniques using fossil fuels, especially regarding carbon capture and robustness in electricity and hydrogen

production. Therefore, technological advancements need to be developed. The main issues, however, are capital costs and reliability. While the integrated coal gasification combined cycle (IGCC) technique has not yet been broadly accepted for power generation, the ability to switch between power and hydrogen generation requires additional capital costs, which must be recovered (Nnabuife et al., 2022). New technologies, like entrained bed gasification, are expected to improve the cost and efficiency of producing hydrogen from coal by approximately 25 % (Nnabuife et al., 2022). However, these new technologies require more time to validate their true capability as they are in the conceptual stages.

2.5.1.7. Methane Pyrolysis

Methane pyrolysis is deemed an appropriate alternative technology for hydrogen production, and it infers the thermal decomposition of methane to form hydrogen and solid carbon (Sánchez-Bastardo et al., 2020). Since the early 1900s, methane pyrolysis has been extensively researched. The first reaction mechanisms, however, were not proposed until the 1960s (Sánchez-Bastardo et al., 2020). It is now widely accepted that the catalytic decomposition of methane follows the essential reactions described by equations 2.10 to 2.14.

$$CH_4^* \rightarrow CH_3^* + H^* \qquad 2.10$$

$$CH_3^* \rightarrow CH_3^* + H^* \qquad 2.11$$

$$CH_2^* \rightarrow CH^* + H^* \qquad 2.12$$

$$CH^* \rightarrow C^* + H^* \qquad 2.13$$

$$2H^* \rightarrow H_2 \qquad 2.14$$

An overall equation can represent this reaction mechanism as in equation 2.15.

$$CH_4 \rightarrow CH_2^* + H_2 \qquad 2.15$$

Pyrolysis is categorized into three types based on operating conditions. These types are slow, fast, and flash pyrolysis. The types vary in heating intensity, reaction temperature, and residence time (Younas et al., 2022). In fast pyrolysis, elevated temperatures are appropriate for rich-hydrogen production. Hydrogen production is favoured by high moisture content, longer residence time, and small particles.

While methane pyrolysis is not a sustainable process because it utilizes a fossil fuel raw material, this technology can be a convenient alternative owing to the large amounts of natural gas reserves available (Sánchez-Bastardo et al., 2020). In contrast to SMR, methane pyrolysis is more environmentally friendly, given that carbon monoxide/carbon dioxide production is circumvented, and only solid carbon is obtained as a reaction by-product (Sánchez-Bastardo et al., 2020).

Nonetheless, the application of methane pyrolysis is limited by the need for a solid catalyst that deactivates quickly (Sánchez-Bastardo et al., 2020). Furthermore, while the carbon product is marketable, there are no established markets for significant carbon by-products. The development of new markets and applications for the produced carbon may improve the economics of this process. However, it is unlikely that such large amounts of carbon will find markets.

2.5.1.8. Plasma reforming

Plasma reforming has a similar reaction mechanism to conventional reforming. However, in this process, free radicals and energy are fed into the reforming reaction via plasma created by electricity or heat. This procedure is commonly used to support autothermal reforming, partial oxidation, and steam reforming syngas production routes. Plasma devices, also known as plasmatrons, generate temperatures greater than 2000 ℃ and necessitate precise temperature control (Tao et al., 2011).

Heat generation is independent of reaction kinetics, and the optimal operating conditions can be controlled across a wide range of gas compositions and feed rates. Gas streams with a high hydrogen content can be produced in plasma reformers from

various hydrocarbon feedstocks, including natural gas, oil, gasoline, biomass, diesel, and jet fuel, with high conversion efficiencies of approximately 100% (Abdin et al., 2020). Plasma conditions, which include high temperature and a high degree of dissociation and ionization, can accelerate thermodynamically favorable reactions without needing a catalyst or supplying the energy required by endothermic reforming processes.

Plasma reforming is classified into two types based on the average gas temperature: thermal (or equilibrium) plasma reforming and non-thermal plasma reforming. Thermal plasmas have been used for dry reforming of methane, and the results show that greenhouse gas conversions achieved with thermal plasma can reach more than 80% while carbon deposition is limited (Abdin et al., 2020). To generate syngas, non-thermal plasmas such as corona discharge, gliding arc, dielectric barrier discharge (DBD), atmospheric-pressure glow discharge (APGD), micro-wave discharge, and spark discharge have been investigated (Tao et al., 2011). Non-thermal plasma conversions of methane and carbon dioxide are generally lower than catalysis and thermal plasma.

Plasma reformers have the following advantages: compactness and low weight, low cost, high conversion efficiencies, the ability to operate with a wide range of fuels, including heavy and dirty hydrocarbons, and fast response time. Plasma reforming can thus be used for both stationary and mobile applications, and the main disadvantages are high-pressure operation and reliance on electrical energy.

2.5.2. Hydrogen production from renewable resources

Although hydrocarbon steam reforming is a popular and cost-effective method of producing industrial hydrogen, it emits significant amounts of carbon dioxide due to its carbonaceous feedstock. However, steam reforming may be of interest in the short term for hydrogen production if it is efficiently developed to reduce carbon dioxide emissions or through a carbon capture and storage process. Hydrogen production from renewable resources has recently gained traction in a quest to produce green hydrogen. Green hydrogen is produced from renewable resources with near-zero emissions.

Hydrogen with a low carbon footprint can significantly reduce energy-related carbon dioxide emissions and limit global warming (Megia et al., 2021). Green hydrogen can be produced from water or biomass-derived compounds in this regard.

2.5.2.1. Hydrogen produced from water

Water is the most abundant resource for hydrogen production. It can be decomposed into hydrogen and oxygen if enough energy is provided without harmful emissions. In its most basic form, water splitting uses an electrical current (electrolysis) passing through two electrodes to split water into hydrogen and oxygen. It can, however, be split using alternative energy sources such as thermal energy (thermolysis), photonic energy (photo electrolysis), and bio photolysis using microorganisms. These aspects are summarized in Table 2.1 (Megia et al., 2021; Martinez-Burgos et al., 2021).

Table 2.1: Summary of hydrogen production technologies from water

Technology	Energy source	Operating conditions	Advantages	Disadvantages	Maturity
Electrolysis	electricity	Pressures up to 30 bar and temperatures between 323-1173K, depending on the method	The most effective technique reaches 60% efficiency; oxygen is the only by-product.	Requires high amounts of energy	Commercial
Photo electrolysis	light	Ambient temperatures	It uses solar, which is renewable	Low energy conversion	Research and development stage
Thermolysis	heat	Temperatures more than 2773 K but less than 1273 K for thermochemical cycles	Solar energy and different types of biomass can be used as a heat source to drive the reaction	High energy demand and maximum efficiency is 40%	Research and development stage
Bio photolysis	microorganisms	Ambient temperatures	Environmentally sustainable and economically feasible	Low hydrogen yield	Research and development stage

Electrolysis

Electrolysis is one of the most basic methods for producing green hydrogen from water using renewable energy. It is defined as converting electrical energy to chemical energy in the form of hydrogen and oxygen as a by-product, with two reactions occurring in each electrode: anode and cathode (Martinez-Burgos et al., 2021). According to Human et al. (2021), water electrolysis is the lone hydrogen production technology viable with intermittent renewable sources and appropriate for disseminated on-site production. The following reactions in equations 2.16 to 2.18 describe the process of electrolysis.

$$H_2O \rightarrow 0.5\ O_2 + 2\ H^+ + 2\ e^- \qquad 2.16$$

$$2\ H^+ + 2\ e^- \rightarrow H_2 \qquad 2.17$$

$$H_2O \rightarrow H_2 + 0.5\ O_2 \qquad 2.18$$

Water electrolysis can be accomplished using various technologies, including alkaline water electrolysis, solid oxide electrolysis, and proton-exchange membrane electrolysis. A gas separator is required in alkaline electrolysis to prevent the mixture of the gas products during alkaline water electrolysis. It employs concentrated lye as an electrolyte and electrodes made of non-noble metals (e.g., nickel). Proton-exchange membrane electrolysis employs humidified polymer membranes as the electrolyte and noble metals such as platinum or iridium oxide as electrocatalysts. For both technologies, the operating temperature ranges from 50 to 80 °C, and the operating pressures can be set up to 30 bar (Megia et al., 2021). However, proton-exchange membrane electrolysis offers many advantages, for example, a higher rate of hydrogen production, improved energy efficiency, and a more solid design (Ishaq et al., 2022).

On the other hand, solid oxide electrolysis converts water into hydrogen and oxygen at high temperatures between 700-900 °C, increasing the thermal demand (Megia et al., 2021). As a result of the lower investment cost and longer unit lifetime, alkaline water electrolysis and proton-exchange membrane (PEM) electrolysis are more promising

technologies for large-scale implementation. Water electrolysis powered by renewable energy sources, such as wind, sea waves, and biomass, is expected to allow for the scaling-up of hydrogen production (high purity of 99.99%) with zero carbon dioxide emissions, allowing on-site hydrogen production without transportation. However, the cost of producing hydrogen via electrolysis is still significantly higher than fossil fuels.

Among the significant disadvantages of electrolysis is the use of costly electro-catalytic metals such as platinum and process efficiency. Despite being the highest among thermolysis methods, high energy demand and observed corrosion at the cathode must be highlighted as opportunities for technology development (Martinez-Burgos et al., 2021). The expense of generating hydrogen through electrolysis relies significantly on the availability and usage of renewable resources. Researchers Parkinson et al. (2019) and Al-Qahtani et al. (2021) assessed the levelized cost of hydrogen (LCOH) from different sources, including nuclear, wind, and PV solar-powered electrolysis using a PEM system. Their findings showed that PV solar-powered electrolysis had the highest LCOH compared to nuclear and wind-based electrolysis.

Thermolysis

Thermolysis is a thermochemical water-splitting process that uses high temperatures to decompose water into hydrogen and oxygen (Megia et al., 2021). Even though this appears to be a simple procedure, water decomposition requires temperatures above 2500 °C (Wang et al., 2019). The heat required for thermolysis can be provided using solar thermal, biomass, or geothermal heat. However, providing solar thermal heat is not ideal, as continuous heat provision is required in thermolysis (Acar & Dincer, 2022). Since the thermolysis process is reversible, one of the primary challenges in the application is the separation of produced hydrogen and oxygen, as the recombination of gaseous products may result in an explosive mixture (Abdin et al., 2020; Acar & Dincer, 2022). Another issue is the scarcity of materials that can withstand the required temperatures. To address these issues, Kogan (1998) proposed using a catalyst in water, which would allow water to be decomposed in multiple steps while significantly lowering the required heating temperature.

The existing semi-permeable membrane based on ZrO_2 and other high-temperature materials can be used at the thermolysis temperature. However, gas separation is only possible when the temperature of the gas mixture drops, at which point palladium membranes can effectively separate the gas mixture (Abdin et al., 2020). Different chemical reagents have been proposed to reduce the operating limitations of thermolysis.

In contrast to thermolysis, thermochemical water-splitting cycles operate at lower maximum operating temperatures, typically less than 1000 °C, producing hydrogen and oxygen in separate steps, avoiding recombination and the need for high-temperature and expensive downstream gas separation. Increasing the number of cycles reduces the temperature required to split water while complicating the experiment. Water-splitting thermochemical cycles are classified as having light operating conditions and high temperatures.

Although the sulfur iodine thermochemical cycle necessitates a high temperature, it is regarded as the most promising cycle, which is why it has received the most attention in the literature. On the other hand, copper chloride (CuCl) and magnesium chloride (MgCl) cycles are the most commonly reported low-temperature cycles. Recent technological advancements have concentrated on using renewable energy sources such as solar or non-fossil fuels such as nuclear energy.

Photo-electrolysis

Although still in the experimental phase, photo-electrolysis has demonstrated considerable potential in performance and cost-effectiveness as a sustainable method of hydrogen production (Qureshi et al., 2023). Currently, it is the most economically viable and methodical approach for generating hydrogen from sustainable energy sources. Photo electrolysis is a process similar to electrolysis but integrating with light energy absorption in a single unit, contributing to the sustainability of the energy supply (Megia et al., 2021). It uses heterogeneous photocatalysts at one electrode of a photovoltaic electrolytic cell exposed to solar radiation. The photoanode of the cell absorbs sunlight, causing electrons to be generated by the semiconductor at the anode.

These electrons are then transferred to the cathode via an external current, producing hydrogen at the cathode.

In addition to solar energy, electricity should support this process; thus, photonic and electrical energies are converted to chemical energy as hydrogen (Megia et al., 2021). Water photo-electrolysis can be accomplished by absorbing photons with energies more significant than the band gaps of semiconducting photoelectrodes, resulting in holes and electrons in photoelectrochemical cells. The semiconductor, for example, TiO_2, uses photons with energies more significant than the semiconductor bandgap to generate electron-hole pairs that are split by the electric field that traverses the electrolyte (Megia et al., 2021). The type of photon-absorbing material, surface properties, crystalline structure, corrosion resistance, and reactivity all contribute to the performance of the system.

Bio-photolysis

Bio-photolysis, similar to plant and algae photosynthesis, generates hydrogen. A water molecule is split into oxygen and hydrogen ions via photosynthesis by green algae in indirect bio-photolysis (Abdin et al., 2020). The hydrogenase enzyme reacts with these hydrogen ions to produce hydrogen, and these enzymes are typically oxygen-sensitive; thus, the process occurs anaerobically (Megia et al., 2021).

The primary benefit of this process is that it can produce hydrogen from water in an aqueous environment at room temperature. From the standpoint of water and carbon dioxide utilization, it could be regarded as an environmentally sustainable and economically feasible method. Due to the low hydrogen yield, this technology requires a large surface area to collect enough sunlight. In contrast, in indirect bio-photolysis, carbohydrates accumulate during the carbon dioxide fixation stage, producing oxygen. In the following stage, hydrogen is produced, and the substrates produced in the previous stages are used as the carbon source, reducing the need to add nutrients to the medium (Megia et al., 2021).

2.5.2.2. Hydrogen produced from biomass

Biomass is a renewable primary energy source from plants and animals, such as forest residues, crops, municipal solid waste, microalgae, or animal by-products (Abdin et al., 2020). It is considered a potential fuel and chemical feedstock resource. In many developed countries, hydrogen production from biomass and residual wastes is technically and economically feasible, given the technology and economic conditions. It has been predicted that biomass will meet more than 25 % of global energy demand by 2050 (Megia et al., 2021).

In contrast to fossil fuels, biomass-to-energy processes reduce net carbon dioxide emissions and absorb carbon dioxide from the natural environment, resulting in a carbon-neutral scenario. This occurs because the carbon dioxide released during the combustion of biomass is roughly equal to the amount of carbon dioxide absorbed by the plants during their growth, thereby creating a balanced carbon cycle. Two main methods for converting biomass into hydrogen are biological and thermochemical, and the thermochemical process is typically much faster than the biological process and produces more hydrogen (Megia et al., 2021).

i. Biological processes

Research on hydrogen obtained from biological processes has increased significantly in recent years due to increased attention to sustainable development and waste minimization (Abdin et al., 2020). Dark fermentative hydrogen production and photo fermentative are the two primary biological processes used for hydrogen production. Anaerobic bacteria are used in dark fermentative processes on carbohydrate-rich substrates, deprived of light, and under anoxic conditions, yielding the original biomass in hydrogen, organic acids, and carbon dioxide. Hydrogen can be produced at any time because it does not require light (Abdin et al., 2020).

Biohydrogen is produced in the dark fermentation process via biochemical reactions involving enzymes at room temperature and pressure (Zhang et al., 2017). Although the maximum hydrogen yield is closely related to substrate type, inoculum, and operation conditions like temperature and pH, the process pathway metabolically limits

the maximum hydrogen yield (Megia et al., 2021). As a result, various advances in the literature have been reported, such as the immobilization technique (Zhang et al., 2017) or metal ions and oxide nanoparticles (Mishra et al., 2019), to maximize hydrogen production.

In photo fermentation, on the other hand, photosynthetic bacteria use sunlight as a source of energy and assimilate small organic molecules present in the biomass, producing hydrogen and carbon dioxide as by-products, allowing for hydrogen production from a variety of substrates (Eroglu & Melis, 2011). Strict environmental control is required to ensure efficient hydrogen production via photo fermentation. The theoretical hydrogen yield for the photo fermentation process is high, as is the chemical oxygen demand removal efficiency, even though the economic viability of hydrogen production is limited by nitrogenase metabolism. This enzyme produces hydrogen during nitrogen fixation and light intensity received. Compared to the yield under sunlight, the hydrogen yield in dark conditions is typically lower (Megia et al., 2021).

ii. Thermochemical processes

Thermochemical processes are other efficient techniques for producing hydrogen-rich gases from biomass (Hossain et al., 2016). The most common technologies are pyrolysis, gasification, and hydrothermal liquefaction (Hosseini & Wahid, 2016). When gasification and pyrolysis are used, the thermochemical conversion of dried biomass is similar to that of fossil fuels. Both technologies generate carbon monoxide and methane, which can boost hydrogen production via steam reforming and water-gas shift reactions (Abdin et al., 2020). Hydrogen is obtained from wet biomass by combining hydrothermal liquefaction with steam reforming.

Biomass pyrolysis

Pyrolysis is the starting point for all thermochemical conversion technologies because it involves all chemical reactions that result in solid, liquid, and gas as the main products with no oxygen concentration (Megia et al., 2021). Advanced research on biomass for liquid fuels has been conducted recently, ranging from pyrolysis, hydrothermal liquefaction, gasification, and biomass-to-liquid technologies to

upgrading processes. Dried biomass pyrolysis is typically carried out at temperatures ranging from 300 to 1000 °C (Zhang et al., 2017). After thermal decomposition, pyrolytic products include biochar, bio-oil, and non-condensable gases such as hydrogen, methane, carbon oxides, and other gaseous hydrocarbons.

Product yields are affected by operational conditions. When the temperature is below 450 °C, biochar formation is encouraged, whereas bio-oil is the main product when the temperature is between 450 and 800 °C (Ong et al., 2019). Pyrolysis is classified into two types based on its operating conditions: fast and conventional pyrolysis. Since charcoal is the primary product of conventional pyrolysis, fast pyrolysis with high temperatures and short residence times is preferred for hydrogen production.

Fast pyrolysis has received much attention in recent years for liquid fuel production because it has advantages in transport and storage, as well as low investment costs and high energy efficiencies compared to other processes. Various pyrolysis reactors are described in the literature, such as fixed-bed, fluidized bed, microwave, or solar reactors, which have the advantage of heating with a renewable energy source. Although most pyrolysis-related research has focused on producing liquid biofuels, hydrogen can be produced directly at high residence time and temperature following the reaction scheme in equation 2.19.

$$biomass + heat \rightarrow H_2 + CO + CH_4 + other\ products \qquad 2.19$$

Furthermore, formed methane and carbon monoxide can react with water to produce additional hydrogen via the steam reforming and water-gas shift reactions. Catalytic pyrolysis with metal (e.g., Ni or alkali metals) or non-metal-based catalysts is proposed to increase hydrogen production (e.g., activated carbon). Both have shown that they can increase hydrogen production. On the contrary, zeolites or basic materials are preferred to improve the bio-oil quality without needing costly pre-upgradation techniques.

Biomass gasification

Biomass gasification is the most convenient and economical process for hydrogen production (Acar & Dincer, 2022). In this process, the conversion of dry biomass into a combustible gas mixture at high temperatures of between 800-900 ℃ increases hydrogen yield (Megia et al., 2021). It is a type of pyrolysis in which the materials are partially oxidized to produce a mixture of hydrogen, methane, carbon monoxide, carbon dioxide, and nitrogen (Ishaq et al., 2022). This mixture is a producer gas (Holladay et al., 2009). An ignitable gaseous producer gas is produced utilizing numerous sorted thermochemical reactions in biomass gasification (Ishaq et al., 2022). Biomass gasification technology permits the production of a much cleaner and more versatile fuel than the original biomass. This process is deemed cleaner because biomass gasification produces fuel in the form of syngas rather than burning it. It prevents many pollutants from being emitted, such as NOx, SOx, and other particulates at higher than gasification temperatures. Gasifiers are classified as either fixed-bed or fluidized-bed reactors. The main advantages of fixed-bed reactors are that they produce less dust and particulates in the product gas than fluidized-bed reactors and are more cost-effective.

On the other hand, the main advantage of using fluidized-bed reactors is their superior heat and mass transfer between both phases, solid and gas, allowing for a homogeneous temperature and, as a result, increasing carbon conversion and decreasing tar formation. Catalytic biomass gasification has also been reported in the literature to maximize syngas production (Holladay et al., 2009). Using a catalyst during the gasification process promotes the cracking reaction and reduces activation energy, lowering energy consumption (Megia et al., 2021).

Gasification reactors are typically built on a large scale and require massive amounts of material to be fed continuously. Due to the lower heating value, gasification reactors can achieve 35-50 % efficiencies (Holladay et al., 2009). One of the issues with this technology is that massive amounts of resources must be used to transport large amounts of biomass to the central processing plant. Currently, high logistics costs limit

the location of gasification plants. Smaller, more efficient distributed gasification plants may be required for this technology to produce hydrogen at a low cost.

Hydrothermal liquefaction

Hydrothermal liquefaction of wet biomass is a process of breaking down the polymer structure of biomass at moderate temperatures of 250-370 ℃ and high pressures between 4-40 MPa (Megia et al., 2021). At these conditions, water remains in a liquid or relatively dense supercritical state. Since this process operates in a wet reaction environment, hydrothermal liquefaction is especially suited to wet feedstocks as the need for drying is assuaged. The primary product from this process is a liquid biocrude and biochar (Castello et al., 2018). A gaseous stream, an aqua phase, and a solid residue are produced as by-products. The aqueous phase can be recycled to the hydrothermal unit to increase the bio-oil yield. In addition, it could also be utilized to produce hydrogen-rich synthesis gas from steam reforming.

The process of hydrothermal liquefaction can be divided into three primary steps. The first step is the depolymerization of the biomass, and the decomposition follows this in monomers. The last step involves the recombining and repolymerization of reactive fragments (Castello et al., 2018). Given the complex mixture of carbohydrates, lignin, proteins, and lipids contained in the original biomass, the reaction chemistry during the transformation of biomass into liquid products is time-consuming. The reactor can operate in either batch or continuous mode. Even though continuous reactors provide higher feedstock conversion, most studies focus on batch conditions (Megia et al., 2021). Batch activities have gained much more interest due to their relative simplicity of operation (Castello et al., 2018).

Furthermore, catalyst selection is critical in increasing bio-oil yield while decreasing the temperature and pressure required for this process. Catalysts can be alkaline, acidic, metal-based, or mineral-based, and the substrate determines their choice. Alkaline catalysts, for example, are preferred for lignocellulosic and microalgae substrates, whereas zeolites or acid catalysts are best for alcohols. The main advantages of

hydrothermal liquefaction over pyrolysis are higher energy efficiency, lower operating temperature, and lower tar yield (Megia et al., 2021).

The primary product from hydrothermal liquefaction, bio-oil, can be processed to increase hydrogen production. Bio-oil is a liquid with a higher energy density than the original biomass, and it primarily comprises oxygenated compounds such as acids, ketones, aldehydes, and phenols. This complex composition depends on the original biomass composition. It is accountable for many harmful properties of bio-oil, such as low heating value, corrosiveness, or immiscibility with other fuels, making it a low-quality fuel. The bio-oil can be divided into two fractions, namely organic and aqueous. However, the organic fraction is composed of nonpolar compounds and can thus be upgraded by hydrotreating to obtain fuels. The aqueous phase has a low value and primarily comprises water and several oxygenated organic compounds with concentrations ranging from 15 to 60 % by weight. As a result, it can be revalued by producing more hydrogen via a catalytic reforming process.

However, the hydrogen yield obtained from this process is influenced by the thermodynamic limitations of the water-gas shift reaction and other secondary reactions, such as methanation and coking. As a result, hydrogen production is reduced. Therefore, the design of suitable catalysts becomes critical to achieving high activity, high selectivity toward hydrogen, and low deactivation primarily due to coke deposition.

Additionally, the catalyst is in charge of cracking C-C, C-H, and O-H bonds. In this regard, noble-metal-based catalysts have been designated active and stable. However, their prices are tremendously high, whereas transition metal-based catalysts, such as Ni- and Co-based, are less expensive and have demonstrated suitable activity in steam reforming. Researchers have paid much more attention to Ni- and Co-based catalysts recently.

2.6. Considerations in selecting a hydrogen production method

The future of hydrogen as an energy carrier and fuel substitute depends on how effective and sustainable hydrogen production technologies will reach maturity commercially. The path to sustainability suggests the need for emission-free and renewable sources in the value chain via sustainable production pathways.

Many studies have been conducted on different sustainability metrics of hydrogen production methods, looking at fossil and renewable methods. Dawood et al. (2020) provided a pathway toward 100 % renewable energy systems and considered the role of hydrogen in the future energy matrix. In addition, the study assessed various hydrogen production methods based on environmental impact, technology maturity level, and efficiencies. El-emam & Ozcan (2019) thoroughly reviewed the literature on clean hydrogen production's technological, economic, and environmental aspects. Their research also highlighted recent advances and developments in the literature to introduce hydrogen production routes compatible with renewable and nuclear sources. Furthermore, the current and future cost expectations for the clean-hydrogen economy were discussed, and the study concluded that clean and carbon-free hydrogen production is economically feasible in the near future.

In another study, Ji & Wang (2021) investigated the current status, recent advances, and barriers of fossil and renewable-based hydrogen production methods. They compared life cycle costs and environmental impacts of various hydrogen production methods. Moreover, they deduced that electrolysis and thermochemical cycles combined with clean energy sources have significant economic and environmental potential. Acar & Dincer (2022) recently conducted a comparative assessment of the sustainability performance of selected hydrogen production methods. The assessment was based on economic, thermodynamic, environmental, social, and technical aspects. The study also outlined the benefits and challenges of hydrogen production methods. The study showed that steam reforming with carbon capture could provide sustainable

hydrogen quickly while increasing the maturity levels and decreasing the costs of other technologies.

Furthermore, Kannah et al. (2021) reviewed the sensitivity analysis of various hydrogen production processes such as pyrolysis, gasification, steam reforming, dark fermentation, photo biolysis, water electrolysis, and liquid reforming to evaluate their pros and cons along with their cost-effectiveness. The review concluded that steam reforming of natural gas is efficient, low-cost, and the best for hydrogen production. However, future research is vital to decrease energy requirements. Norouzi (2022) examined and ranked various hydrogen production methods from economic, social, environmental, energy, and exergy aspects. The authors concluded that solar electrolysis was preferable on a small scale, and thermochemical hydrogen production was preferable on a large scale.

Hermesmann & Müller (2022) examined nine hydrogen production configurations based on four hydrogen production methods. The selected methods, conventional steam reforming, steam reforming with carbon capture, electrolysis, and methane pyrolysis, represented different colors of hydrogen, which are grey, blue, green, and turquoise. The study compared the pathways according to the life cycle analysis (LCA), and results showed that electrolysis is the least harmful, while conventional steam reforming has the highest environmental impact. However, it is not enough to choose a pathway based on one concept; other criteria like cost need to be considered.

The number of options available for hydrogen production methods with different features and capabilities does not allow a straightforward decision. Table 2.2 summarizes the advantages and disadvantages of each discussed hydrogen production technique. The economic, social, and environmental performance of the pathways vary greatly; therefore, choosing a pathway is not straightforward (Abdel-Basset et al., 2021). It requires various criteria to be taken into consideration and the tradeoffs thereof. Most models in the existing research focus on optimizing a financial measure, typically the cost, when designing a hydrogen production facility. However, this approach overlooks other essential objectives that should be considered. By solely

emphasizing cost minimization, there is a risk of creating a system that disregards environmental concerns. This means opting for inexpensive technologies while avoiding cleaner yet more expensive alternatives like electrolysis and SMR with CCS.

Conversely, prioritizing environmental friendliness may lead to a system that is not the most cost-effective. As a result, selecting a hydrogen production pathway requires multi-criteria decision-making methods to be utilized. These methods involve decision-making considering tradeoffs between two or more conflicting criteria or objectives.

Table 2.2: Summary of each discussed hydrogen production method's advantages and disadvantages

Process	Advantages	Disadvantages
Steam reforming	High hydrogen yield Cheaper production of hydrogen Oxygen not required	Carbon dioxide emissions High energy is required
Partial oxidation	Faster start-up times Faster transient response	Decreased hydrogen and carbon dioxide production efficiencies Soot formation
Autothermal reforming	Optimum high hydrogen yield with low carbon monoxide content Shut down and started rapidly while producing a more significant amount of hydrogen	Difficult during purity control and the final product Requires air or oxygen Catalyst deactivation
Dry reforming	Possibility of using carbon dioxide	Coking of catalyst High energy demand
Coal gasification	Increased efficiency	Carbon dioxide emissions
Methane pyrolysis	High hydrogen rate	Carbon dioxide emissions High energy requirements
Biomass gasification	Abundant and cheap feedstock Moderate hydrogen yield	More purification steps are required due to tar formation
Biomass pyrolysis	Abundant and cheap feedstock Carbon dioxide neutral Moderate hydrogen yield	High operating temperatures required Requires more purification steps
Biomass photolysis	Oxygen is the only by-product Works in mild conditions	Requires energy input from sunlight; therefore, weather constraint
Dark fermentation	Free of carbon dioxide emissions Cheap feedstock	Low hydrogen yield
Photo fermentation	Contributes to waste recycling Carbon dioxide neutral	Requires sunlight as energy input Low hydrogen yield

Electrolysis	Free of pollution The feedstock is water	Moderate temperatures required High cost
Thermolysis	Oxygen is the only by-product Abundant feedstock, which is water	Corrosion problem High cost High toxicity
Photo-electrolysis	Oxygen is the by-product Abundant feedstock, which is water	Sunlight is the energy input Low hydrogen yield

2.7. Multi-criteria decision-making (MCDM) in hydrogen production

Multi-criteria decision-making (MCDM) is an essential and integrative field that has been considered in recent years. It is categorized into two types, which are multi-objective decision-making (MODM) and multi-attribute decision-making (MADM) (Keshavarz-Ghorabaee et al., 2021). MADM focuses on problems with discrete decision space, and MODM involves several contending objectives that must be optimized simultaneously (Zavadskas et al., 2019). From an applied perspective, MADM is related to problems in which the number of alternatives is pre-set, and the decision maker (DM) opts for, prioritizes, or ranks a fixed number of paths. On the other hand, MODM is related to situations in which the alternatives are not known from the onset. The MCDM methods aim to estimate the ranking of alternatives and criteria (Keshavarz-Ghorabaee et al., 2018).

Typically, there are four steps in the assessment process employing MCDM methods. The steps are as follows (Keshavarz-Ghorabaee et al., 2021):

(i) specifying the alternatives and criteria linked to the problem,
(ii) defining weights of each quantity,
(iii) allocating individual performance to each alternative on each quantity and
(iv) assessing the different options based on the collective performance of all criteria.

MCDM methods have been proven practical tools for tackling decision issues categorized by large dimensionality with contrary goals and different stakeholders. Hence, various MCDM methods have been developed for the sustainability assessment

and prioritization of hydrogen production technologies in the literature. Some of the standard methods in MCDM include the Weighted Sum Model (WSM), Weighted Aggregated Sum Product Assessment (WASPAS), Technique for Order of Preference by Similarity to Ideal Solution (TOPSIS), Vise Kriterijumska Optimizacija I Kompromisno Resenje (VIKOR), Preference Ranking Organization METHod for Enrichment of Evaluations (PROMETHEE), ELimination Et Choix Traduisant la REalité (ELECTRE), COmplex PRoportional Assessment (COPRAS), Evaluation based on Distance from Average Solution (EDAS), Analytic Hierarchy Process (AHP), Analytic Network Process (ANP) and Best- Worst Method (BWM). Figure 2.5 shows some standard MCDM methods.

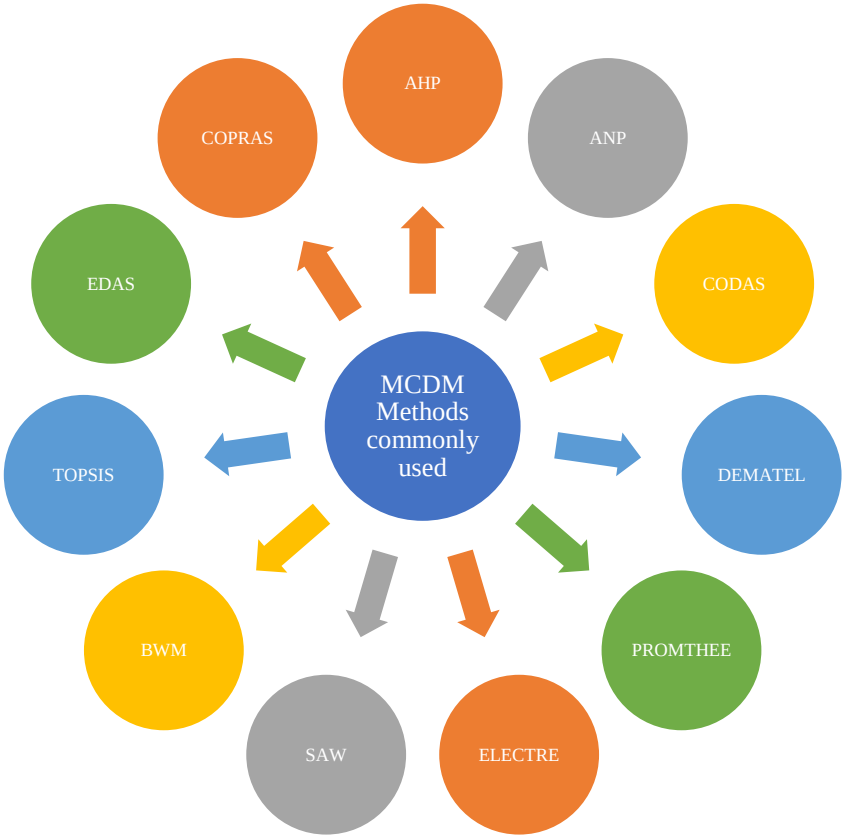

Figure 2.5:Some standard methods used in multi-criteria decision making

Pilavachi et al. (2009) assessed seven hydrogen production technologies using the Analytic Hierarchy Process (AHP) method, and five criteria were utilized in the

assessment. In another study, Chung et al. (2014) utilized the AHP method to study hydrogen production selection problem in Korea. Ren et al. (2013a) used the decision-making trial and evaluation laboratory (DEMATEL) method to improve hydrogen production sustainability and further combined extension theory and the AHP method to prioritize hydrogen production technologies (Ren et al. 2013b). Ramazankhani et al. (2016) used the technique for order preference by similarity to an ideal solution (TOPSIS) and the VIKOR methods to investigate the hydrogen production problem in Iran.

Furthermore, Acar et al. (2018) compared the sustainability of available hydrogen production technologies by considering five factors: economic, technological, environmental, social, and availability/reliability. The hesitant fuzzy AHP method was utilized in the study to select and evaluate six hydrogen production technologies. Ren et al. (2016) developed a novel approach to decision-making in which the criteria weights were calculated using a combined fuzzy AHP and the Analytic Network Process (ANP) method. The sustainability ranking was implemented using a PROMTHEE approach. However, all these methods depend on human opinions, and decision-maker's judgments are subjective and vague, causing uncertainties.

Lin et al. (2021) developed a novel multi-criteria framework for the sustainability prioritization of five hydrogen production pathways under hybrid information accounting for the vagueness and ambiguity in human judgments. Firstly, the Z-number Best Worst Method (ZBWM) was employed to accurately determine the criteria weights using Z numbers to capture the vagueness and ambiguity in decision makers' opinions. Then, an extended ELECTRE model was developed for the sustainability prioritization of hydrogen production pathways based on the decision-making matrix with hybrid information. However, a limitation of the preferences/ opinions of different decision makers not allowed to be merged in the decision-making process simultaneously still existed.

Abdel-Basset et al. (2021) evaluated hydrogen production options considering five sustainability criteria and seventeen sub-indicators. Additionally, they proposed a new

model consisting of three MCDM methods, AHP-COPRAS-EDAS, with AHP applied to calculate the proportional importance of the selected criteria. COPRAS and EDAS were used to rank the pathways. Wind electrolysis was shown to be the most sustainable pathway in the near future. Although a novel MCDM-based approach was developed in this study, some limitations still need to be addressed in the future, including better consideration of the opinions of multiple stakeholders during the decision-making since only four were used in the study.

In another study, Li et al. (2020) developed a novel MCDM framework to objectively determine the sustainability assessment of nine hydrogen production technologies, considering nine criteria. The framework utilizes the grey relational analysis (GRA) method incorporated into the conventional DEMATEL approach to identify the causal relationships among criteria and objectively determine the criteria weights by calculating the grey relational coefficients that measure the correlation among criteria. Furthermore, the sustainability of the alternative hydrogen production pathways was ranked using a GRA approach, in which the grey correlation coefficients were calculated as an indicator to measure the closeness of each concerning the ideal scheme. However, the developed method did not specify the interaction among criteria.

Ren et al. (2020) developed a novel two-stage MCDM framework to select the most sustainable eight hydrogen production technologies. In the first stage, the initial sustainability ranking of the alternatives was attained by utilizing the fuzzy best-worst method (FBWM) to establish the weights of the criteria and the fuzzy TOPSIS method to prioritize the sustainability of the alternatives. In the second stage, a newly proposed Preference Ranking Linear Programming Method (PRLPM) was used to obtain the final decision using the initial sustainability ranking obtained in the first stage to establish the new decision-making matrix. It was concluded that the proposed method was more accurate in reflecting the alternative preference of the decision-maker for selecting the preferred alternative among various hydrogen production techniques. However, determining the criteria weights did not account for the interdependency

between criteria. Also, the method was not extended to the framework of multi-actor decision-making.

Seker & Aydin (2022) proposed a novel fuzzy-based stepwise weight assessment ratio analysis (SWARA) and Weighted Aggregated Sum Product Assessment integrated with the intuitionistic fuzzy sets (IVIF-WASPAS) method to determine the most suitable hydrogen production method in the Black Sea. Eight criteria were considered based on decision-makers' viewpoints and a comprehensive literature review. The fuzzy-based SWARA method was conducted to obtain criteria weights. Then, the IVIF-WASPAS method was employed to assess and rank the alternatives. Accordingly, electrochemical was selected to be the best method. However, the number of experts contributing to this study was a limitation.

Another study by Chau et al. (2022) provided a framework for assessing the most desirable hydrogen production technique based on efficiency, safety, and infrastructure using an integrated AHP and life-cycle index (LInX) approach. The study concluded that steam reforming was the most desirable technique based on the chosen criteria. They further employed fuzzy set theory to address subjectivity and uncertainty challenges in the data. They found that although the technologies based on electrolysis are environmentally benign, more significant insecurities were present than with non-renewable technologies.

Literature has used various MCDM methods to prioritize various hydrogen production paths based on different situations. However, the methods utilized are mainly subjective, having to depend on decision-makers' opinions. Table 2.3 summarizes the main advantages and disadvantages of some of the MCDM methods (Siksnelyte-Butkiene et al., 2020; Alsalem et al., 2018; Pond & Bond, 2022). As much as decision makers directly express how they feel about the relative importance of the criteria and give some perspective into the processes, inconsistencies exist. Subjective MCDM methods are regularly time-consuming, given that decision-makers might not agree on the problem under consideration. In addition, the MCDM methods applied for prioritizing hydrogen production techniques usually require two methods: one for

calculating the criteria weights and another for ranking the alternatives. Keshavarz-Ghorabaee et al. (2018) proposed a novel method, the simultaneous evaluation of criteria and alternatives (SECA), which is objective and simultaneously calculates the criteria weights and ranks the alternatives.

Table 2.3:Advantages and disadvantages of some standard MCDM methods

Method	Brief description	Advantages	Disadvantages
WSM	This method evaluates alternatives based on several decision criteria. WSM allows for the comparison of options by assigning weights and then utilizing these weights and generating fundamental values for the alternatives under consideration	• Simple to use • Suitable for single-dimension problems management	• Only evaluates a one-dimensional problem • No possibility of integrating multiple preferences
AHP	This method echoes the natural behavior of human thinking. It solves complex problems by decomposing them into a hierarchy of more easily known sub-problems having decision alternatives at the lowest levels	• It can be easily applied to different problems • Simple computation • Quick evaluation process • Contains comprehensible logic • Based on a hierarchical structure, therefore, better focus on each criterion	• It depends on expert opinions • Time-consuming • Complex as more decision-makers are involved • The additional analysis required to verify the results • Interdependence between alternatives and objectives can lead to inaccuracy
TOPSIS	This technique is based on the idea that the ideal alternative has the highest level for all attributes, whereas the negative ideal has the lowest level for all attributes	• Works with a fundamental ranking • The data need not be independent • The method has a coherent logic, and the concept	• The method is based on Euclidean distance, and negative and positive values do not influence calculations

		is in a relatively simple mathematical form • Simple computational process • Results obtained quickly	• A substantial deviation of one indicator from the ideal solution strongly impacts the results • The method is appropriate when the indicators of options do not vary strongly
CRITIC	This method uses standard deviation to measure the contrast intensity of each criterion. It necessitates that a criterion with a higher contrast intensity or standard deviation is assigned with a higher weight	• One of the most objective methods where there is no need for decision-makers • Involves basic statistical operations • Simple calculation process	• The limitation of the method lies in its hypothesis that the evaluation criteria are compensatory • It only shows some properties of the initial data • It does not consider the type of criteria
WASPAS	This technique is a unique combination of the weighted sum model (WSM) and weighted product model (WPM)	• Shorter calculation stages • The method weights cost and benefit criteria separately • Valid for the complete ranking • High accuracy	• Considers only minimum and maximum values and does not consider all the performance values
PROMETHEE	A method for scoring or ranking a finite number of alternatives by considering multiple criteria associated with the alternatives. MCDM is concerned with evaluating and selecting alternatives that are compatible with the goals and requirements	• Useful for options that are difficult to harmonize • Works with qualitative and quantitative information • Uncertain and fuzzy information can be incorporated into calculations	• The computation process is quite long • Calculations are very complicated
VIKOR	This method evaluates the compromise ranking list and the solution attained with given	• Most significant for real-world problems	• Lacks provision to weigh elicitation and check the

	weights. It aims to rank and select from a set of alternatives in the presence of conflicting criteria	• Ability to recognize the proper alternative • Applicable to situations with many alternatives and criteria • Appropriate to use when quantitative or objective information is offered	consistency of judgments
ELECTRE	Utilized to choose the best choice with maximum advantage and most minor conflict	• Outranking is used	• Time-consuming • Not adequate for many interactions between criteria
ANP	This method is a mathematical theory that can systematically handle all dependencies. It can be used in numerous fields. It includes a multi-criteria decision-making method that compares different alternatives to select the best alternative	• Considers dependent and independent criteria	• Unable to single out an element to identify its strengths and weaknesses.
COPRAS	Utilized to evaluate the maximizing and minimizing index values, and the effect of maximizing and minimizing attribute indexes on results evaluation is considered separately	• Suitable for the evaluation of a single alternative • Robust method • Not requiring minimization of criteria	• Less stable in data variation case in comparison to some other methods • Sensitive to slight variations in data.
GRA	This method deals with all incomplete data	• Provides a unique solution for perfect data	• The optimal solution is difficult to obtain
SAW	The basic logic of this method is to acquire the weighted sum of the performance ratings of each alternative over all attributes by scaling the values of all attributes to make them comparable and sum up	• Considers all criteria/attribute • Offers simple calculation • Makes decisions intuitively	• Does not commonly discover the actual situation • All criteria values must be positive, and maximum

	the values of all attributes for each alternative		
BWM	This is a technique that compares the best attribute to all other attributes and all other factors to the worst factor	• It achieves more reliable outcomes • Easy to use • decreases the times of comparison • Ensures the reliability of the results by making fewer comparisons • Contains consistency index	• Determining the importance level of the best criterion over the other criteria, as well as the importance of all the criteria over the worst one, is difficult
DEMATEL	It deals with assessing interdependent relationships among factors and acquiring the critical ones through a visual structural model	• Evaluates the direct and indirect relationships between criteria	• The mechanism that consents to the assimilation of indirect /direct relations is uncertain

2.8. The Simultaneous Evaluation of Criteria and Alternatives (SECA)

This objective MCDM method was proposed by Keshavarz-Ghorabaee et al. (2018). Unlike other MCDM methods, this method can simultaneously evaluate criteria and alternatives. It is a multi-objective, non-linear mathematical model developed to calculate criteria weights and rank alternatives simultaneously. A multi-objective non-linear mathematical model is developed for the evaluation process. There are three objective functions in the model. The first goal is to maximize the overall performance of alternatives, while the second and third goals maximize variation information within and between criteria. The standard deviation measures within-criterion variation, while the correlation considers between-criterion variation. The overall performance scores of alternatives and the objective weights of criteria can be determined simultaneously by optimizing the developed mathematical model.

The SECA model has been applied in several fields for the prioritization of electric vehicles (Ecer, 2021; Lu et al., 2022), renewable energy resources (Assadi et al., 2022), wastewater allocation (Azbari et al., 2021), an asymmetric traveling salesman (Bazrafshan et al., 2021), KPI's (Baradari et al., 2021), pharmaceutical supply (Amoozad Mahdiraji et al., 2022), SME's (Amoozad Mahdiraji et al., 2022), finance (Ozcalici, 2022), E-waste scenario management (Keshavarz-Ghorabaee et al., 2022), aerospace and defense (Rasmussen et al., 2023) and machining processes (Das & Chakraborty, 2022). However, the method has not been applied in the hydrogen production field, thus forming the basis of this work.

2.9. References

Ã, Y. L., Wang, Y., Zhang, X., & Mi, Z. (2008). Thermodynamic analysis of autothermal steam and CO 2 reforming of methane. 33, 2507–2514. https://doi.org/10.1016/j.ijhydene.2008.02.051

Abbasi, S., Abbasi, M., Tabkhi, F., & Akhlaghi, B. (2020). Syngas production plus reducing carbon dioxide emission using dry reforming of methane: Utilizing low-cost Ni-based catalysts. Oil and Gas Science and Technology, 75(10), 1–19. https://doi.org/10.2516/ogst/2020016

Abdel-Basset, M., Gamal, A., Chakrabortty, R. K., & Ryan, M. J. (2021). Evaluation of sustainable hydrogen production options using an advanced hybrid MCDM approach: A case study. International Journal of Hydrogen Energy, 46(5), 4567–4591. https://doi.org/10.1016/j.ijhydene.2020.10.232

Abdin, Z., Zafaranloo, A., Rafiee, A., Mérida, W., Lipiński, W., & Khalilpour, K. R. (2020). Hydrogen as an energy vector. Renewable and Sustainable Energy Reviews, 120(December 2019). https://doi.org/10.1016/j.rser.2019.109620

Acar, C., Beskese, A., & Temur, G. T. (2018). Sustainability analysis of different hydrogen production options using hesitant fuzzy AHP. International Journal of Hydrogen Energy, 43(39), 18059–18076. https://doi.org/10.1016/j.ijhydene.2018.08.024

Acar, C., & Dincer, I. (2022). Selection criteria and ranking for sustainable hydrogen production options. International Journal of Hydrogen Energy, 47(95), 40118–40137. https://doi.org/10.1016/j.ijhydene.2022.07.137

Ajanovic, A., Sayer, M., & Haas, R. (2022). The economics and the environmental benignity of different colors of hydrogen. International Journal of Hydrogen Energy, 47(57), 24136–24154. https://doi.org/10.1016/j.ijhydene.2022.02.094

Al-Qahtani, A., Parkinson, B., Hellgardt, K., Shah, N., & Guillen-Gosalbez, G. (2021). Uncovering the true cost of hydrogen production routes using life cycle monetisation. Applied Energy, 281, 115958. https://doi.org/10.1016/j.apenergy.2020.115958

Alsalem, M. A., Zaidan, A. A., Zaidan, B. B., Hashim, M., Albahri, O. S., Albahri, A. S., Hadi, A., & Mohammed, K. I. (2018). Systematic Review of an Automated Multiclass Detection and Classification System for Acute Leukaemia in Terms of Evaluation and Benchmarking, Open Challenges, Issues and Methodological Aspects. Journal of Medical Systems, 42(11). https://doi.org/10.1007/s10916-018-1064-9

Amoozad Mahdiraji, H., Govindan, K., Yaftiyan, F., Garza-Reyes, J. A., & Razavi Hajiagha, S. H. (2022). Unveiling coordination contracts' roles considering circular economy and eco-innovation toward pharmaceutical supply chain resiliency: Evidence of an emerging economy. Journal of Cleaner Production, November, 135135. https://doi.org/10.1016/j.jclepro.2022.135135

Amoozad Mahdiraji, H., Yaftiyan, F., Abbasi-Kamardi, A., & Garza-Reyes, J. A. (2022). Investigating potential interventions on disruptive impacts of Industry 4.0 technologies in circular supply chains: Evidence from SMEs of an emerging economy. Computers and Industrial Engineering, 174(October), 108753. https://doi.org/10.1016/j.cie.2022.108753

Arora, S., & Prasad, R. (2016). An overview on dry reforming of methane: Strategies to reduce carbonaceous deactivation of catalysts. RSC Advances, 6(110), 108668–108688. https://doi.org/10.1039/c6ra20450c

Assadi, M. R., Ataebi, M., Ataebi, E. sadat, & Hasani, A. (2022). Prioritization of renewable energy resources based on sustainable management approach using simultaneous evaluation of criteria and alternatives: A case study on Iran's electricity industry. Renewable Energy, 181, 820–832. https://doi.org/10.1016/j.renene.2021.09.065

Azbari, K. E., Ashofteh, P. S., Golfam, P., & Singh, V. P. (2021). Optimal wastewater allocation with the development of an SECA multi-criteria decision-making method. Journal of Cleaner Production, 321(March), 129041. https://doi.org/10.1016/j.jclepro.2021.129041

Bahari, N. A., Wan Isahak, W. N. R., Masdar, M. S., & Yaakob, Z. (2019). Clean hydrogen generation and storage strategies via CO2 utilization into chemicals and fuels: A review. International Journal of Energy Research, 43(10), 5128–5150. https://doi.org/10.1002/er.4498

Baradari, I., Shoar, M., Nezafati, N., & Motadel, M. (2021). A new approach for KPI ranking and selection in ITIL processes: Using simultaneous evaluation of criteria and alternatives (SECA). Journal of Industrial Engineering and Management Studies (JIEMS), 8(1), 157. https://doi.org/10.22116/jiems.2020.228519.1356

Bazrafshan, R., Hashemkhani Zolfani, S., & Al-E-hashem, S. M. J. M. (2021). Comparison of the sub-tour elimination methods for the asymmetric traveling salesman problem applying the SECA method. Axioms, 10(1), 1–14. https://doi.org/10.3390/axioms10010019

Bharadwaj, S. S., & Schmidt, L. D. (1994). Synthesis gas formation by catalytic oxidation of methane in fluidized bed reactors. Journal of Catalysis, 146(1), 11–21. https://doi.org/10.1016/0021-9517(94)90003-5

Carapellucci, R., & Giordano, L. (2020). Steam, dry and autothermal methane reforming for hydrogen production: A thermodynamic equilibrium analysis. Journal of Power Sources, 469(June), 228391. https://doi.org/10.1016/j.jpowsour.2020.228391

Castello, D., Pedersen, T. H., & Rosendahl, L. A. (2018). Continuous hydrothermal liquefaction of biomass: A critical review. Energies, 11(11). https://doi.org/10.3390/en11113165

Chanburanasiri, N., Ribeiro, A. M., Rodrigues, A. E., Arpornwichanop, A., Laosiripojana, N., Praserthdam, P., & Assabumrungrat, S. (2011). Hydrogen production via sorption enhanced steam methane reforming process using Ni/CaO multifunctional catalyst. Industrial and Engineering Chemistry Research, 50(24), 13662–13671. https://doi.org/10.1021/ie201226j

Chau, K., Djire, A., & Khan, F. (2022). Review and analysis of the hydrogen production technologies from a safety perspective. International Journal of Hydrogen Energy, 47(29), 13990–14007. https://doi.org/10.1016/j.ijhydene.2022.02.127

Chih, Y. K., Chen, W. H., You, S., Hsu, C. H., Lin, H. P., Raza Naqvi, S., & Ashokkumar, V. (2023). Statistical optimization of hydrogen production from bio-methanol steam reforming over Ni-Cu/Al2O3 catalysts. Fuel, 331(P1), 125691. https://doi.org/10.1016/j.fuel.2022.125691

Chung, Y., Hong, S., & Kim, J. (2014). Which of the technologies for producing hydrogen is the most prospective in Korea?: Evaluating the competitive priority of those in near-, mid-, and long-term. Energy Policy, 65, 115–125. https://doi.org/10.1016/j.enpol.2013.10.020

Clerici, A., & Alimonti, G. (2015). World energy resources. EPJ Web of Conferences, 98, 1–15. https://doi.org/10.1051/epjconf/20159801001

Das, P. P., & Chakraborty, S. (2022). Application of simultaneous evaluation of criteria and alternatives (SECA) method for parametric optimization of hybrid machining processes. International Journal on Interactive Design and Manufacturing, 16(4), 1497–1509. https://doi.org/10.1007/s12008-022-00842-z

Dash, S. K., Chakraborty, S., & Elangovan, D. (2023). A Brief Review of Hydrogen Production Methods and Their Challenges. Energies, 16(3). https://doi.org/10.3390/en16031141

Dawood, F., Anda, M., & Shafiullah, G. M. (2020). Hydrogen production for energy: An overview. International Journal of Hydrogen Energy, 45(7), 3847–3869. https://doi.org/10.1016/j.ijhydene.2019.12.059

De Souza, T. L., Rossi, C. D. C. R. D. S., Alonso, C. G., Guirardello, R., Cabral, V. F., Fernandes-Machado, N. R. C., Specchia, S., Zabaloy, M. S., & Cardozo-Filho, L. (2014). Thermodynamic analysis of autothermal reforming of methane via entropy maximization: Hydrogen production. International Journal of Hydrogen Energy, 39(16), 8257–8270. https://doi.org/10.1016/j.ijhydene.2014.03.078

DOE. (2019). The South African Energy Sector Report. In Department of Energy, SA (Vol. 33, Issue 1). http://dx.doi.org/10.1016/j.powtec.2017.06.008%0Ahttps://doi.org/10.1016/j.jwpe.2017.08.012%0Ahttps://doi.org/10.1016/j.jhazmat.2021.125853%0Ahttps://doi.org/10.1080/10962247.2018.1521349%0Ahttp://www.energy.gov.za

Durán, F. J., Dorado, F., & Sanchez-Silva, L. (2020). Exergetic and Economic Improvement for a Steam Methane-Reforming Industrial Plant: Simulation Tool. Energies, 13(15). https://doi.org/10.3390/en13153807

Ecer, F. (2021). A consolidated MCDM framework for performance assessment of battery electric vehicles based on ranking strategies. Renewable and Sustainable Energy Reviews, 143(January), 110916. https://doi.org/10.1016/j.rser.2021.110916

El-emam, R. S., & Ozcan, H. (2019). Comprehensive review on the techno-economics of sustainable large-scale clean hydrogen production. 220. https://doi.org/10.1016/j.jclepro.2019.01.309

El Hajj Chehade, A. M., Daher, E. A., Assaf, J. C., Riachi, B., & Hamd, W. (2020). Simulation and optimization of hydrogen production by steam reforming of natural gas

for refining and petrochemical demands in Lebanon. International Journal of Hydrogen Energy, 45(58), 33235–33247. https://doi.org/10.1016/j.ijhydene.2020.09.077

Eroglu, E., & Melis, A. (2011). Photobiological hydrogen production: Recent advances and state of the art. Bioresource Technology, 102(18), 8403–8413. https://doi.org/10.1016/j.biortech.2011.03.026

Faheem, H. H., Tanveer, H. U., Abbas, S. Z., & Maqbool, F. (2021). Comparative study of conventional steam-methane-reforming (SMR) and auto-thermal-reforming (ATR) with their hybrid sorption enhanced (SE-SMR & SE-ATR) and environmentally benign process models for the hydrogen production. Fuel, 297(February), 120769. https://doi.org/10.1016/j.fuel.2021.120769

Giwa, A., & Giwa, S. O. (2013). Simulation, Sensitivity Analysis and Optimization of Hydrogen Production by Steam Reforming of Methane Using Aspen Plus. International Journal of Engineering Research & Technology, 2(7), 1719–1729.

Hermesmann, M., & Müller, T. E. (2022). Green, Turquoise, Blue, or Grey? Environmentally friendly Hydrogen Production in Transforming Energy Systems. Progress in Energy and Combustion Science, 90(September 2021), 100996. https://doi.org/10.1016/j.pecs.2022.100996

Holladay, J. D., Hu, J., King, D. L., & Wang, Y. (2009). An overview of hydrogen production technologies. Catalysis Today, 139(4), 244–260. https://doi.org/10.1016/j.cattod.2008.08.039

Hossain, M. A., Jewaratnam, J., & Ganesan, P. (2016). Prospect of hydrogen production from oil palm biomass by thermochemical process – A review. International Journal of Hydrogen Energy, 41(38), 16637–16655. https://doi.org/10.1016/j.ijhydene.2016.07.104

Hosseini, S. E., & Wahid, M. A. (2016). Hydrogen production from renewable and sustainable energy resources: Promising green energy carrier for clean development.

Renewable and Sustainable Energy Reviews, 57, 850–866. https://doi.org/10.1016/j.rser.2015.12.112

Hrabovsky, M., Hlina, M., Kopecky, V., Maslani, A., Krenek, P., Serov, A., & Hurba, O. (2018). Steam Plasma Methane Reforming for Hydrogen Production. Plasma Chemistry and Plasma Processing, 38(4), 743–758. https://doi.org/10.1007/s11090-018-9891-5

Human, G., van Schoor, G., & Uren, K. R. (2021). Genetic fuzzy rule extraction for optimised sizing and control of hybrid renewable energy hydrogen systems. International Journal of Hydrogen Energy, 46(5), 3576–3594. https://doi.org/10.1016/j.ijhydene.2020.10.238

IEA. (2021). World Energy Outlook 2021 : Part of the World Energy Outlook. International Energy Agency, 386. https://www.iea.org/reports/world-energy-outlook-2021

Incer-Valverde, J., Korayem, A., Tsatsaronis, G., & Morosuk, T. (2023). "Colors" of hydrogen: Definitions and carbon intensity. Energy Conversion and Management, 291(June), 117294. https://doi.org/10.1016/j.enconman.2023.117294

Ishaq, H., Dincer, I., & Crawford, C. (2022). A review on hydrogen production and utilization: Challenges and opportunities. International Journal of Hydrogen Energy, 47(62), 26238–26264. https://doi.org/10.1016/j.ijhydene.2021.11.149

Ji, M., & Wang, J. (2021). ScienceDirect Review and comparison of various hydrogen production methods based on costs and life cycle impact assessment indicators. *International Journal of Hydrogen Energy*, *46*(78), 38612–38635. https://doi.org/10.1016/j.ijhydene.2021.09.142

Kannah, R. Y., Kavitha, S., Karthikeyan, O. P., Kumar, G., Dai-viet, N. V., & Banu, J. R. (2021). Bioresource Technology Techno-economic assessment of various hydrogen production methods – A review. Bioresource Technology, 319(September 2020), 124175. https://doi.org/10.1016/j.biortech.2020.124175

Keshavarz-Ghorabaee, M., Amiri, M., Zavadskas, E. K., Turskis, Z., & Antucheviciene, J. (2018). Simultaneous evaluation of criteria and alternatives (SECA) for multi-criteria decision-making. Informatica (Netherlands), 29(2), 265–280. https://doi.org/10.15388/Informatica.2018.167

Keshavarz-Ghorabaee, M., Amiri, M., Zavadskas, E. K., Turskis, Z., & Antucheviciene, J. (2021). Determination of objective weights using a new method based on the removal effects of criteria (Merec). Symmetry, 13(4), 1–20. https://doi.org/10.3390/sym13040525

Keshavarz-Ghorabaee, M., Amiri, M., Zavadskas, E. K., Turskis, Z., & Antucheviciene, J. (2022). A Fuzzy Simultaneous Evaluation of Criteria and Alternatives (F-SECA) for Sustainable E-Waste Scenario Management. Sustainability (Switzerland), 14(16). https://doi.org/10.3390/su141610371

Kogan, A. (1998). Direct solar thermal splitting of water and on-site separation of the products - II. Experimental feasibility study. International Journal of Hydrogen Energy, 23(2), 89–98. https://doi.org/10.1016/s0360-3199(97)00038-4

Lavoie, J. M. (2014). Review on dry reforming of methane, a potentially more environmentally-friendly approach to the increasing natural gas exploitation. Frontiers in Chemistry, 2(NOV), 1–17. https://doi.org/10.3389/fchem.2014.00081

Li, W., Ren, X., Ding, S., & Dong, L. (2020). A multi-criterion decision making for sustainability assessment of hydrogen production technologies based on objective grey relational analysis. International Journal of Hydrogen Energy, 45(59), 34385–34395. https://doi.org/10.1016/j.ijhydene.2019.11.039

Lu, F., Yan, L., & Huang, B. (2022). Site selection for shared charging and swapping stations using the SECA and TRUST methods. Energy Reports, 8, 14606–14622. https://doi.org/10.1016/j.egyr.2022.10.378

Lu, Q., Hou, Y., Laraib, S. R., Khalifa, O., Li, K., Xie, W. luan, Cui, M. shu, & Yang, Y. ping. (2019). Electro-catalytic steam reforming of methane over Ni-CeO2/Γ-

Al2O3-MgO catalyst. Fuel Processing Technology, 192(October 2018), 57–64. https://doi.org/10.1016/j.fuproc.2019.04.021

Luo, M., Yi, Y., Wang, S., Wang, Z., Du, M., Pan, J., & Wang, Q. (2018). Review of hydrogen production using chemical-looping technology. Renewable and Sustainable Energy Reviews, 81(July 2017), 3186–3214. https://doi.org/10.1016/j.rser.2017.07.007

Majewski, A. J., & Wood, J. (2014). Tri-reforming of methane over Ni@SiO2 catalyst. International Journal of Hydrogen Energy, 39(24), 12578–12585. https://doi.org/10.1016/j.ijhydene.2014.06.071

Martinez-Burgos, W. J., de Souza Candeo, E., Pedroni Medeiros, A. B., Cesar de Carvalho, J., Oliveira de Andrade Tanobe, V., Soccol, C. R., & Sydney, E. B. (2021). Hydrogen: Current advances and patented technologies of its renewable production. Journal of Cleaner Production, 286. https://doi.org/10.1016/j.jclepro.2020.124970

Matamba, T., Iglauer, S., & Keshavarz, A. (2022). A progress insight of the formation of hydrogen rich syngas from coal gasification. Journal of the Energy Institute, 105(June), 81–102. https://doi.org/10.1016/j.joei.2022.08.001

Megia, P. J., Vizcaino, A. J., Calles, J. A., & Carrero, A. (2021). Hydrogen Production Technologies: From Fossil Fuels toward Renewable Sources. A Mini Review. Energy and Fuels, 35(20), 16403–16415. https://doi.org/10.1021/acs.energyfuels.1c02501

Midilli, A., Kucuk, H., Topal, M. E., Akbulut, U., & Dincer, I. (2021). A comprehensive review on hydrogen production from coal gasification: Challenges and Opportunities. International Journal of Hydrogen Energy, 46(50), 25385–25412. https://doi.org/10.1016/j.ijhydene.2021.05.088

Minutillo, M., & Perna, A. (2010). A novel approach for treatment of CO2 from fossil fired power plants. Part B: The energy suitability of integrated tri-reforming power plants (ITRPPs) for methanol production. *International Journal of Hydrogen Energy*, *35*(13), 7012–7020. https://doi.org/10.1016/j.ijhydene.2010.04.091

Mishra, P., Krishnan, S., Rana, S., Singh, L., Sakinah, M., & Ab Wahid, Z. (2019). Outlook of fermentative hydrogen production techniques: An overview of dark, photo and integrated dark-photo fermentative approach to biomass. Energy Strategy Reviews, 24(July 2017), 27–37. https://doi.org/10.1016/j.esr.2019.01.001

Nikolaidis, P., & Poullikkas, A. (2017). A comparative overview of hydrogen production processes. Renewable and Sustainable Energy Reviews, 67, 597–611. https://doi.org/10.1016/j.rser.2016.09.044

Nnabuife, S. G., Ugbeh-Johnson, J., Okeke, N. E., & Ogbonnaya, C. (2022). Present and Projected Developments in Hydrogen Production: A Technological Review∗. Carbon Capture Science & Technology, 3(January), 100042. https://doi.org/10.1016/j.ccst.2022.100042

Norouzi, N. (2022). Hydrogen production in the light of sustainability: A comparative study on the hydrogen production technologies using the sustainability index assessment method. Nuclear Engineering and Technology, 54(4), 1288–1294. https://doi.org/10.1016/j.net.2021.09.035

Olaniyi, O., Incer-Valverde, J., Tsatsaronis, G., & Morosuk, T. (2023). Exergetic and Economic Evaluation of Natural Gas/Hydrogen Blends for Power Generation. Journal of Energy Resources Technology, Transactions of the ASME, 145(6), 1–9. https://doi.org/10.1115/1.4056448

Ong, H. C., Chen, W. H., Farooq, A., Gan, Y. Y., Lee, K. T., & Ashokkumar, V. (2019). Catalytic thermochemical conversion of biomass for biofuel production: A comprehensive review. Renewable and Sustainable Energy Reviews, 113(July), 109266. https://doi.org/10.1016/j.rser.2019.109266

Ozcalici, M. (2022). Asset Allocation With Multi-Criteria Decision Making Techniques. Decision Making: Applications in Management and Engineering, 5(2), 78–119. https://doi.org/10.31181/dmame0305102022o

Parkinson, B., Balcombe, P., Speirs, J. F., Hawkes, A. D., & Hellgardt, K. (2019). Levelized cost of CO2 mitigation from hydrogen production routes. Energy and Environmental Science, 12(1), 19–40. https://doi.org/10.1039/c8ee02079e

Pilavachi, P. A., Chatzipanagi, A. I., & Spyropoulou, A. I. (2009). Evaluation of hydrogen production methods using the Analytic Hierarchy Process. International Journal of Hydrogen Energy, 34(13), 5294–5303. https://doi.org/10.1016/j.ijhydene.2009.04.026

Pond, K., & Bond, T. (2022). Water and environmental health. In Clay's Handbook of Environmental Health (Vol. 4, Issue November). https://doi.org/10.1201/9781003035640-15

Quarton, C. J., & Samsatli, S. (2020). The value of hydrogen and carbon capture, storage and utilisation in decarbonising energy: Insights from integrated value chain optimisation. Applied Energy, 257(June 2019), 113936. https://doi.org/10.1016/j.apenergy.2019.113936

Qureshi, F., Yusuf, M., Arham Khan, M., Ibrahim, H., Ekeoma, B. C., Kamyab, H., Rahman, M. M., Nadda, A. K., & Chelliapan, S. (2023). A State-of-The-Art Review on the Latest trends in Hydrogen production, storage, and transportation techniques. Fuel, 340(December 2022), 127574. https://doi.org/10.1016/j.fuel.2023.127574

Ramazankhani, M. E., Mostafaeipour, A., Hosseininasab, H., & Fakhrzad, M. B. (2016). Feasibility of geothermal power assisted hydrogen production in Iran. International Journal of Hydrogen Energy, 41(41), 18351–18369. https://doi.org/10.1016/j.ijhydene.2016.08.150

Rasmussen, A., Sabic, H., Saha, S., & Nielsen, I. E. (2023). Supplier selection for aerospace & defense industry through MCDM methods. 12(December 2022).

Ratshomo, K. (2021). The South African energy sector report 2021. In Treatise on Geophysics: Second Edition (Vol. 0).

Rebouillat, S., Lyons, M. E. G., Brandon, M. P., & Doyle, R. L. (2011). Paving the way to the integration of smart Nanostructures: Part II: Nanostructured microdispersed hydrated metal oxides for electrochemical energy conversion and storage applications. International Journal of Electrochemical Science, 6(11), 5830–5917.

Ren, J., Manzardo, A., Toniolo, S., & Scipioni, A. (2013a). Sustainability of hydrogen supply chain. Part I: Identification of critical criteria and cause-effect analysis for enhancing the sustainability using DEMATEL. International Journal of Hydrogen Energy, 38(33), 14159–14171. https://doi.org/10.1016/j.ijhydene.2013.08.126

Ren, J., Manzardo, A., Toniolo, S., & Scipioni, A. (2013b). Sustainability of hydrogen supply chain. Part II: Prioritizing and classifying the sustainability of hydrogen supply chains based on the combination of extension theory and AHP. International Journal of Hydrogen Energy, 38(32), 13845–13855. https://doi.org/10.1016/j.ijhydene.2013.08.078

Ren, J., Xu, D., Cao, H., Wei, S., Dong, L., & Goodsite, M. E. (2016). Sustainability decision support framework for industrial system prioritization. AIChE Journal, 62(1), 108–130. https://doi.org/10.1002/aic.15039

Ren, X., Li, W., Ding, S., & Dong, L. (2020). Sustainability assessment and decision making of hydrogen production technologies: A novel two-stage multi-criteria decision making method. International Journal of Hydrogen Energy, 45(59), 34371–34384. https://doi.org/10.1016/j.ijhydene.2019.12.134

Riera, J. A., Lima, R. M., & Knio, O. M. (2023). A review of hydrogen production and supply chain modeling and optimization. International Journal of Hydrogen Energy, 48(37), 13731–13755. https://doi.org/10.1016/j.ijhydene.2022.12.242

Sánchez-Bastardo, N., Schlögl, R., & Ruland, H. (2020). Methane Pyrolysis for CO2-Free H2 Production: A Green Process to Overcome Renewable Energies Unsteadiness. Chemie-Ingenieur-Technik, 92(10), 1596–1609. https://doi.org/10.1002/cite.202000029

Seker, S., & Aydin, N. (2022). Assessment of hydrogen production methods via integrated MCDM approach under uncertainty. International Journal of Hydrogen Energy, 47(5), 3171–3184. https://doi.org/10.1016/j.ijhydene.2021.07.232

Shimura, K., Kato, S., Yoshida, T., Itoh, H., Hattori, T., & Yoshida, H. (2010). Photocatalytic steam reforming of methane over sodium tantalate. Journal of Physical Chemistry C, 114(8), 3493–3503. https://doi.org/10.1021/jp902761x

Siksnelyte-Butkiene, I., Zavadskas, E. K., & Streimikiene, D. (2020). Multi-criteria decision-making (MCDM) for the assessment of renewable energy technologies in a household: A review. Energies, 13(5). https://doi.org/10.3390/en13051164

Song, C., & Pan, W. (2004). Tri-reforming of methane: A novel concept for catalytic production of industrially useful synthesis gas with desired H2/CO ratios. Catalysis Today, 98(4), 463–484. https://doi.org/10.1016/j.cattod.2004.09.054

Taherian, Z., Khataee, A., Han, N., & Orooji, Y. (2022). Hydrogen production through methane reforming processes using promoted-Ni/mesoporous silica: A review. Journal of Industrial and Engineering Chemistry, 107(xxxx), 20–30. https://doi.org/10.1016/j.jiec.2021.12.006

Tao, X., Bai, M., Li, X., Long, H., Shang, S., Yin, Y., & Dai, X. (2011). CH4-CO2 reforming by plasma - Challenges and opportunities. Progress in Energy and Combustion Science, 37(2), 113–124. https://doi.org/10.1016/j.pecs.2010.05.001

Tetteh, D. A., & Salehi, S. (2023). The Blue Hydrogen Economy: A Promising Option for the Nearto- Mid-Term Energy Transition. Journal of Energy Resources Technology, Transactions of the ASME, 145(4), 1–16. https://doi.org/10.1115/1.4055205

U.S Energy Information Administration. (2021). Country Analysis Executive Summary: South Africa. Independent Statistic & Analysis, 2 August, 1–15. https://www.eia.gov/international/overview/country/ZAF

Voitic, G., Pichler, B., Basile, A., Iulianelli, A., Malli, K., Bock, S., & Hacker, V. (2018). Hydrogen production. In Fuel Cells and Hydrogen: From Fundamentals to Applied Research. Elsevier Inc. https://doi.org/10.1016/B978-0-12-811459-9.00010-4

Wang, M., Wang, G., Sun, Z., Zhang, Y., & Xu, D. (2019). Review of renewable energy-based hydrogen production processes for sustainable energy innovation. Global Energy Interconnection, 2(5), 436–443. https://doi.org/10.1016/j.gloei.2019.11.019

York, A. P. E., Xiao, T., & Green, M. L. H. (2003). Brief overview of the partial oxidation of methane to synthesis gas. Topics in Catalysis, 22(3–4), 345–358. https://doi.org/10.1023/A:1023552709642

Younas, M., Shafique, S., Hafeez, A., Javed, F., & Rehman, F. (2022). An Overview of Hydrogen Production: Current Status, Potential, and Challenges. Fuel, 316(February), 123317. https://doi.org/10.1016/j.fuel.2022.123317

Zavadskas, E. K., Antucheviciene, J., & Kar, S. (2019). Multi-objective and multi-attribute optimization for sustainable development decision aiding. Sustainability (Switzerland), 11(11), 1–6. https://doi.org/10.3390/su11113069

Zhang, C., Kang, X., Liang, N., & Abdullah, A. (2017). Improvement of Biohydrogen Production from Dark Fermentation by Cocultures and Activated Carbon Immobilization. Energy and Fuels, 31(11), 12217–12222. https://doi.org/10.1021/acs.energyfuels.7b02035

Zhang, H., Gao, Z., Ao, W., Li, J., Liu, G., Fu, J., Ran, C., Mao, X., Kang, Q., Liu, Y., & Dai, J. (2017). Microwave-assisted pyrolysis of textile dyeing sludge using different additives. Journal of Analytical and Applied Pyrolysis, 127(February), 140–149. https://doi.org/10.1016/j.jaap.2017.08.014

Zhang, H., Sun, Z., & Hu, Y. H. (2021). Steam reforming of methane: Current states of catalyst design and process upgrading. Renewable and Sustainable Energy Reviews, 149(June), 111330. https://doi.org/10.1016/j.rser.2021.111330

CHAPTER 3

FRAMEWORK DEVELOPMENT

3.1. Introduction

The proposed framework developed and explained in this section comprises two main components, i.e., the superstructure development and the analysis thereof.

3.2. Superstructure development

A superstructure is developed, which comprises possible alternative pathways that lead to hydrogen production and its utilization that can be potentially selected in the final flowsheet. The proposed superstructure comprises 3 modules, i.e., the hydrogen production module, the hydrogen storage module, and the hydrogen utilization module. However, this study focuses mainly on the hydrogen production module utilizing a systematic approach and not a superstructure approach.

For this study on hydrogen production, a systematic approach was chosen over a superstructure approach due to the need for accuracy, focus, and thorough analysis. The adoption of a systematic approach in this study guarantees methodological clarity, enabling researchers to explore the nuances of hydrogen generation, refine procedures, and lay the groundwork for future research stages that may involve possible synergies with storage and utilization modules. The ultimate purpose of this focused analysis is to advance sustainable energy solutions by offering nuanced insights into the potential and problems related to hydrogen production.

The superstructure is shown in Figure 3.1.

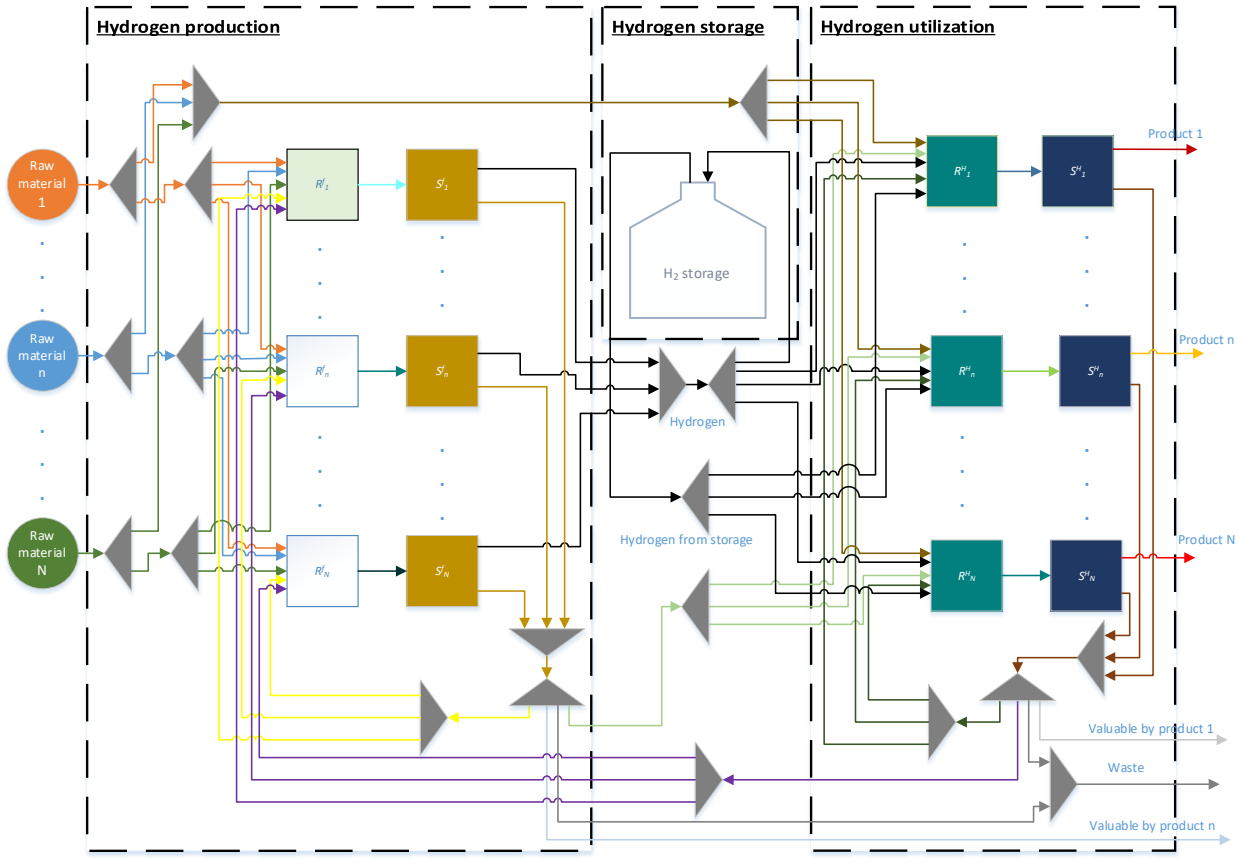

Figure 3.1:Superstructure for hydrogen production and utilization pathways

3.3. Search space reduction

Many pathways can be utilized for hydrogen production, and it would be illogical and difficult to work with all pathways simultaneously. Therefore, a search space reduction model is adopted to reduce the manageable pathways for rigorous optimization. A Pathway Database (PD) is constructed, containing possible alternative pathways. The pathways are selected from literature based on the information that addresses the availability, the economics, and the greenhouse gas emissions of the hydrogen production pathways. This information allows the pathways to be evaluated using the criteria of availability, cost, and environmental sustainability.

The Simultaneous Evaluation of Criteria and Alternatives by Keshavarz-Ghorabaee et al. (2018) is adopted as the search space reduction model. The model is a multi-objective nonlinear mathematical model that has three objective functions: (1)

maximizing the overall performance of alternatives, (2) minimizing the deviation of criterion weights from the reference point based on the within-criterion variation information, and (3) minimizing the deviation of criterion weights from the reference point based on the between criterion variation information. It does not require expert opinions for scoring criteria. Two reference points, the standard deviation and the correlation, are recommended, and the deviation of criteria weights from the reference points is minimized.

Due to the normalization method used in the original SECA model, an evaluation matrix with zero as an element cannot be evaluated. Therefore, this study uses a different normalization method to accommodate different evaluation matrices.

Suppose there is a multi-criteria decision-making problem with *n* alternatives and *m* criteria, and the weight of each criterion $(w_j, j \in \{1,2, \dots m\})$ is unknown. The matrix of this problem can be defined as follows:

$$x = \begin{bmatrix} x_{11} & x_{12} & \cdots & x_{1m} \\ x_{21} & x_{22} & \dots & x_{2m} \\ \vdots & \vdots & \ddots & \vdots \\ x_{n1} & x_{n2} & \cdots & x_{nm} \end{bmatrix} \qquad 3.1$$

Where x_{ij} is the element in the decision matrix of the $i^{th}(i \in \{1,2, \dots n\})$ alternative on the $j^{th}(j \in \{1,2, \dots m\})$ criterion and $x_{ij} \geq 0$.

Based on Equation 3.1, the normalized decision matrix can be constructed using Equations 3.2 and 3.3. The elements of the decision-making matrix are normalized according to the benefit or cost criterion using Equation 3.3.

$$x^N = \begin{bmatrix} x_{11}^N & x_{12}^N & \cdots & x_{1m}^N \\ x_{21}^N & x_{22}^N & \dots & x_{2m}^N \\ \vdots & \vdots & \ddots & \vdots \\ x_{n1}^N & x_{n2}^N & \cdots & x_{nm}^N \end{bmatrix} \qquad 3.2$$

Where,

$$x_{ij}^{N} = \begin{cases} \dfrac{x_{ij} - max\, x_{ij}}{max\, x_{ij} - min\, x_{ij}}, j \in BC \\ \dfrac{max\, x_{ij} - x_{ij}}{max\, x_{ij} - min\, x_{ij}}, j \in CC \end{cases} \quad 3.3$$

and BC and CC are sets of benefit and cost criteria, respectively.

In the SECA model, the weight of the criteria is calculated based on the decision matrix information. Therefore, two fundamental concepts in the statistics field are utilized: standard deviation and correlation indexes. In statistics, the standard deviation index indicates the dispersion of data. In MCDM methods, it is used to calculate the contrast intensity of the interaction of the alternatives in each criterion. In addition, the correlation index indicates the strength of the linear relationship between two variables in statistics. In MCDM methods, it is used to calculate the conflicting character between the criteria (Diakoulaki et al., 1995).

The standard deviation of the elements of each vector (σ_j) evaluated using Equation 3.4 gets the within-criterion variation information. The correlation is used to capture the between criterion variation information from the decision matrix. The correlation is denoted by $r_{jl}(j\ and\ l \in \{1,2,\dots,m\})$. Then Equation 3.5 reflects the degree of conflict between the j^{th} criterion and other criteria.

$$\sigma_j = \sqrt{\frac{1}{m}\sum_{i=1}^{m}\left(X_{ij} - \overline{X_{\iota J}}\right)^2} \quad 3.4$$

$$\pi_j = \sum_{l=1}^{m}\left(1 - r_{jl}\right) \quad 3.5$$

An increase in the variation within the vector of a criterion (σ_j), as well as an increase in the degree of conflict between a criterion and other criteria (π_j), intensifies the objective of that criterion. Accordingly, we define the normalized values of (σ_j) and

(π_j) as the reference points of the weights of criteria. These values are calculated as follows:

$$\sigma_j^N = \frac{\sigma_j}{\sum_{i=1}^{m} \sigma_l} \quad 3.6$$

$$\pi_j^N = \frac{\pi_j}{\sum_{i=1}^{m} \pi_l} \quad 3.7$$

Based on the above description, a multi-objective nonlinear programming model, including three objective functions and two constraints, is formulated as follows:

$$max\, S_i = \sum_{j=1}^{m} w_j\, x_{ij}^N \qquad \forall_i \in \{1,2,\dots,n\} \quad 3.8$$

$$min\, \lambda_b = \sum_{j=1}^{m} \left(w_j - \sigma_j^N\right)^2 \quad 3.9$$

$$min\, \lambda_c = \sum_{j=1}^{m} \left(w_j - \pi_j^N\right)^2 \quad 3.10$$

$$s.t \quad \sum_{j=1}^{m} w_j = 1 \quad 3.11$$

$$\varepsilon \le w_j \le 1 \qquad \forall_j \in \{1,2,\dots,m\} \quad 3.12$$

In the preceding model, the weighted sum method is used to maximize the overall performance of alternatives using Equation 3.8. The sum of squared deviations from the reference points is used to minimize the deviation of criteria weights from the reference points of each criterion. The deviations within and between criteria are

calculated using Equations 3.9 and 3.10. Equation 3.11 guarantees that the sum of the weights equals 1, and Equation 3.12 guarantees that the criteria weights are in the interval [ε,1]. The parameter ε is a small positive value that necessitates the lower bound of the criteria weights and is considered equal to 10^{-3}.

To optimize Equations 3.8 – 3.12, techniques of multi-objective optimization are utilized to transform the model to Equations 3.13-3.19 as follows:

$$max\ Z = \lambda_a - \beta(\lambda_b + \lambda_c) \tag{3.13}$$

$$s.t\ \ \lambda_a \leq S_i \qquad \forall_i \in \{1,2,\dots,n\} \tag{3.14}$$

$$S_i = \sum_{i=1}^{m} x_{ij}^N w_j \qquad \forall_i \in \{1,2,\dots,n\} \tag{3.15}$$

$$\lambda_b = \sum_{j=1}^{m} \left(w_j - \sigma_j^N\right)^2 \tag{3.16}$$

$$\lambda_c = \sum_{j=1}^{m} \left(w_j - \pi_j^N\right)^2 \tag{3.17}$$

$$s.t \quad \sum_{j=1}^{m} w_j = 1 \tag{3.18}$$

$$\varepsilon \leq w_j \leq 1 \qquad \forall_j \in \{1,2,\dots,m\} \tag{3.19}$$

According to the objective function of Equation 3.13, the minimum overall performance score of alternatives (λ_a) is maximized. The deviations from reference points are deducted from the objective function as they should be minimized. The

coefficient, β, is used to merge the objectives into a single objective and minimize deviation from reference points of criteria. The sets of alternative rankings are created, considering different coefficient values to optimize the results of the SECA model and obtain the maximum performance of alternatives.

The overall performance score of each alternative (S_i) and the objective weight of each criterion (w_j) are determined by solving Equations 3.13-3.19.

3.4. Process flow description and analysis

After reducing the search space, the top three ranked pathways are extracted from the SECA model results, and a process flow is developed to show the possible configurations of the three pathways. The reactor and separation sections of the hydrogen production module are expanded to show the auxiliary units and possible configurations of the top three ranked pathways, which are further analyzed. Possible auxiliary units include compressors, heat exchangers, phase separators, pressure swing adsorbers (PSA), and absorbers.

3.5. Gibbs free energy minimization

For simplicity, Gibbs free energy minimization is used to pre-calculate the equilibrium compositions and equivalent energy balance for the pathways. The following thermodynamic assumptions are considered:

- All components of the system operate at a steady state
- Kinetic and potential energies are negligible
- Carbon formation is negligible at high temperatures
- Pressure drop is negligible
- The processes are isothermal
- The gases are assumed to behave ideally

The Gibbs free energy is at its lowest at equilibrium. If the pressure of the system and temperature are constant, the total Gibbs free energy for a system is given as the sum of the product of the number of moles and the partial molar Gibbs free energy. It can be expanded as in Equation 3.20:

$$G_{total} = \sum_{i=1}^{N} n_i \, \overline{G}_i = \sum_{i=1}^{N} n_i \, \mu_i = \sum_{i=1}^{N} n_i \left(G_i^0 + RT \, In \, (y_i P) \right) \qquad 3.20$$

The equation calculates the total Gibbs free energy to be minimized (G_{total}) as a product sum of the number of moles of species i (n_i) and the partial molar Gibbs free energy on species i, ($\overline{G}_i$) or the chemical potential (μ_i). The total Gibbs free energy is also calculated as a product sum of the number of moles and the sum of the standard Gibbs free energy (G_i^o) to the product of the universal gas constant (R), the temperature in Kelvin (T), and the natural log of the product of the mole fraction (y_i) and the pressure of the system P. The mole fractions and total moles are calculated in Equations 3.21 and 3.22, respectively.

$$y_i = \frac{n_i}{n_{total,gas\ product}} \qquad 3.21$$

and

$$n_{total,gas\ product} = \sum_{i=gas\ products} n_i \qquad 3.22$$

To find the set of n_i that minimizes the value of G_{total} , it is vital that the values of n_i fulfil the elemental mass balances as indicated by Equation 3.23:

$$\sum_{i=1}^{N} a_{ji} \, n_i = b_j \qquad for\ 1 \le j \le M \qquad 3.23$$

Equation 3.23 gives the elemental balance value b_j by multiplying the number of gram-atoms of element j (a_{ij}) with the number of moles of element i for M number of elements present in the reacting mixture is, say, C, H, O.

The variables that are considered in the Gibbs free energy minimization model with their associated bounds are as follows:

- Pressure, bounded between 10-25 bar
- Temperature bounded between 500-1500 K
- The feed ratio of methane to steam between 1:1-1:6
- The feed ratio of methane to oxygen between 4:1-1:1

The number of moles at equilibrium is monitored, and the optimum results at each feed ratio are extracted. The SECA model is then employed to get the best reactor conditions. Economic costs, environmental sustainability, and availability are the selection criteria. The operating temperature is selected to represent the economics because a process's energy requirements are the most intensive part. The higher the temperature, the higher the energy required for the process and, thus, the higher the costs. Carbon dioxide emissions represent the emissions as this is the main constituent of greenhouse gases. The amount of hydrogen produced is considered to represent availability because if a process can produce high amounts of hydrogen, it increases the availability of hydrogen.

3.6. Mathematical modeling of the hydrogen production process flow

The following assumptions were made during the development of the model

- The plant operates for 8,000 hours per year
- The lifetime of the plant is 15 years
- The interest rate is 10 %
- All heat exchangers are isobaric
- The processes are isobaric and operate at a steady state

- The reactors are isothermal
- The recovery of the absorber is set to 96 %
- The specific heat is a function of temperature
- The phase separator to remove water accomplishes perfect separation
- The pressure swing adsorption (PSA) comprises 90 % of the hydrogen in the inlet stream with a 99 % purity
- The feed is assumed to enter the process at standard conditions

3.6.1. Mass and energy balances

Compression constraints

The feed is compressed using stagewise compression from 1 bar to the process pressure. Stagewise compression abides by the allowable compression ratio of less than 3. Since the minimum process pressure allocated for the pathways is 10 bar, a single compressor going from 1-10 bar requires much energy and can be impractical. Thus, it gets worse when the pressure increases. The power for the compressors is calculated using Equation 3.24. Equation 3.25 is a constraint that calculates the temperature at the compressor outlet (P_i^{out}) by adding pressure at the inlet (P_i) to the change in the inlet pressure (ΔP_i). Equation 3.26 is a constraint that ensures that the change in pressure does not exceed the maximum pressure (P_{max}), which is set to the process pressure. Equation 3.27 ensures that the compression limit in stagewise compression is not exceeded.

$$Power_i^{comp} = \left(\frac{\gamma}{\gamma - 1}\right)\eta^{-1}R_g T_{feed}\sum_{i=1}^{n} F_{ij}^{comp}\left[\left(\frac{P_i^{out}}{P_i}\right)^{\left(\frac{\gamma}{\gamma-1}\right)} - 1\right] \quad 3.24$$

$$P_i^{out} = P_i + \Delta P_i \quad 3.25$$

$$0 \leq \Delta P_i \leq P_{max} \quad 3.26$$

$$P_i^{out} \leq 3P_i \qquad 3.27$$

The heat capacity ratio (Υ) is assumed to be constant at 1.5, and the compressor efficiency (η) is fixed at 0.8. Compression of a gas adiabatically increases its internal energy. Since temperature is a measure of internal energy, the temperature increases. The outlet temperature of the compressed gas is then calculated using Equation 3.28 by multiplying the inlet temperature of the compressor ($T_{feed,n}$) with the ratio of the inlet and outlet pressure.

$$T_n^{out} = T_{feed,n}\left(\frac{P_{i,n}^{out}}{P_{i,n}}\right)^{\left(\frac{\gamma-1}{\gamma}\right)} \qquad 3.28$$

Heat exchangers are introduced to cool the streams to maintain the outlet temperature limit of the compressors in stagewise compression of not more than 400 K. The heat exchangers cool the gas to the feed temperature of 298 K. The cooling required for each heat exchanger ($\hat{Q}_n^{hx}$) is calculated using Equation 3.29, which is given by the integral of the product of the moles in the steam (n) with the specific heat capacity of the component (C_p) from the initial temperature (T_o) to the final temperature (T_n).

$$\hat{Q}_n^{hx} = \int_{To}^{Tn} nC_p dT \qquad 3.29$$

Mixing constraints

Before entering the reactor, the feed is compressed to the same pressure to enable adequate mixing, as mixing cannot happen at different pressures, the temperature of the mixture (T_{mix}) is calculated using Equation 3.30.

$$T_{mix} = \frac{\sum n_j C_{p,j} T_j^{out}}{\sum n_j C_{p,j}} \qquad 3.30$$

Heat exchanger constraints

Heat exchangers must adjust the temperature for each given unit and task. The energy balance around the heat exchangers is given by Equation 3.31.

$$\frac{dH}{dt} = V_r \frac{dP}{dt} + \sum_{j=1}^{N} F_{ij}^{0} \overline{H_{lJ}^{0}} - \sum_{j=1}^{N} F_{ij}^{out} \overline{H_{lJ}} + \hat{Q}_{hx} \qquad 3.31$$

Since the heat exchangers are assumed to be isobaric, there is no change in pressure $\left(\frac{dP}{dt}\right)$. The heat exchangers are operated at a steady state since no reaction takes place. Therefore, there is no change in enthalpy $\left(\frac{dH}{dt}\right)$. Equation 3.31 then reduces to Equation 3.32, where the cooling or heating required for the reactor ($\hat{Q}_{hx}$) is given by the difference between the enthalpy flow of the inlet ($\overline{H}_{ij}^{0}$) and outlet ($\overline{H}_{ij}$).

$$\hat{Q}_{hx=} \sum_{j=1}^{N} F_{ij}^{out} \overline{H_{lJ}} - \sum_{j=1}^{N} F_{ij}^{0} \overline{H_{lJ}^{0}} \qquad 3.32$$

The amount of heat required for the heat exchanger can also be written as the sum of the product of the moles in the stream (n) and the specific heat capacity of the components (C_p) according to Equation 3.33.

$$\hat{Q}_{hx} = \sum_{i=1}^{N} nC_p \, dT \qquad 3.33$$

Reactor constraints

Since the conversions are pre-determined using the Gibbs minimization model, the reactor effluent is computed using the following relations:

$$F_{ij}^{out} = X_{ij} F_{methane}^{0} \qquad 3.34$$

$$X_{ij} = \frac{kmol\ of\ component\ j\ exiting\ process\ i}{kmol\ of\ fresh\ limiting\ reagent\ entering\ the\ process} \quad 3.35$$

The reactor effluent is calculated by multiplying the initial feed of methane ($F^0_{methane}$) adding the initial feed (F^0_{ij}) with the ratio of component *j* exiting process *i* and the fresh feed of the limiting reagent (X_i). Equation 3.36 is a constraint that enforces the law of conservation of mass around the reactor. The total mass that flows into the reactor, which is calculated by multiplying the inlet moles with the molar mass (M) for each component, should be equal to the total mass flowing out of the reactor. The total mass flowing out of the reactor is calculated similarly but with the reactor outlet moles.

$$\sum_{j=1}^{N} F_{ij}^{out}\, M = \sum_{j=1}^{N} F_{ij}^{0}\, M \quad 3.36$$

The reactors are assumed to operate isothermally. Depending on whether the reaction is exothermic or endothermic, cooling or heating is required. For an exothermic reaction, heat is removed to maintain a fixed system temperature; that is, energy is produced by the reaction to maintain isothermal conditions. Since reactions occur in the reactors, it is essential to account for the enthalpy of the reaction. The reverse is true for an endothermic reaction. The heating or cooling required by the reactor at specific conditions is equal to the heat of the reaction ($\Delta H_{rxn}(T)$) at those conditions. The following relations (Equations 3.37-3.39) are used to perform the energy balances of the reactors:

$$\Delta H_{rxn}(25℃, 1\ atm) = \sum_{i}^{flowout} \left(n_i^{in} + v_i\xi\right)\Delta\hat{H}_{fi}^{o} - \sum_{i}^{flowin} \left(n_i^{in}\right)\Delta\hat{H}_{fi}^{o} = \xi \sum v_i \Delta\hat{H}_{fi}^{o} = \xi\Delta H_{rxn}^{o} \quad 3.37$$

$$H_i(T_i) - H_i(25℃) = n_i \int_{25\ ℃}^{Ti} C_p dT + n_i \Delta\hat{H}_{i,phase\ change} \quad 3.38$$

$$\Delta H_{rxn}(T) = \sum_{i}^{reactants} n_i\left[\widehat{H}_i(25\ ℃) - \widehat{H}_i(T)\right] + \Delta H_{rxn}(25\ ℃) + \sum_{i}^{products} n_i\left[\widehat{H}_i(T) - \widehat{H}_i(25\ ℃)\right] \quad 3.39$$

Evaluating the energy balances for the reactors considers the standard specific enthalpy of the components at standard conditions ($\widehat{H}_{fi}^{0}, \widehat{H}_i(25\ ℃)$) and the extent of reaction (ξ) as well as any phase change that may take place in the process ($\Delta\widehat{H}_{i,phase\ change}$).

Absorber constraints

The absorber operates with a 96 % CO_2 recovery. The absorber mass balances are calculated as follows:

$$F_{ij}^{abs\ out} = F_{ij}^{abs\ in} \qquad \forall j \backslash \{CO_2\} \quad 3.40$$

$$F_{i,CO_2}^{abs\ out} = F_{i,CO_2}^{abs\ in} - F_{i,CO_2} \quad 3.41$$

$$F_{i,CO_2} = 0.96 F_{i,CO_2}^{abs\ in} \quad 3.42$$

$$0 \leq F_{ij}^{abs\ in} \leq F_{max} \quad 3.43$$

$$0 \leq F_{ij}^{abs\ out} \leq F_{max} \quad 3.44$$

$$0 \leq F_{i,CO_2} \leq F_{max} \quad 3.45$$

The outlet flowrate to the absorber $\left(F_{ij}^{abs.out}\right)$ is equal to the inlet flowrate $\left(F_{ij}^{abs.in}\right)$ for all components except for carbon dioxide, according to Equation 3.40. The absorbed carbon dioxide $\left(F_{i,CO_2}\right)$ is calculated from the difference between the carbon

dioxide at the inlet and the outlet streams. This is to say, according to the assumption made, 96 % of the carbon dioxide at the inlet stream is absorbed. Equations 3.43, 3.44, and 3.45 are constraints that ensure that the flowrates are bounded between zero and the maximum allowable flowrate (F_{max}).

Flash constraints

The flash separator removes water $\left(F_{i,H2O}\right)$ in a simple mass balance, allowing the rest of the components to pass through. The flash separator is essential since water is present in all the alternatives. The flash is assumed to dry the syngas completely. The mass balances around the flash are as in Equations 3.46 and 3.47.

$$F_{ij}^{flash\ out} = F_{ij}^{flash\ in} \qquad \forall j \backslash \{H_2O\} \tag{3.46}$$

$$F_{i,H_2O} = F_{i,H_2O}^{flash\ in} \tag{3.47}$$

Pressure Swing Adsorption constraints

Pressure swing adsorption (PSA) requires a maximum of 30 bar to carry out hydrogen adsorption while it is desorbed at 1 bar. The low hydrogen content PSA effluent is assumed to maintain a pressure of 30 bar at the exit of the PSA. Then, this flow can be recycled to the reactor to continue the superstructure path or purged to avoid build-up. If the conversions are high enough, recycling is not necessary. Thus, the flow is allowed to exit the superstructure. The recovery of the PSA is assumed to be 90 %. The following relations give the balances around the PSA:

$$F_{ij}^{PSA\ out} = F_{ij}^{PSA\ in} \qquad \forall j \backslash \{H_2\} \tag{3.48}$$

$$F_{i,H_2}^{PSA\ out} = F_{i,H_2}^{PSA\ in} - F_{i,H_2} \tag{3.49}$$

$$F_{i,H_2}^{PSA\ out} = 0.1 F_{i,H_2}^{PSA\ in} \tag{3.50}$$

$$Power_i^{PSA} = \left(\frac{\gamma}{\gamma - 1}\right)\eta^{-1}R_g T_{feed}\sum_{i=1}^{n} F_{ij}^{PSA\ in}\left[\left(\frac{P_i^{out}}{P_i}\right)^{\left(\frac{\gamma}{\gamma-1}\right)} - 1\right] \quad 3.51$$

$$0 \leq F_{ij}^{PSA\ in} \leq F_{max} \quad 3.52$$

$$0 \leq F_{ij}^{PSA\ out} \leq F_{max} \quad 3.53$$

$$0 \leq F_{i,H_2} \leq F_{max} \quad 3.54$$

3.6.2. Cost calculations

Cost is one of the criteria for selecting the most suitable hydrogen production pathway. It is essential to calculate the cost of capital, operating costs, and raw materials, which are calculated differently for each unit.

Raw materials

Raw materials are an essential part of a process. Without raw materials, there are no products that are produced. The total cost of raw materials (raw_i) is calculated by summing the product of the cost of each component that is fed to the process (δ_{ij}), the amount of feed required per unit time (F_{ij}^0) and the number of hours of the plant per year (t_h) as in Equation 3.55.

$$raw_i = \sum_j \delta_j F_{ij}^0 t_h \quad 3.55$$

Capital costs

The procedure to cost the equipment unit operations, including the heat exchangers, compressors, and process vessels, was adapted from Turton et al. (2015). All the constants, tables, and graphs can be found in Appendix 8.2.

1. Calculate the C_p^o value based on Equation 3.56

$$log_{10}C_p^o = K_1 + K_2 log_{10}(A) + K_3(log_{10}(A))^2 \quad 3.56$$

Equation 3.56 determines the purchased ambient cost at standard conditions (C_p^o) using the capacity of the unit (*A*) and the purchased cost constants (K_1, K_2, and K_3).

2. Calculate the pressure factor of the unit operation using Equation 3.57. This step does not occur for the compressor, pumps, and turbines.

$$log_{10}F_p = C_1 + C_2 log_{10}(P) + C_3(log_{10}(P))^2 \quad 3.57$$

Equation 3.57 evaluates the pressure factor (F_p) employing the operating pressure of the unit operation (*P*) and the pressure factor constants (C_1, C_2, and C_3).

For process vessels, the pressure factor is calculated using Equation 3.58. The equation evaluates a process vessel's pressure factor using the unit (P) operating pressure and diameter (*D*). However, if the pressure within the process within the process vessel is less than 0.5 barg, the pressure factor is 1.25.

$$F_p = \frac{\frac{(P+1)D}{2(850 - 0.6(P+1))} + 0.00315}{0.0063} \quad 3.58$$

3. The material factor (F_M) depends on the material of construction for the unit operation (Turton et al., 2015); the material factor identification numbers and the associated graph are shown in Appendix 8.2 of this dissertation.
4. The bare module cost is calculated using Equation 3.59. For units that do not need the pressure factor, for example, the compressors, the bare module cost is calculated using Equation 3.60. The bare module cost is used as a cost basis when accounting for inflation.

$$C_{BM} = C_p^o + (B_1 + B_2 F_M F_p) \quad 3.59$$

$$C_{BM} = C_p^o F_{BM} \qquad 3.60$$

Equations 3.59 and 3.60 calculate the bare module costs of the unit operations (C_{BM}) using the purchased cost at ambient conditions (C_p^o), the material factor (F_M), the pressure factor (F_p), the bare module factor (F_{BM}), and bare module cost constants (B_1 and B_2).

5. The procedure for calculating the bare module cost is based on 2001. The base cost date is 2001, and the prices are assumed to be accurate to within ± 25 %. To get the value of the cost to the current year ($Present\ cost$) accounting for inflation, the cost from 2001 ($original\ cost\ at\ time\ t$) is multiplied by the ratio of the Chemical Engineering Plant Cost Index of the current year ($CEPCI_{now}$) to the one for 2001 ($CEPCI_{then}$) as in equation 3.61.

$$Present\ cost = (original\ cost\ at\ time\ t)\left(\frac{CEPCI_{now}}{CEPCI_{then}}\right) \qquad 3.61$$

Sizing the heat exchangers for costing

The bare cost depends on the size of the heat exchanger, and therefore, the area is calculated by dividing the heat transferred per unit of time (Q) with the overall heat transfer coefficient $(U)$and the logarithmic mean temperature difference, the temperature-driving force (ΔT_{lm}) as in Equation 3.62.

$$A = \frac{Q}{U\Delta T_{lm}} \qquad 3.62$$

Assuming counter-current flow in the heat exchanger, the logarithmic mean temperature is calculated from the terminal temperature differences, i.e., the difference between the temperature at the outlet and inlet of the heat exchanger. The cold fluid temperature at the inlet $(t_2)$is subtracted from the hot fluid temperature at the outlet (T_1). Likewise, the cold fluid temperature at the inlet (t_1) is subtracted from the hot fluid temperature at the outlet (T_2) as in Equation 3.63.

$$\Delta T_{lm} = \frac{(T_1 - t_2) - (T_2 - t_1)}{ln\frac{(T_1 - t_2)}{(T_2 - t_1)}} \quad 3.63$$

Operating costs

An estimate of the operating costs is essential to judge the process's viability and enable choices to be made between possible alternative pathways. The operating cost of the absorber is calculated using Equation 3.64 from Medrano-García et al. (2017).

$$Op_{abs} = 1.89 F_{CO_{2i}} t_h \quad 3.64$$

The utility costs are considered for other units, as these comprise significant operating costs. These are calculated by multiplying the utility requirement $(\hat{Q})$ with the cost of the utility (Ut_i) and the number of hours the plant operates in a year, as in Equation 3.65.

$$Op_{ut} = \hat{Q} Ut_i t_h \quad 3.65$$

After all the costs are calculated, the Total Annualized Cost (*TAC*) of the system is calculated using Equation 3.66, and the annualizing factor (AF) is calculated using Equation 3.67, considering the interest rate (IR).

$$TAC = \left(\sum_i Cap_i\right) AF + \sum_i (Op_i + raw_i) \quad 3.66$$

$$AF = \frac{IR(IR+1)^{years}}{(IR+1)^{years} - 1} \quad 3.67$$

The levelized cost of hydrogen (LCOH) is calculated using Equation 3.68. LCOH is a variable that shows how much it costs to produce 1 kg of hydrogen, considering the

estimated costs of the investment required and the operating costs involved in the production.

$$LCOH = \frac{TAC}{mass_{hydrogen\ produced}} \quad 3.68$$

3.6.3. Global Warming Potential

The Global Warming Potential (GWP) is estimated based on the amount of carbon dioxide produced in each alternative. Thus, this means the amount of carbon dioxide at the outlet streams of the process, excluding the absorber outlet, because the absorbed carbon dioxide is not released into the atmosphere. The GWP is calculated as the amount of carbon dioxide produced per mass of hydrogen produced $\left(mass_{hydrogen\ produced}\right)$ as in equation 3.69.

$$GWP = \frac{\sum_i F_{CO_{2,i}}^{out} Mt_h}{mass_{hydrogen\ produced}} \quad 3.69$$

3.6.4. Availability and reliability

The availability and reliability of each pathway are assessed by the amount of hydrogen produced. As hydrogen is an energy carrier, producing more hydrogen from a particular pathway guarantees energy security.

3.7. Heat integration

Pinch Analysis technology is applied to design minimum energy targets and minimize the utility required. This is done using MATLAB utilizing the following steps from Tewari et al. (2015):

1. Input the temperatures of the hot and cold fluid streams at the inlet and outlet.
2. Input the heat transfer rate $\left(\hat{Q}\right)$ or the heat capacity flow rate of the streams $(\dot{m}C_p)$.
3. Evaluate the heat capacity flow rate if the heat transfer rate is given using the relation in equation 3.70.

$$\hat{Q} = \dot{m} C_p \Delta T \qquad 3.70$$

4. Input the minimum temperature approach (ΔT_{min}).
5. The adjusted temperatures $(Adj\ T)$ of the hot streams are calculated using equation 3.71.

$$Adj\ T = stream\ T - \Delta T_{min} \qquad 3.71$$

6. The unique ranking of each temperature is defined in decreasing order.
7. The enthalpy of each temperature interval (ΔH_i) is then calculated by finding the difference between the heat capacity flowrates of the hot and cold streams (C) using equation 3.72 as follows:

$$\Delta H_i = \left(\sum C_{hot} - \sum C_{cold}\right)(T_{i-1} - T_i) \qquad 3.72$$

8. The cumulative enthalpy is then calculated, assuming an initial heat load of 0.
9. Check where the heat is zero, assuring that the remaining enthalpy is positive, and then that interval temperature is the pinch point temperature. The initially given heat is the minimum heating load, and the remaining is the minimum cooling load.
10. If any enthalpy is negative, take the most negative enthalpy as the initial heat and calculate the new cumulative enthalpy of each temperature interval. Repeat step 9.

3.8. Objective function

The best hydrogen production pathway selection requires multi-objective optimization to cater to the chosen criteria: affordability, availability, and environmental sustainability. The objectives are to minimize the total annualized and levelized costs of hydrogen, minimize global warming potential, and maximize the amount of

hydrogen produced. These are conflicting objectives that require to be solved simultaneously. The objectives are as follows:

$$\begin{matrix} min\{TAC, LCOH\} \\ s.t. constraints \end{matrix} \quad 3.73$$

$$\begin{matrix} min\,\{GWP\} \\ s.t. constraints \end{matrix} \quad 3.74$$

$$\begin{matrix} max\{mass_{hydrogen\ produced}\} \\ s.t. constraints \end{matrix} \quad 3.75$$

The SECA model is employed for the optimization, and it is a nonlinear programming model that is solved using GAMS.

3.9. References

Diakoulaki, D., Mavrotas, G., & Papayannakis, L. (1995). Determining objective weights in multiple criteria problems: The critic method. Computers and Operations Research, 22(7), 763–770. https://doi.org/10.1016/0305-0548(94)00059-H

Keshavarz-Ghorabaee, M., Amiri, M., Zavadskas, E. K., Turskis, Z., & Antucheviciene, J. (2018). Simultaneous evaluation of criteria and alternatives (SECA) for multi-criteria decision-making. Informatica (Netherlands), 29(2), 265–280. https://doi.org/10.15388/Informatica.2018.167

Medrano-García, J. D., Ruiz-Femenia, R., & Caballero, J. A. (2017). Multi-objective optimization of combined synthesis gas reforming technologies. Journal of CO2 Utilization, 22(September), 355–373. https://doi.org/10.1016/j.jcou.2017.09.019

Turton, R., Bailie R, C., Whiting W. B., Shaeiwitz J. A., & Debangsu Bhattacharyya. (2015). *Analysis, Synthesis and Design of Chemical Processes.* United States of America: Pearson Education Inc.

Tewari, K., Agrawal, S., & Kumar Arya, R. (2015). Generalized Pinch Analysis Scheme Using MATLAB. Chemical Engineering and Technology, 38(3), 530–536. https://doi.org/10.1002/ceat.201400475

CHAPTER 4

FRAMEWORK APPLICATION

4.1. Introduction

In this chapter, the framework developed in the previous chapter is applied to a pathway database to demonstrate its applicability. The pathway database was carefully chosen to ensure the pathways have enough data to satisfy the criteria. The benefits of using the framework are revealed in the application. Firstly, a pathway database is constructed. Secondly, the search space is reduced to recognize the top 3 pathways, which are then used to develop a process flow description for further analysis. Finally, the final pathway is obtained, and its flowsheet and literature are compared.

4.2. Pathway database

A pathway database was developed from the literature. The data was collected according to affordability, availability, and environmental sustainability criteria. The affordability was characterized by the cost of hydrogen ($/kg), and the data was adapted from (Nikolaidis & Poullikkas, 2017b). Table 4.1 shows the data collected representing the affordability.

Table 4.1: Affordability of hydrogen processes

Process	Hydrogen cost [$/kg]	Study year
SMR with CCS	2.27	2005
SMR without CCS	2.08	2005
CG with CCS	1.63	2005
CG without CCS	1.34	2005
ATR of methane with CCS	1.48	2005
Methane pyrolysis	1.59-170	1992
Biomass pyrolysis	1.25-2.20	2004

Biomass gasification	1.77-2.05	2004
Direct bio photolysis	2.13	2002
Indirect bio photolysis	1.42	2002
Dark fermentation	2.57	2014
Photo fermentation	2.83	2014
Solar PV electrolysis	5.78-23.27	2007
Solar thermal electrolysis	5.10-10.49	2007
Wind electrolysis	5.89-6.03	2005
Nuclear electrolysis	4.15-7.00	2006
Nuclear thermolysis	2.17-2.63	2007
Solar thermolysis	7.98-8.40	2007
Photo-electrolysis	10.36	2014

Environmental sustainability data was collected from different sources in the literature. This criterion was characterized by global warming potential (GWP), which is the amount of carbon dioxide produced by the process per amount of hydrogen produced (kg CO_2 / kg H_2). Table 4.2 shows the data collected for environmental sustainability and the respective sources.

Table 4.2: Global warming potential for hydrogen processes

Process	**GWP (kgCO_2/ kg H_2)**	**Source**
SMR with CCS	3.40	Mehmeti et al. (2018)
SMR without CCS	12.00	Cetinkaya et al. (2012)
CG with CCS	15.50	Acar & Dincer (2014)
CG without CCS	24.20	Mehmeti et al. (2018)
ATR of methane with CCS	3.98	Antonini et al. (2020)
Methane pyrolysis	5.00	Al-Qahtani et al. (2021)
Biomass pyrolysis	2.40	Bhandari et al. (2014)
Biomass gasification	2.67	Mehmeti et al. (2018)
Direct bio photolysis	0.70	Acar & Dincer (2014)
Indirect bio photolysis	67.00	Barole and Greig, 2019
Dark fermentation	16.29	Mehmeti et al. (2018)
Photo fermentation	0.60	Dincer & Acar (2014)
Solar PV electrolysis	2.00	Bhandari et al. (2014)
Solar thermal electrolysis	2.50	Bhandari et al. (2014)
Wind electrolysis	0.97	Bhandari et al. (2014)

Nuclear electrolysis	2.00	Utgikar & Thiesen (2006); Bhandari et al. (2014)
Nuclear thermolysis	0.63	Bhandari et al. (2014)
Solar thermolysis	0.68	Bhandari et al. (2014)
Photo-electrolysis	2.00	Dincer & Acar (2014)

Availability is the third criterion, and it measures the raw materials required in a particular process to obtain hydrogen. The measure was rated regarding how much raw material is available. Raw material availability was chosen because neglecting resource availability may cause a model to select a production process that is not well suited to a region of interest. In this research, a rigorous methodology to calculate the availability rating of critical raw materials was employed. The availability rating was determined using the following formula:

$$Availability\ rating = \frac{Total\ raw\ material\ available}{Total\ raw\ material\ required} \qquad 4.1$$

The study considered the total quantities of raw materials required for a 100-year projection assuming stoichiometric calculations. The availability rating for each raw material was calculated individually, offering a detailed assessment of their respective contributions to the overall availability. Furthermore, an average availability rating was computed to provide a holistic perspective on the raw material supply chain. The results reveal a surplus beyond the required quantities, emphasizing the robustness of the production system and its capability to meet demands efficiently. This comprehensive approach to assessing availability contributes valuable insights to the optimization of hydrogen production processes.

Table 4.3 shows the estimated total available units for the different raw materials used for the selected processes in the context of the resources available in South Africa.

Table 4.3: Total availability units for raw materials

Raw material	Total available units	Reference
Natural gas	390 trillion ft^3	Botha et al., 2019; Chukwuma et al., 2023
Oxygen	45 000 tonnes per day	Air Liquide, n.d.
Water	33 900 million m^3	du Plessis, 2022
Coal	53 billion tons	Snyman & Botha, 2021
Biomass	24 million tons	Mfopa & Pienaar, n.d.

The average raw material availability required for a particular pathway was used as the availability rating for the pathway. *Table 4.4* shows the final availability rating of the pathways.

Table 4.4: Availability rating of the pathways

Process	Availability rating
SMR with CCS	11.65
SMR without CCS	11.65
CG with CCS	2.10
CG without CCS	2.10
ATR of methane with CCS	7.78
Methane pyrolysis	3.02
Biomass pyrolysis	6.26
Biomass gasification	6.26
Direct bio photolysis	6.26
Indirect bio photolysis	6.26
Dark fermentation	6.26
Photo fermentation	3.13
Solar PV electrolysis	3.13
Solar thermal electrolysis	3.13
Wind electrolysis	3.13
Nuclear electrolysis	3.13
Nuclear thermolysis	3.13
Solar thermolysis	3.13
Photo-electrolysis	3.13

4.3. Search space reduction

After constructing the pathway database consisting of 19 pathways, the SECA was applied to reduce the search space to the top three pathways. The model was solved using GAMS modelling software. The costs were first standardized, and then an evaluation matrix was constructed. Table 4.5 shows the evaluation matrix.

Table 4.5: The evaluation matrix of the pathway database

Process	Cost ($/kg)	GWP (kgCO_2/ kg H_2)	Availability rating
SMR with CCS	4.84	3.40	11.65
SMR without CCS	4.43	12.00	11.65
CG with CCS	3.48	15.50	2.10
CG without CCS	2.86	24.20	2.10
ATR of methane with CCS	3.16	3.98	7.78
Methane pyrolysis	3.18	5.00	3.02
Biomass pyrolysis	3.75	2.40	6.26
Biomass gasification	4.14	2.67	6.26
Direct bio photolysis	3.77	0.70	6.26
Indirect bio photolysis	2.51	67.00	6.26
Dark fermentation	4.65	16.29	6.26
Photo fermentation	5.12	0.60	3.13
Solar PV electrolysis	28.23	2.00	3.13
Solar thermal electrolysis	15.15	2.50	3.13
Wind electrolysis	12.71	0.97	3.13
Nuclear electrolysis	11.25	2.00	3.13
Nuclear thermolysis	4.66	0.63	3.13
Solar thermolysis	15.91	0.68	3.13
Photo-electrolysis	18.73	2.00	3.13

During the analytical phase of the model, data standardization is essential. Ensuring a neutral and fair assessment of the 19 routes under consideration was crucial. Affordability and the environmental sustainability measure were identified as cost criteria given that they need to be minimised. Conversely, availability was identified as a benefit criterion given that it needs to be maximised. The normalised evaluation matrix is constructed and shown in Table 4.6.

Table 4.6: The normalised evaluation matrix of the pathway database

Process	Affordability	Environmental sustainability	Availability
SMR with CCS	0.91	0.96	1.00
SMR without CCS	0.93	0.83	1.00
CG with CCS	0.96	0.78	0.00
CG without CCS	0.99	0.64	0.00
ATR of methane with CCS	0.97	0.95	0.59
Methane pyrolysis	0.97	0.93	0.10
Biomass pyrolysis	0.95	0.97	0.44
Biomass gasification	0.94	0.97	0.44
Direct bio photolysis	0.95	1.00	0.44
Indirect bio photolysis	1.00	0.00	0.44
Dark fermentation	0.92	0.76	0.44
Photo fermentation	0.90	1.00	0.11
Solar PV electrolysis	0.00	0.98	0.11
Solar thermal electrolysis	0.51	0.97	0.11
Wind electrolysis	0.60	0.99	0.11
Nuclear electrolysis	0.66	0.98	0.11
Nuclear thermolysis	0.92	1.00	0.11
Solar thermolysis	0.48	1.00	0.11
Photo-electrolysis	0.37	0.98	0.11

4.3.1. Criteria weight analysis

Determining criteria weights is crucial as it gives insight into which criteria should be prioritized when selecting a process. The SECA model was solved using data in Table 4.6 using different values for the β parameter (β = 0.1, 0.2, 0.3, 0.4, 0.5, 1, 2, 3, 4, 5, 6, and 7). By solving the model, 12 sets of criteria weights are evaluated. The criteria weights related to changing β are shown in Table 4.7. The variation of the criteria weights is shown in Figure 4.1. The parameter β was chosen so that changing it results in almost constant weights for the criteria obtained from the model. The model was solved independently for each value of β. In a mathematical context, the constant weight is translated so that the weight of the model's solution for two consecutive β's is less than 0.01. In other words, the difference between all weights is less than 0.01.

Table 4.7: Sets of criteria weights determined by changing β

β	**0.1**	**0.2**	**0.3**	**0.4**	**0.5**	**1**	**2**	**3**	**4**	**5**	**6**	**7**
Affordability weight	0.494	0.404	0.364	0.344	0.332	0.308	0.297	0.298	0.306	0.310	0.314	0.316
Environmental sustainability weight	0.505	0.459	0.438	0.428	0.422	0.409	0.403	0.394	0.381	0.373	0.368	0.365
Availability weight	0.001	0.137	0.198	0.228	0.246	0.282	0.300	0.308	0.313	0.316	0.318	0.320

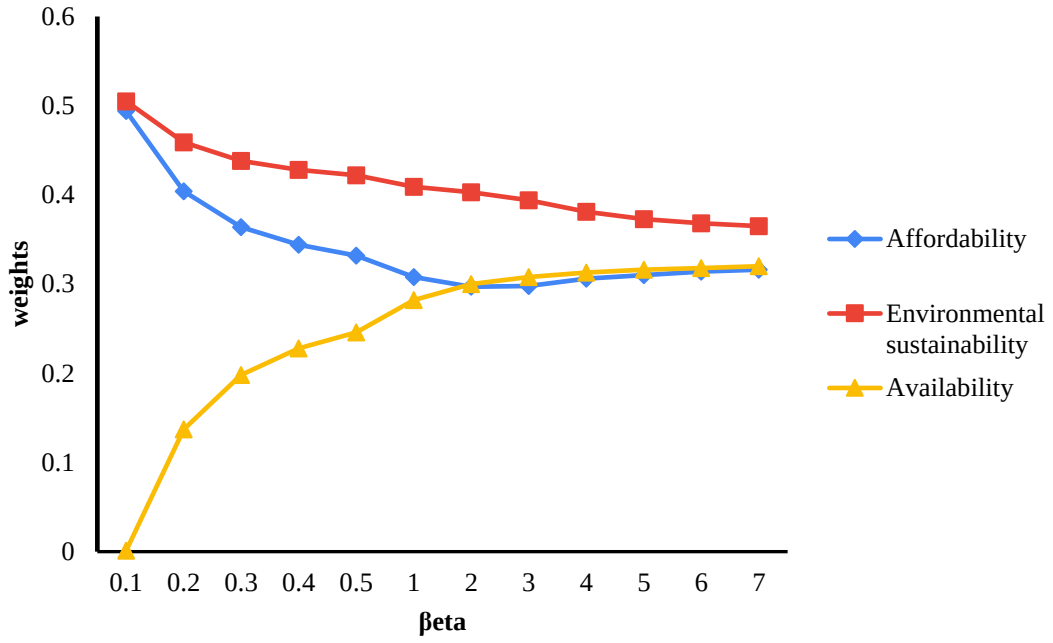

Figure 4.1: The variation of criteria weights related to β

Additionally, the objective function value of the model decreased with an increase of β, as shown in Figure 4.2. The β parameter was also where the criteria weights became more stable, and the objective function was at its maximum.

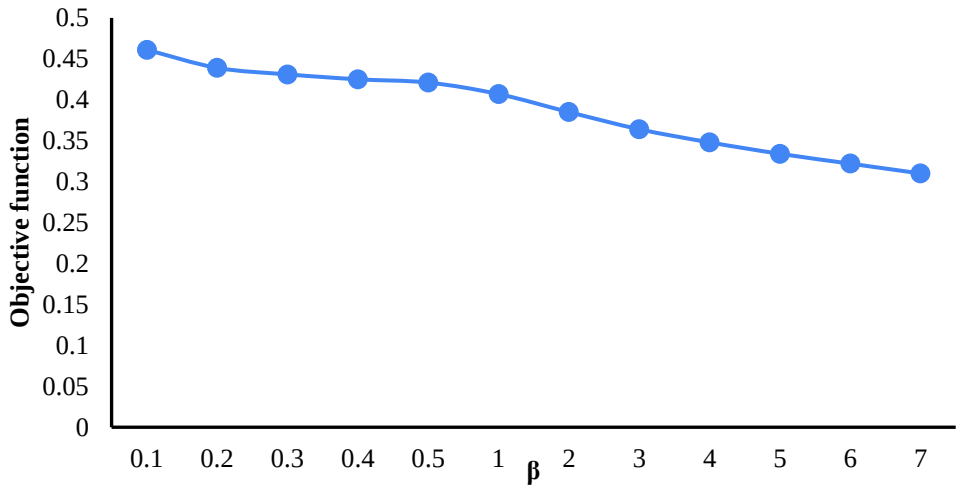

Figure 4.2: Objective function with varying β

The criteria weights became more stable when β was more significant than 3. The difference between two consecutive weights was less than 0.01, where β was 4. Therefore, the criteria weights were determined from a β value of 5. The criteria weights chosen revealed that for the data set, environmental sustainability was a crucial criterion to be considered. It weighed 0.373. The availability criterion, represented by raw material availability, was the second priority, with a weight of 0.316. The least essential criterion was affordability, with a weight of 0.310.

4.3.2. Analysis of the performance of alternatives

The overall performance score of each alternative (S_i) by solving the SECA model based on the data on the normalized data in Table 4.6. The same values for β that were used for criteria weights were used. The overall performance scores obtained are presented in Table 4.8, and the corresponding ranks of the alternatives are shown in Table 4.9. S1 to S19 and P1 to P19 correspond with the pathway's position in the pathway database. For example, S1 and P1 correspond to SMR with CCS. Furthermore, a graphical view of the performance scores is presented in Figure 4.3.

Table 4.8: The performance overall performance scores for different alternatives

β	0.1	0.2	0.3	0.4	0.5	1	2	3	4	5	6	7
S1	0.934	0.944	0.949	0.951	0.952	0.955	0.956	0.956	0.956	0.956	0.956	0.956
S2	0.876	0.891	0.898	0.901	0.903	0.907	0.909	0.910	0.912	0.913	0.913	0.914
S3	0.867	0.745	0.690	0.663	0.647	0.614	0.598	0.593	0.590	0.588	0.587	0.587
S4	0.813	0.694	0.642	0.615	0.600	0.568	0.552	0.548	0.547	0.547	0.547	0.547
S5	0.961	0.911	0.888	0.877	0.871	0.857	0.850	0.848	0.846	0.845	0.844	0.844
S6	0.953	0.835	0.783	0.757	0.741	0.710	0.694	0.688	0.684	0.682	0.680	0.679
S7	0.962	0.891	0.859	0.843	0.834	0.815	0.805	0.801	0.798	0.797	0.795	0.795
S8	0.952	0.883	0.852	0.836	0.827	0.809	0.799	0.795	0.792	0.790	0.789	0.788
S9	0.974	0.902	0.870	0.854	0.844	0.825	0.815	0.811	0.808	0.806	0.805	0.804
S10	0.494	0.464	0.450	0.444	0.439	0.431	0.427	0.432	0.442	0.448	0.452	0.455
S11	0.839	0.781	0.755	0.752	0.734	0.718	0.711	0.708	0.708	0.708	0.707	0.707
S12	0.949	0.837	0.787	0.762	0.747	0.717	0.702	0.695	0.690	0.687	0.684	0.683
S13	0.494	0.464	0.450	0.444	0.439	0.431	0.427	0.419	0.407	0.400	0.395	0.392
S14	0.742	0.666	0.632	0.615	0.605	0.585	0.575	0.568	0.560	0.555	0.552	0.549
S15	0.800	0.717	0.677	0.658	0.647	0.624	0.612	0.605	0.597	0.593	0.590	0.588
S16	0.821	0.731	0.691	0.671	0.659	0.635	0.623	0.616	0.609	0.605	0.602	0.600
S17	0.958	0.844	0.793	0.768	0.753	0.722	0.707	0.701	0.695	0.692	0.690	0.688
S18	0.741	0.667	0.633	0.617	0.607	0.587	0.577	0.570	0.561	0.556	0.552	0.550
S19	0.677	0.613	0.585	0.571	0.562	0.545	0.537	0.529	0.520	0.514	0.511	0.508

Table 4.9:The ranks of alternatives based on different values of β

β	0.1	0.2	0.3	0.4	0.5	1	2	3	4	5	6	7
P1	8	1	1	1	1	1	1	1	1	1	1	1
P2	9	4	2	2	2	2	2	2	2	2	2	2
P3	10	11	12	12	12	13	13	13	13	13	13	13
P4	13	14	14	15	16	16	16	16	16	16	16	16
P5	3	2	3	3	3	3	3	3	3	3	3	3
P6	5	9	9	9	9	10	10	10	10	10	10	10
P7	2	4	5	5	5	5	5	5	5	5	5	5
P8	6	6	6	6	6	6	6	6	6	6	6	6
P9	1	3	4	4	4	4	4	4	4	4	4	4
P10	18	18	18	18	18	18	18	18	18	18	18	18
P11	11	10	10	10	10	8	7	7	7	7	7	7
P12	7	8	8	8	8	9	9	9	9	9	9	9
P13	18	18	18	18	18	18	18	19	19	19	19	19

P14	15	16	16	15	15	15	15	15	15	15	14	15
P15	14	13	13	13	12	12	12	12	12	12	12	12
P16	12	12	11	11	11	11	11	11	11	11	11	11
P17	4	7	7	7	7	7	8	8	8	8	8	8
P18	16	15	15	14	14	14	14	14	14	14	14	14
P19	17	17	17	17	17	17	17	17	17	17	17	17

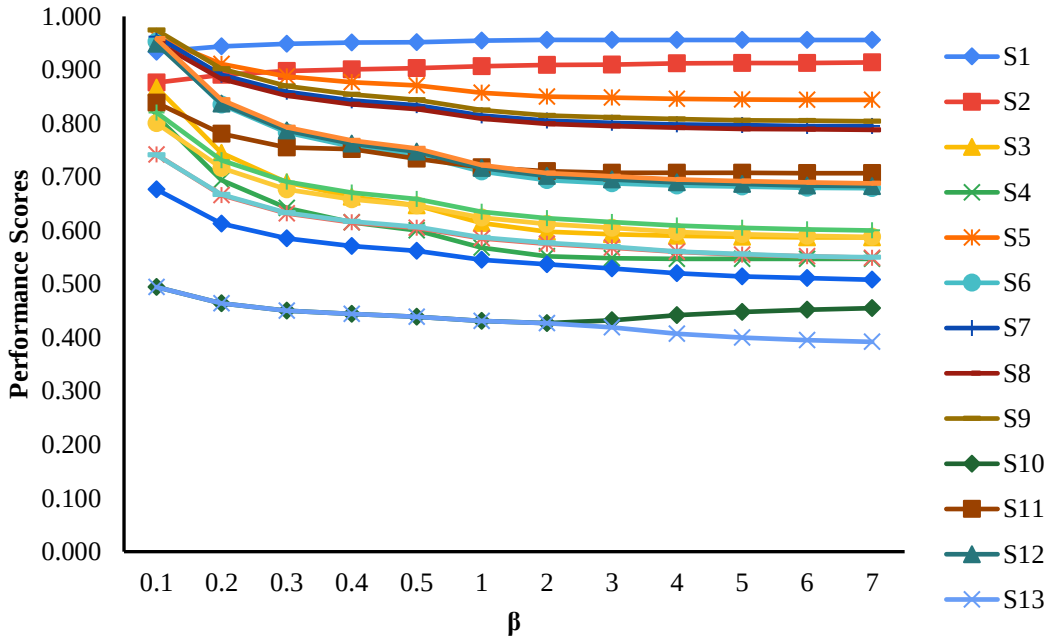

Figure 4.3: Variations in the performance scores related to β

Spearman's correlation coefficient was calculated for various β values against the ranks to analyze the final alternative ranking, as displayed in Table 4.10. It was observed that the alternative ranking remained stable for β values greater than or equal to 3, resulting in a correlation coefficient of 1. Consequently, substantiating the selection of $\beta = 5$ to determine the overall performance and ranking of the alternatives.

Table 4.10: Spearman's rank correlation for ranks of alternatives

β	0.1	0.2	0.3	0.4	0.5	1	2	3	4	5	6	7
0.1	1	0.897	0.863	0.857	0.850	0.828	0.816	0.818	0.818	0.818	0.815	0.818
0.2	0.897	1	0.992	0.989	0.986	0.978	0.972	0.972	0.972	0.972	0.969	0.972
0.3	0.863	0.992	1	0.997	0.994	0.987	0.982	0.981	0.981	0.981	0.978	0.981
0.4	0.857	0.989	0.997	1	0.998	0.992	0.986	0.986	0.986	0.986	0.985	0.986
0.5	0.850	0.986	0.994	0.998	1	0.994	0.988	0.988	0.988	0.988	0.987	0.988
1	0.828	0.978	0.987	0.992	0.994	1	0.998	0.997	0.997	1	1	1
2	0.816	0.972	0.982	0.986	0.988	0.998	1	0.999	0.999	1	1	1
3	0.818	0.972	0.981	0.986	0.988	0.997	0.999	1	1	1	1	1
4	0.818	0.972	0.981	0.986	0.988	0.997	0.999	1	1	1	1	1
5	0.818	0.972	0.981	0.986	0.988	0.997	0.999	1	1	1	1	1
6	0.815	0.969	0.978	0.985	0.987	0.996	0.998	0.999	0.999	1	1	1
7	0.818	0.972	0.981	0.986	0.988	0.997	0.999	1	1	1	1	1

The performance scores revealed that from the pathway database, the top three pathways had performance scores of 0.956, 0.913, and 0.845. These pathways were SMR with CCS, SMR without CCS, and ATR of methane with CCS, respectively. The selected pathways were investigated further.

4.4. Process flow description and analysis results

A process flow description was developed according to the three pathways determined to be the top three. Although these are three pathways, they are generally two with a difference in handling the carbon dioxide produced from the processes as this impacts the overall environmental impact of the process. The process flow description allowed both the pathways, steam reforming and autothermal reforming, to be with or without CCS. Figure 4.4 shows the resulting process flow description. The reactor and

separation sections of the hydrogen production module are expanded to show the auxiliary units. The initial feedstock to the process, which enters at 25 °C, and 1 bar is composed of methane and steam or methane, steam, and oxygen. The feed enters a compression stage and is pressurized to the working pressure of 10 bar. The mixture is preheated before entering the reformer. The reformer effluent is cooled to 250 °C before being sent to the separation stage. The single-pass conversion of the reactor is precalculated using the Gibbs free energy minimization for simplicity.

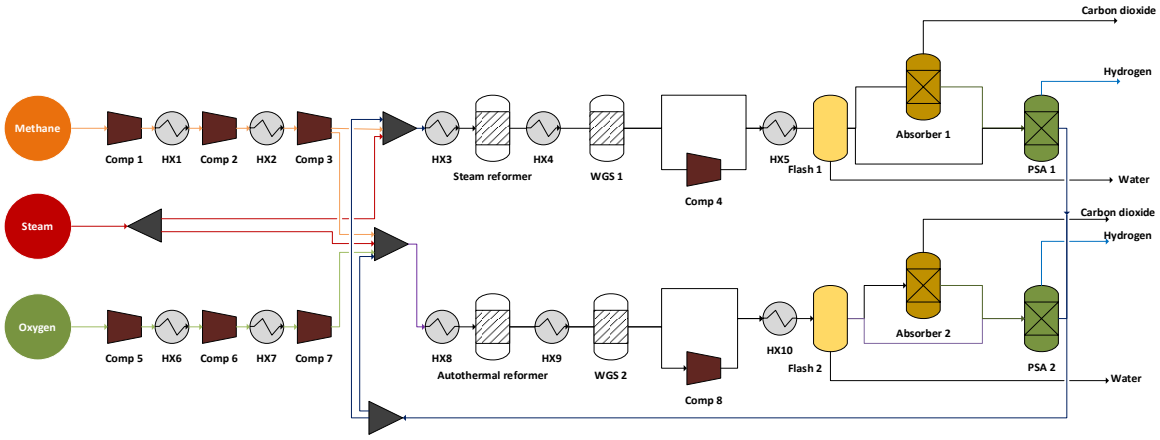

Figure 4.4: The developed process flow description

4.4.1. Thermodynamic trends

MATLAB was used to solve the Gibbs free energy minimization model for the two reforming choices and to plot graphs illustrating the influence of changes to reformer feed ratios and operating conditions on equilibrium compositions. The model calculates equilibrium compositions for specified operating and feed conditions and determines reactor energy balance. Water production in the reactor makes determining the direct conversion of water challenging. As a result, apparent conversion is assessed.

4.4.1.1. Effect of temperature on equilibrium compositions in steam reforming

Figure 4.5 shows the effect of temperature on the equilibrium composition for steam reforming.

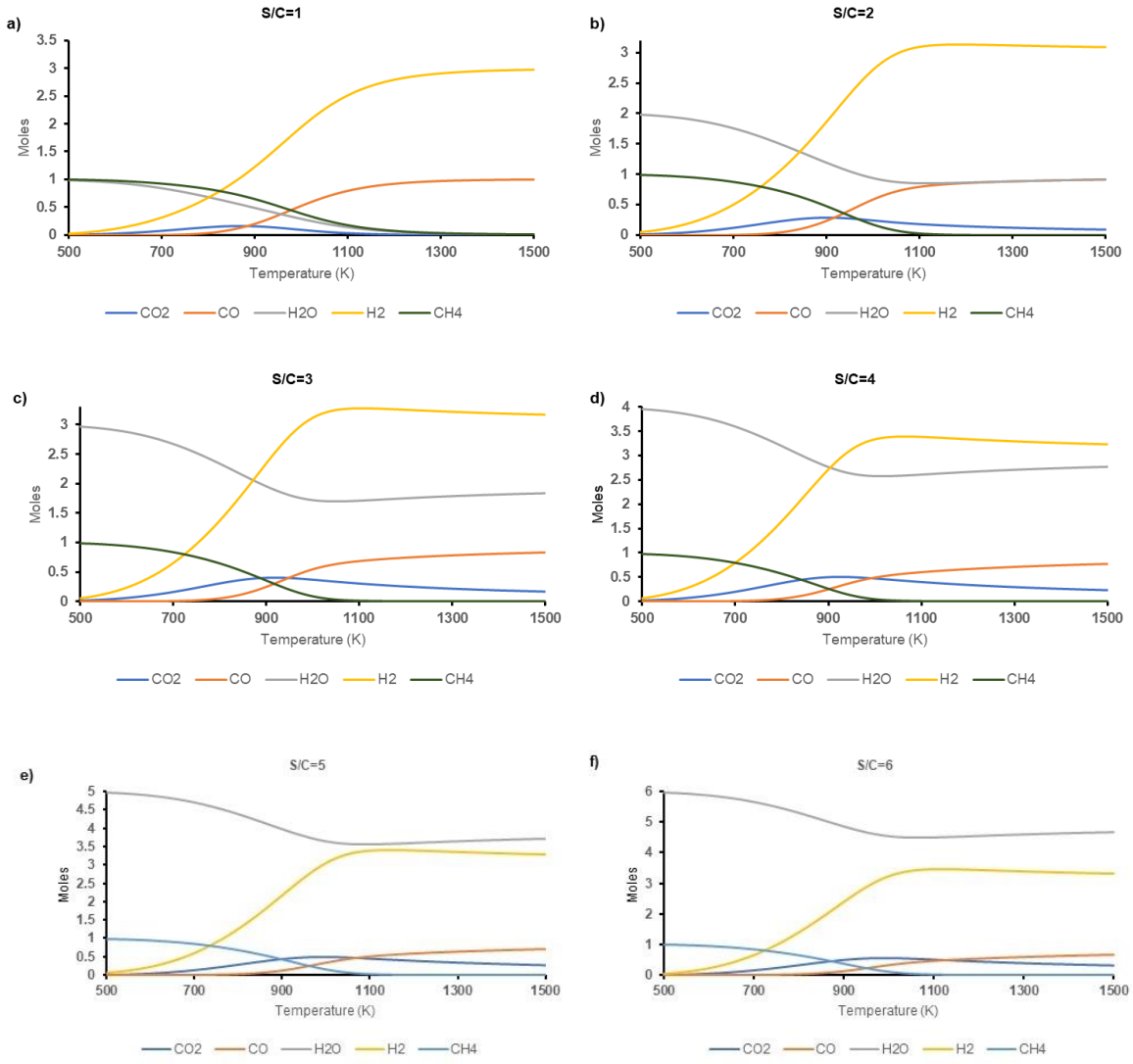

Figure 4.5: Effect of temperature on equilibrium for steam reforming at different steam-to-carbon ratios

The reaction temperature predominantly affects the equilibrium composition, notably H_2 and CO production. Higher temperatures promote increased H_2 and CO production and higher CH_4 conversion while decreasing CO_2 production. according to Le Chatelier's principle, increasing the steam-to-carbon ratio in methane conversion reactions promotes the formation of hydrogen and carbon dioxide by shifting the equilibrium toward the production of these products, thereby enhancing the efficiency

of the conversion process. At higher temperatures, the H_2/CO ratio approaches 3:1, as predicted by literature and stoichiometry.

As the ratio of steam to methane increases, the conversion of CH_4 increases. The increase in the steam being fed to the system increases the amount of hydrogen entering the system, and thus, more hydrogen is generated. However, this also leads to lower steam conversion and CO yield. As the steam flowrate to the system increases, the equilibrium shifts, transforming CO and steam to hydrogen and CO_2 in the water gas shift reaction. Therefore, more CO is converted when more steam is fed, lowering the amount of CO produced. As more steam is fed, more H_2 forms simultaneously with increased CO_2.

As the steam feed rate increases, the energy intake increases due to the endothermic nature of steam reforming. These findings are supported by experimental data from Seo et al. (2002) thermodynamic investigations. There is a trade-off that necessitates an appropriate steam/methane ratio to optimize the value of steam addition. These findings support industrial hydrogen generation and steam reforming at temperatures exceeding 1000 K. Elevated steam-to-methane ratios (3:1) increase hydrogen generation while minimizing solid carbon formation. However, when energy costs and environmental limitations become more rigid, it needs new options for maximizing hydrogen production while adapting to these new limitations.

4.4.1.2. Effect of temperature on equilibrium compositions in autothermal reforming

Figure 4.6 shows the effect of temperature on the equilibrium composition for autothermal reforming.

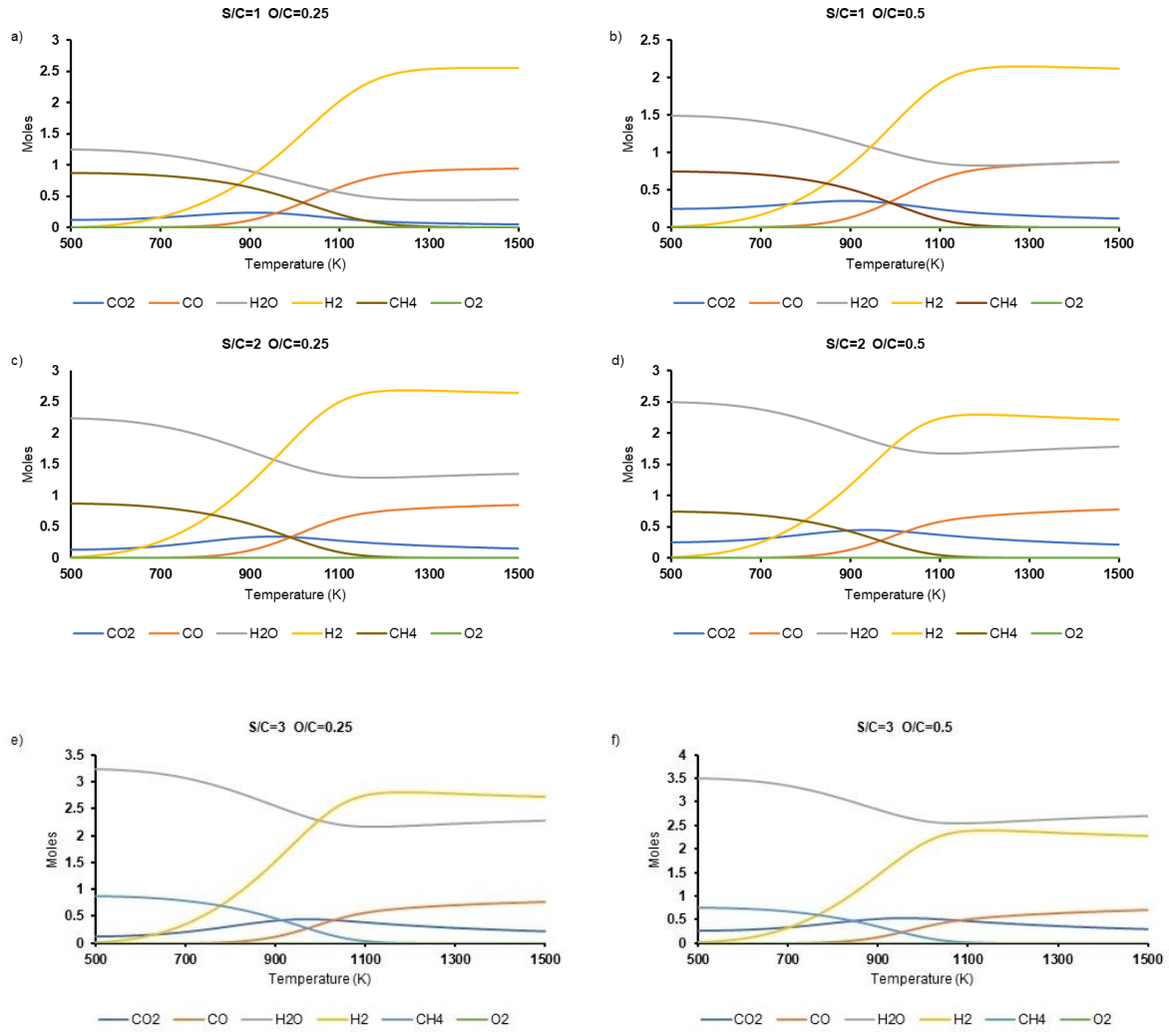

Figure 4.6: Effect of temperature on equilibrium for autothermal reforming at different steam-to-carbon ratios and oxygen-to-carbon ratios

The addition of steam does not affect the conversion of O_2, but adding another oxidizer reduces the apparent conversion of steam. Due to its exothermic nature, the partial oxidation process is preferred over steam reforming in terms of reaction, which illustrates why O_2 conversion is unaffected. The methane conversion decreases at a constant oxygen feed rate, and the temperature rises as the steam-to-carbon ratio rises.

When steam is introduced into the reformer, the steam reforming reaction, a highly endothermic process, begins. As a result, a lower reactor temperature occurs from a more considerable steam-to-carbon ratio, and the conversion is decreased due to the

lower reactor temperature. At a methane-to-oxygen ratio of 4:1, the molar flow rate of H_2 and CO peaks. The H_2 molar flow rate rises as the steam-to-carbon ratio rises, whereas the CO_2 molar flow rate decreases. This reveals that increasing the steam-to-carbon ratio increases the hydrogen-to-carbon dioxide ratio. On the other hand, if the methane-to-oxygen ratio is more than 4:1, the H_2 molar flow rate reduces more steeply than the CO molar flow rate due to H_2 oxidizing more quickly than CO in areas with a high oxygen ratio. These observations provide helpful information for reformer design.

4.4.2. Optimal reactor conditions

The developed MATLAB code allowed to obtain the conditions at which the most hydrogen was produced at each different feed ratio. There was observed to be higher conversion at lower pressures; thus, the pressure was maintained at the lower bound of 10 bar for both processes. Table 4.11 shows the optimum results for the steam reforming process. A key observation is that as the feed ratio increases, the temperature required for the process decreases. Also, as the feed ratio increases, the amount of hydrogen produced increases; however, it decreases because the temperature is much lower. As the feed ratio increases, it is also noted that the carbon dioxide produced increases.

Table 4.11: Optimum results for steam reforming at different feed ratios at 10 bar

Feed ratio (Methane: Steam)	Optimum temperature (K)	Mole H_2/ mole CH_4 fed	Mole CO_2/ mole CH_4 fed
1:1	1500	2.93	0.0026
1:2	1340	3.10	0.12
1:3	1230	3.22	0.24
1:4	1180	3.32	0.35
1:5	1140	3.58	0.44
1:6	1120	3.47	0.50

The optimum results for the autothermal reformer are shown in Table 4.12. As more oxygen is fed, less hydrogen is produced, and the carbon dioxide increases. The temperature for the system decreases as the amount of oxygen fed increases.

Table 4.12: Optimum results for autothermal reforming at different feed ratios at 10 bar

Feed ratio (Methane: Steam: Oxygen)	Optimum temperature (K)	Mole H_2/ mole CH_4 fed	Mole CO_2/ mole CH_4 fed
1:1:0.25	1420	2.56	0.063
1:1:0.50	1280	2.15	0.167
1:1:0.75	1190	1.78	0.303
1:1:1	1130	1.42	0.452
1:2:0.25	1250	2.69	0.210
1:2:0.50	1190	2.29	0.320
1:2:0.75	1130	1.92	0.448
1:2:1	1090	1.55	0.574
1:3:0.25	1180	2.81	0.337
1:3:0.50	1140	2.41	0.439
1:3:0.75	1100	2.20	0.548
1:3:1	1060	1.63	0.660
1:4:0.25	1140	2.90	0.437
1:4:0.50	1110	2.50	0.528
1:4:0.75	1070	2.10	0.628
1:4:1	1030	1.70	0.726
1:5:0.25	1110	2.98	0.517
1:5:0.50	1080	2.57	0.602
1:5:0.75	1050	2.16	0.686
1:5:1	1020	1.75	0.767
1:6:0.25	1090	3.05	0.580
1:6:0.50	1060	2.63	0.657
1:6:0.75	1030	2.21	0.733
1:6:1	1000	1.78	0.804

The results for both processes were used as input data into the SECA model to obtain the overall optimum conditions. Economic costs, environmental sustainability, and availability were considered the selection criteria. The operating temperature was selected to represent the economics because the energy requirements of a process are the most intensive. The higher the temperature, the higher the energy required for the process and the higher the costs. Carbon dioxide emissions represent the environmental impact as this is the main constituent of greenhouse gases. The amount of hydrogen produced was considered to represent availability because if a process can produce high amounts of hydrogen, it increases the availability of hydrogen. Table 4.13 illustrates the optimal conditions that were obtained for the reforming processes.

Table 4.13: Overall optimum results for the reforming options

Reforming technology	**$H_2O:CH_4$ ratio**	**$O_2:CH_4$ ratio**	**Mole H_2/mole CH_4**	**T(K)**	**Mole CO_2/mol CH_4**
Steam reforming	3:1		3.22	1230	0.24
Autothermal reforming	6:1	1:4	3.05	1090	0.58

4.4.3. Pathway simulations

Four process flowsheet configurations differing in operating conditions and unit operations were extracted from the process flow description in Figure 4.4 and simulated in MATLAB for each process. The different configurations are possible pathways that can be used to produce hydrogen. Figure 4.7-Figure *4.14* show the different possible flowsheet configurations. The calculated results using the framework developed in the previous chapter are summarised in Table 4.14.

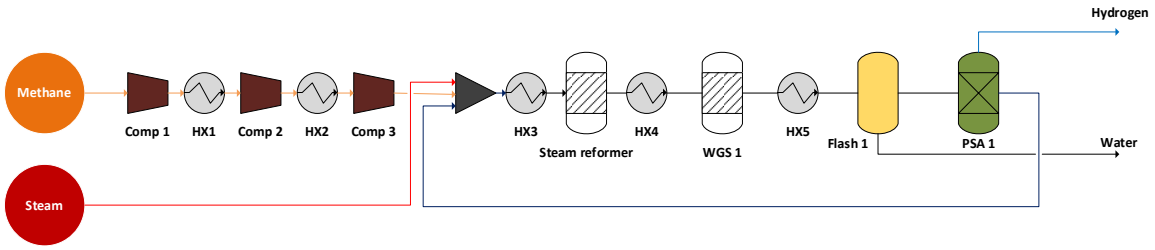

Figure 4.7: SMR flowsheet configuration 1 without compressor after the WGS reactor and no absorber

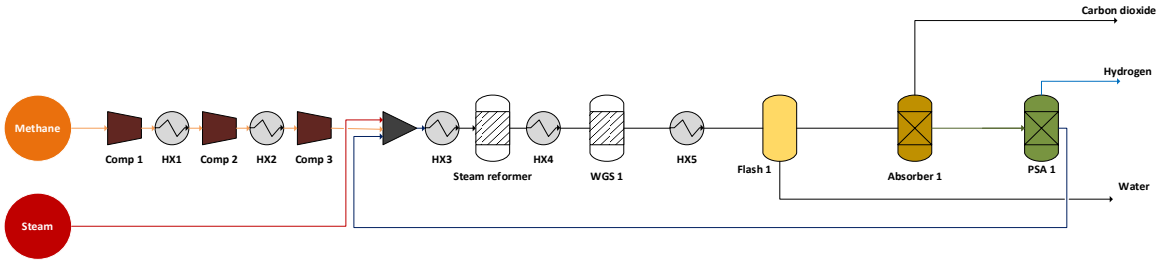

Figure 4.8:SMR flowsheet configuration 2 without compressor after the WGS reactor, with absorber

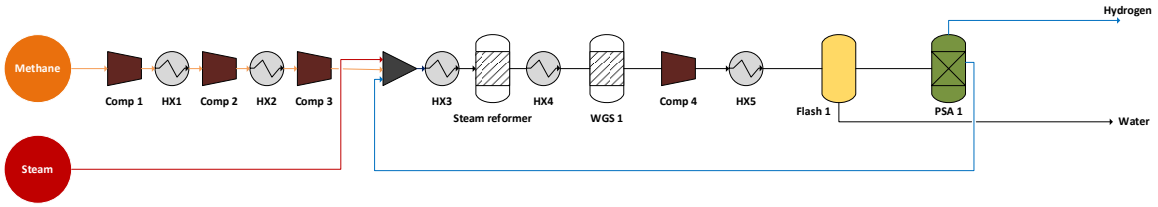

Figure 4.9:SMR flowsheet configuration 3 with compressor after the WGS reactor and no absorber

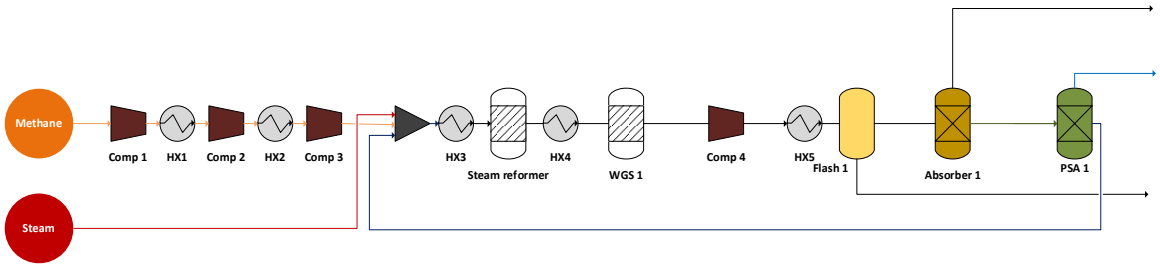

Figure 4.10: SMR flowsheet configuration 4 without compressor after the WGS reactor and an absorber

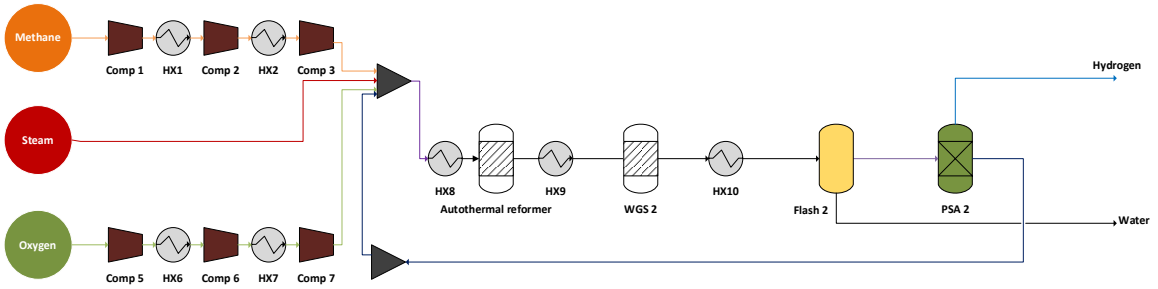

Figure 4.11: ATR flowsheet configuration 1 without compressor after the WGS reactor and no absorber

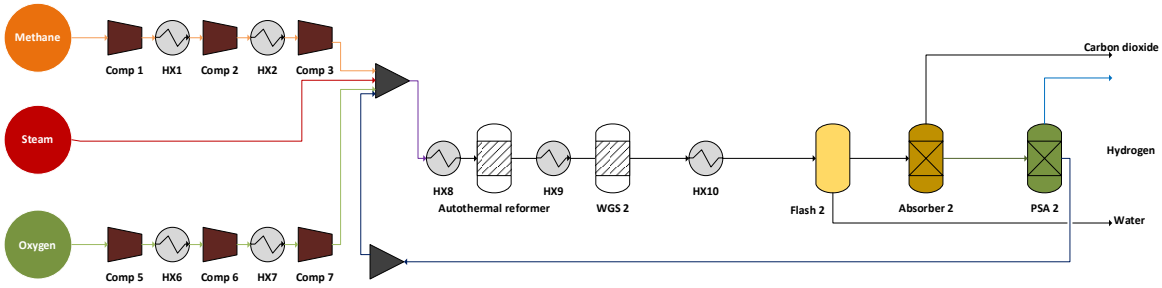

Figure 4.12: ATR flowsheet configuration 2 without compressor after the WGS reactor, with absorber

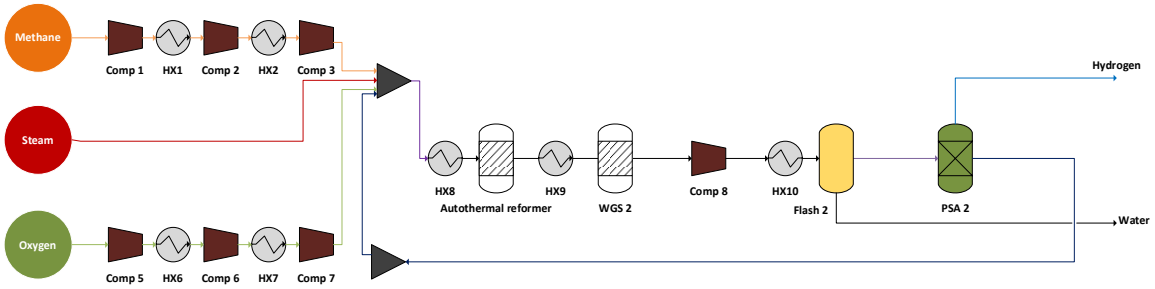

Figure 4.13: ATR flowsheet configuration 3 with compressor after the WGS reactor and no absorber

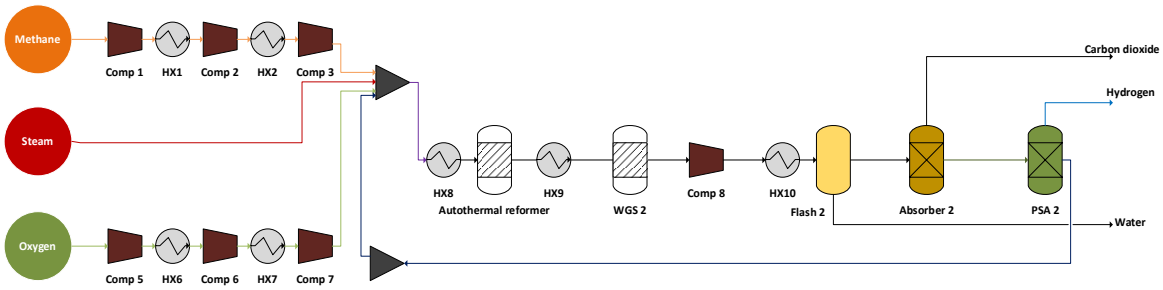

Figure 4.14: ATR flowsheet configuration 4 without compressor after the WGS reactor and an absorber

Table 4.14: Summary of simulated results for the different flowsheet configurations

Flowsheet configuration	**Total Annualized Cost (TAC)-M$/year**	**Levelized cost of hydrogen (LCOH)-$/kg**	**Amount of hydrogen produced /year (mol/year)**	**Amount of carbon dioxide emissions-kg CO_2/kg H_2**
SMR flowsheet configuration 1	328.88	1.61	0.20	5.70
SMR flowsheet configuration 2	329.16	1.61	0.20	0.23
SMR flowsheet configuration 3	308.80	1.51	0.20	5.70
SMR flowsheet configuration 4	332.83	1.63	0.20	0.23
ATR flowsheet configuration 1	388.10	2.17	0.18	6.72
ATR flowsheet configuration 2	430.55	2.41	0.18	0.27
ATR flowsheet configuration 3	404.81	2.26	0.18	6.72
ATR flowsheet configuration 4	405.07	2.26	0.18	0.27

The autothermal reforming options are more costly due to the required compression of two streams. These are the methane and the oxygen streams. In addition, the raw materials are more than those required in steam reforming options. Obtaining oxygen is expensive. In as much as it is available in the air, air separation is costly. If air is used, obtaining pure hydrogen will be costly due to nitrogen, which is not easy to separate downstream. More oxygen produces more carbon dioxide in the autothermal reforming options.

Economically, SMR flowsheet configuration 3 is much more ideal. Adding a compressor after the WGS reactor increases the downstream pressure, thus decreasing the power required for the PSA. Consequently, the overall cost decreases. More hydrogen is produced in steam reforming; thus, steam reforming guarantees more availability than autothermal reforming. Regarding being environmentally friendly, SMR flowsheet configurations 2 and 4 are the best, including carbon capture via the absorber.

4.4.4. Final flowsheet configuration

The flowsheet configurations have different economic, environmental, and availability capabilities. For example, SMR flowsheet configuration 3 has the lowest economic costs, but its carbon dioxide emissions are unfavorable. The SECA mode was applied using data in Table 4.14 to obtain the final flowsheet configuration. The weights of the criteria for this data are shown in Figure 4.15, and the performance scores of the flowsheets are shown in Figure 4.16.

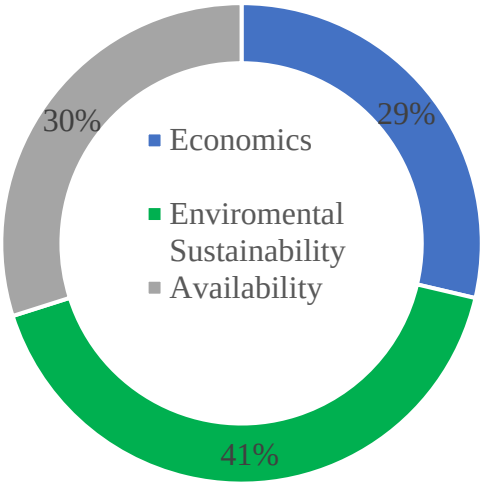

Figure 4.15:Criteria weights

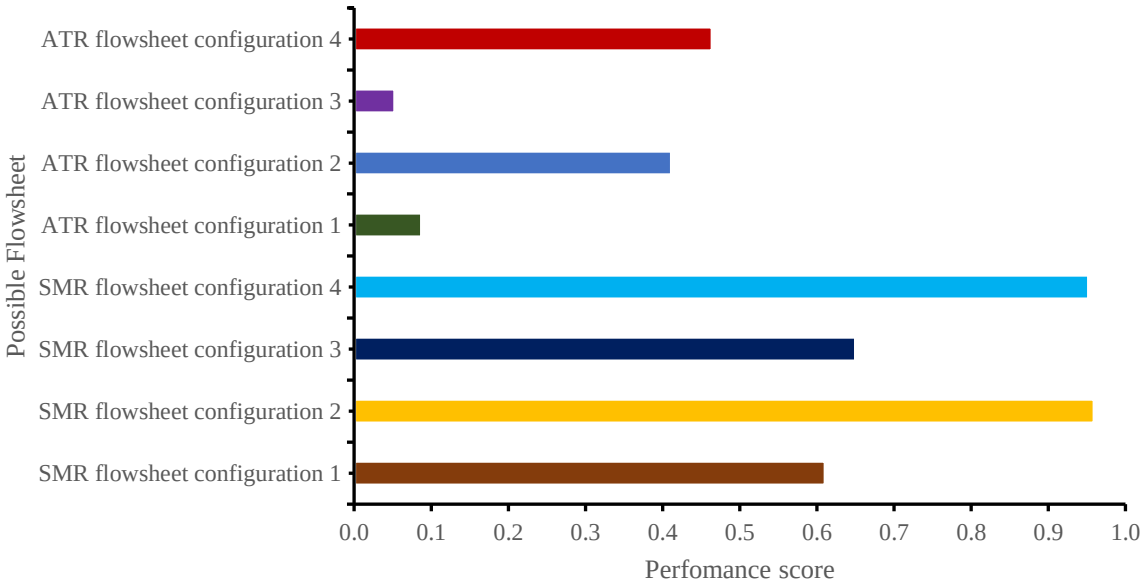

Figure 4.16: Rankings of the flowsheet configurations

From Figure 4.15, the most favoured criterion is environmental sustainability, followed by availability. The least essential criterion is affordability. The prioritization of the weights concurs with the search space reduction, where the same trend is followed. SMR flowsheet configuration 2 has the highest performance score of 0.96, followed by

SMR flowsheet configuration 4 with a performance score of 0.95. ATR flowsheet configuration 3 has the lowest performance score.

4.5. Energy-saving analysis and heat integration of the selected flowsheet configuration

Figure 4.17 shows the selected flowsheet configuration showing the utilities required for the process.

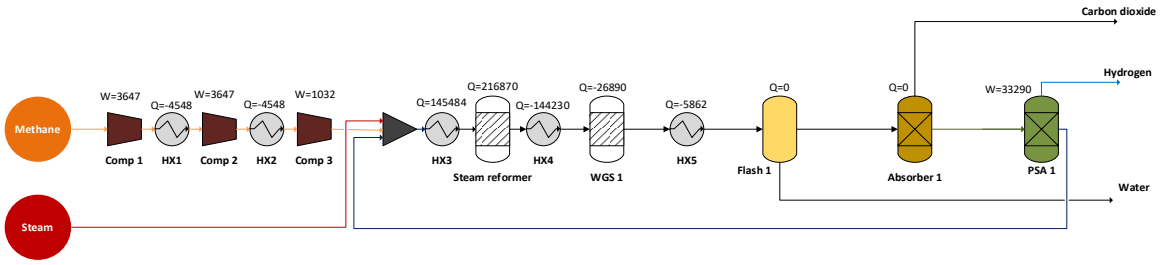

Figure 4.17: Final flowsheet showing utilities required before heat integration

All the existing heat exchanger data must be known to perform heat integration on a plant. Table 4.15 details the data extracted for the heat exchangers to perform heat integration. The process comprises 4 hot steams and 1 cold stream, comprising 5 heat exchangers.

Table 4.15:Data extraction for the process

Stream	Supply Temperature (℃)	Target Temperature (℃)	Q (kW)
Hot 1	142	25	-4548
Hot 2	142	25	-4548
Hot 3	957	250	-144230
Hot 4	250	220	-5862
Cold 1	151	957	145484

Pinch analysis was applied utilizing the data extracted in Table 4.15 to determine potential savings on the utilizes required for the process. Table 4.16 shows the utilities required before and after heat integration. It can be seen that the process consists of opportunities for energy savings, ultimately impacting utility costs. The streams can be

integrated, and less costs will be allocated to purchasing utilities. Figure 4.18 shows the final flowsheet configuration after heat integration.

Table 4.16: Potential savings of the process based on pinch technology.

	Before HI	After HI	Savings	% of Actual
Total utilities (kW)	304672	17314	287358	94.32
Heating utilities (kW)	145484	1805	143679	98.76
Cooling utilities (kW)	159188	15509	143679	90.26

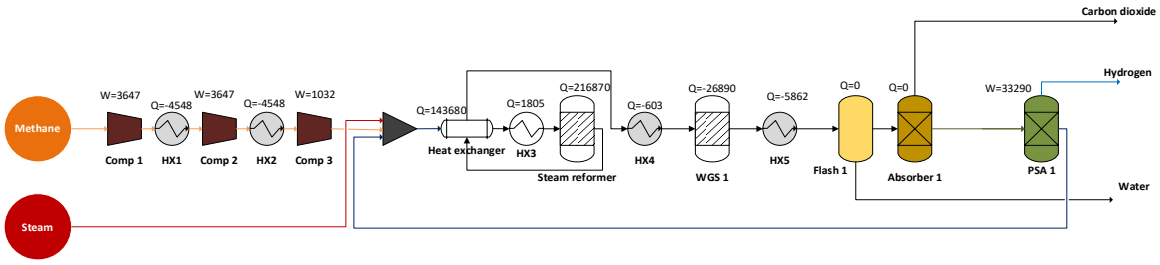

Figure 4.18: Final flowsheet after heat integration

4.6. References

Acar, C., & Dincer, I. (2014). Comparative assessment of hydrogen production methods from renewable and non-renewable sources. International Journal of Hydrogen Energy, 39(1), 1–12. https://doi.org/10.1016/j.ijhydene.2013.10.060

Al-Qahtani, A., Parkinson, B., Hellgardt, K., Shah, N., & Guillen-Gosalbez, G. (2021). Uncovering the true cost of hydrogen production routes using life cycle monetisation. Applied Energy, 281, 115958. https://doi.org/10.1016/j.apenergy.2020.115958

Antonini, C., Treyer, K., Streb, A., van der Spek, M., Bauer, C., & Mazzotti, M. (2020). Hydrogen production from natural gas and biomethane with carbon capture and storage - A techno-environmental analysis. Sustainable Energy and Fuels, 4(6), 2967–2986. https://doi.org/10.1039/d0se00222d

Bhandari, R., Trudewind, C. A., & Zapp, P. (2014). Life cycle assessment of hydrogen production via electrolysis - A review. Journal of Cleaner Production, 85, 151–163. https://doi.org/10.1016/j.jclepro.2013.07.048

Cetinkaya, E., Dincer, I., & Naterer, G. F. (2012). Life cycle assessment of various hydrogen production methods. International Journal of Hydrogen Energy, 37(3), 2071–2080. https://doi.org/10.1016/j.ijhydene.2011.10.064

Dincer, I., & Acar, C. (2014). Review and evaluation of hydrogen production methods for better sustainability. International Journal of Hydrogen Energy, 40(34), 11094–11111. https://doi.org/10.1016/j.ijhydene.2014.12.035

DST. (2016). Bioenergy Atlas of South Africa - Synopsis Report. 1–124. http://dx.doi.org/10.15493/SAEON.BEA.DOcS.10000001%0Ahttp://dx.doi.org/10.15493/SAEON.BEA.DOCS.10000001

DWAF. (2004). Overview of the South African Water Sector. National Water Resource Strategy, 1, 1–35.

EDF. (2015). South Africa : an Emissions Trading. https://www.edf.org/sites/default/files/south_africa_case_study.pdf

Mehmeti, A., Angelis-Dimakis, A., Arampatzis, G., McPhail, S. J., & Ulgiati, S. (2018). Life cycle assessment and water footprint of hydrogen production methods: From conventional to emerging technologies. Environments - MDPI, 5(2), 1–19. https://doi.org/10.3390/environments5020024

Monteleone, D. M. (2014). Environmental affairs. Flexo, 26(12), 57.

Mukumba, P., Makaka, G., & Mamphweli, S. (2016). Biogas Technology in South Africa, Problems, Challenges and Solutions. International Journal of Sustainable Energy and Environmental Research, 5(4), 58–69. https://doi.org/10.18488/journal.13/2016.5.4/13.4.58.69

Nikolaidis, P., & Poullikkas, A. (2017). A comparative overview of hydrogen production processes. Renewable and Sustainable Energy Reviews, 67, 597–611. https://doi.org/10.1016/j.rser.2016.09.044

Seo, Y. S., Shirley, A., & Kolaczkowski, S. T. (2002). Evaluation of thermodynamically favourable operating conditions for production of hydrogen in three different reforming technologies. Journal of Power Sources, 108(1–2), 213–225. https://doi.org/10.1016/S0378-7753(02)00027-7

Snyman, C. P., & Botha, W. J. (2021). Coal in South Africa. Journal of African Earth Sciences, 16(1–2), 171–180. https://doi.org/10.1016/0899-5362(93)90165-M

Utgikar, V., & Thiesen, T. (2006). Life cycle assessment of high temperature electrolysis for hydrogen production via nuclear energy. International Journal of Hydrogen Energy, 31(7), 939–944. https://doi.org/10.1016/j.ijhydene.2005.07.001

CHAPTER 5

FRAMEWORK VALIDATION

5.1. Introduction

In this chapter, the framework developed and the application in the previous chapters is validated to demonstrate that the framework complies and agrees with other studies. The framework validation was done by comparing it to the literature. Three comparisons were made which are:

(i) Comparing the Gibbs results,

(ii) Comparing results obtained using MATLAB vs. those obtained using Aspen Plus,

(iii) Comparing the obtained flowsheet with flowsheets modified from literature.

5.2. Comparison of the Gibbs free energy minimization

The Gibbs free energy minimisation method used in this study was validated by comparing the simulated results to results in literature at selected similar operational conditions. The parameters measured for comparison are equilibrium compositions for the steam reformer and methane conversion for the autothermal reformer. Selectivity was also compared for the autothermal reformer. Table 5.1 and Table 5.2 compare the calculated equilibrium compositions, conversion data, and selectivity obtained for steam reforming and autothermal reforming under the same operating conditions. The data for comparison was obtained from Ávila-Neto et al. (2009), where the methods of equilibrium constants and Lagrange multipliers were used. The comparison revealed that a good correlation close to 1 existed between the equilibrium model results.

Table 5.1:Comparison between simulated and literature equilibrium data for steam reforming at 10 atm

Compounds	773K		873K		973K		1073K		1173K		1273K	
	Lit.	This work	Lit.	This work	Lit.	This work	Lit.	This work	Lit.	This work	Lit.	This work
CH_4	0.260	0.261	0.202	0.202	0.126	0.125	0.054	0.051	0.013	0.012	0.003	0.002
H_2O	0.524	0.526	0.240	0.424	0.309	0.313	0.222	0.225	0.181	0.184	0.173	0.177
CO	0.002	0.003	0.016	0.019	0.056	0.064	0.115	0.123	0.154	0.160	0.168	0.173
CO_2	0.041	0.040	0.063	0.060	0.068	0.062	0.053	0.053	0.038	0.033	0.030	0.026
H_2	0.173	0.169	0.299	0.295	0.441	0.438	0.556	0.556	0.614	0.611	0.626	0.621

Table 5.2: Comparison between simulated and literature equilibrium data for autothermal reforming at 1 atm

Feed				Variable	573K		673K		773K		873K		973K		1073K	
CH_4	H_2O	O_2	N_2		Lit.	This work	Lit.	This work	Lit.	This work	Lit.	This work	Lit.	This work	Lit.	This work
1	2.5	0.1	2.4	CH_4 conv.	11.5	11.4	25.4	25.1	49.9	49.9	82.1	83.0	98.1	98.4	99.9	99.9
1	2.5	0.1	2.4	Selectivity	2.26	2.24	3.18	3.16	3.44	3.42	3.34	3.30	3.20	3.20	3.13	3.10
1	2.5	0.3	2.2		1.10	1.10	2.22	2.20	2.84	2.82	2.95	2.92	2.88	2.85	2.80	2.80
1	2.5	0.5	2.0		0.690	0.680	1.66	1.65	2.38	2.36	2.60	2.60	2.55	2.51	2.47	2.44
1	2.5	1.0	1.5		0.300	0.320	0.910	0.940	1.55	1.57	1.77	1.76	1.72	1.70	1.65	1.62

5.3. Comparison of the MATLAB and Aspen Plus results

MATLAB and Aspen Plus were compared to ensure that the framework calculations correspond. Generally, MATLAB and Aspen Plus are both software programs, but they serve different purposes and are used for different applications. MATLAB is a numerical computing environment and programming language used for matrix manipulations, plotting functions and data, implementation of algorithms, and visualization of data. On the other hand, Aspen Plus is a process simulation software used in the chemical and process industries to model, design, and optimize process flows. It simulates distillation, heat exchanger networks, and reaction kinetics to help

engineers design, optimize, and scale chemical processes. In this study, MATLAB was used to obtain simulation results.

Table 5.3 compares MATLAB and Aspen Plus in the moles at equilibrium. The moles were compared for the reformers in this study and a literature study by Antzara et al. (2015). The comparison showed a relative agreement with the percentage differences being less than 15%, and the correlation was very close to 1.

Table 5.3: Comparison of Aspen Plus and MATLAB results in terms of moles at equilibrium

	Steam reforming at 10 bar and 1230 K			**Autothermal reforming at 10 bar and 1090 K**			**Steam reforming at 25 bar and 1123K (Antzara et al., 2015)**		
	MATLAB	**Aspen plus**	**% Difference**	**MATLAB**	**Aspen Plus**	**% Difference**	**MATLAB**	**Aspen plus**	**% Difference**
CH_4	0.01	0.01	13.65	0.01	0.01	6.81	0.19	0.20	5.66
H_2O	1.77	1.74	1.50	4.93	4.90	0.68	1.90	1.89	0.53
CO_2	0.24	0.27	9.71	0.58	0.61	5.79	0.29	0.31	7.71
CO	0.75	0.73	3.49	0.41	0.37	9.08	0.52	0.49	6.52
H_2	3.22	3.24	0.56	3.05	3.08	1.03	2.72	2.70	0.74
O_2	-	-	-	0.00	0.00	-	-	-	-
Conversion	0.99	0.99	0.12	0.99	0.99	0.10	0.81	0.80	1.37
Selectivity	3.25	3.27	0.68	3.08	3.12	1.10	3.35	3.38	0.63

Table 5.4 shows the comparison of MATLAB and Aspen Plus in terms of the heating and cooling requirements. The comparison was done only for the steam reforming process that was selected to be the best, as well as the process adapted from Antzara et al. (2015). The comparison showed a relative agreement with the percentage differences being less than 10%, and the correlation was very close to 1. The coefficient measures the degree of linear association between the two variables, with higher values indicating a stronger relationship.

Table 5.4: Comparison of Aspen Plus and MATLAB results in terms of utility requirements

	Steam reforming at 10 bar and 1230 K			Steam reforming at 25 bar and 1123K (Antzara et al. 2015)		
	MATLAB	**Aspen plus**	**%difference**	**MATLAB**	**Aspen plus**	**% Difference**
Reformer utility requirement (kW)	216870.00	216123.00	0.35	232140.00	240486.00	3.53
WGS total utilities (kW)	-26890.00	-25367.10	5.83	-18339.20	-17799.00	2.99
Total compressor power (kW)	8325.20	7876.28	5.54	12599.00	12491.37	0.86
Total heating utility (kW)	145490.00	147809.70	1.58	206950.00	203560.30	1.65
Total cooling utility (kW)	-159180.00	-157517.81	1.05	-193030.00	-210597.66	8.70

Various aspects contributed to the difference in the results obtained in Aspen Plus and MATLAB software. Both Aspen Plus and MATLAB used the same inputs and ideal models. However, it was assumed that the heat capacity ratios were constant in MATLAB, a fixed value was used, and the heat of vaporization values were taken as constant at 25 ℃.

5.4. Comparison of the obtained flowsheet with flowsheets in the literature

The obtained flowsheet was compared with flowsheets from the literature to determine its accuracy and reliability. The comparison process included the assessment of equipment, heat and mass balance calculations, and process conditions. The flowsheet obtained in this study is considered to be better than those from the literature in several ways:

1. Cost: The flowsheet in this study uses a cost-effective process that reduces the overall cost of production compared to the flowsheets modified from Antzara et al. (2015) and Faheem et al. (2021). The use of efficient process operations helps to minimize the cost of production.

2. Global Warming Potential (GWP): This study focuses on reducing the carbon footprint of the process, which contributes to reducing the GWP. The flowsheet in this study uses carbon capture and energy-efficient processes to reduce the emissions of greenhouse gases. However the flowsheet from Faheem et al. (2021) does not consider carbon capture.
3. Hydrogen Produced: This study focuses on increasing the hydrogen production efficiency, reflected in the higher hydrogen production compared to other flowsheets modified from literature. Using higher temperatures helps increase the hydrogen production rate by increasing the conversion.
4. Number of Units: The flowsheet in this study uses a modular design that reduces the number of units required compared to other flowsheets in the literature. The use of compact and integrated systems helps to minimize the number of units required, which reduces the cost of production and increases the efficiency of the process.
5. Conversion: The flowsheet in this study focuses on increasing the conversion rate, which is reflected in the higher conversion compared to other flowsheets. According to Le Chatelier's principle, increasing the temperature of an endothermic reaction favors the forward reaction. Since steam reforming is an endothermic reaction, increasing the temperature helps to increase the conversion rate, contributing to higher hydrogen production and reduced carbon footprint.
6. Utility Requirements: The flowsheet in this study focuses on reducing the utility requirements, which is reflected in the lower utility requirements compared to other flowsheets. The use of energy-efficient processes helps to reduce utility requirements, which contributes to lower costs.

In conclusion, the flowsheet in this study is better than those from the literature regarding cost, GWP, hydrogen produced, number of units, conversion, and utility requirements, making it a more sustainable and efficient process for hydrogen production. Table 5.5 compares the process flowsheet configuration obtained in this study with the flowsheets modified from the literature before heat integration.

Table 5.5:Comparison of flowsheets before heat integration

	Flowsheet modified from Antzara et al.	Flowsheet modified from Faheem et al.	This study
Number of heat exchangers	9	5	6
Number of compressors	3	-	3
Number of separation units	3	1	3
Number of reformers	1	1	1
Number of WGS reactors	2	2	1
Reformer temperature (K)	1123	923	1230
Reformer pressure (bar)	25	30	10
Conversion	0.81	0.32	0.99
WGS1 temperature (K)	673	673	523
WGS1 conversion	0.76	0.76	0.90
WGS2 temperature (K)	483	523	-
WGS2 conversion	0.92	0.78	-
Feed ratio (Carbon: Steam)	1:3	1:3	1:3
Total power required (kW)	13450	-	8325
Total heating required (kW)	214090	245200	145484
Total cooling required (kW)	-193030	-206970	159188
Hydrogen produced (Mt/year)	0.19	0.07	0.20
Carbon dioxide produced (kg CO_2/kg H_2)	0.53	0.54	0.23
Total Annualized Cost (M$/year)	337.09	319.67	329.16
Levelized cost of hydrogen ($/kg)	1.79	4.34	1.61

Heat integration was done on the flowsheets to obtain the potential savings on the utility requirements. Table 5.6 shows the utility requirements and the potential savings after heat integration. The results show that the flowsheet modified from Antzara et al. (2015) has the highest savings on utility requirements. However, it still requires more total utilities than the flowsheet obtained in this study. As a result, the flowsheet in this study emerges as the best in terms of the amount of utilities required after heat integration despite having lower savings than Antzara et al. (2015). Reducing the need

for external heating and cooling improves the overall efficiency of a process. This results in lower utility costs and ultimately lower overall operational costs of a process.

Table 5.6: Potential savings of the processes after heat integration

	Total utilities before HI	Total utilities after HI	Savings	% of actual
Antzara et al.	407120	21058	386062	94.83
Faheem et al.	452170	137892	314278	69.50
This study	304762	17314	287448	94.32

5.5. References

Antzara, A., Heracleous, E., Bukur, D. B., & Lemonidou, A. A. (2015). Thermodynamic analysis of hydrogen production via chemical looping steam methane reforming coupled with in situ CO2 capture. International Journal of Greenhouse Gas Control, 32, 115–128. https://doi.org/10.1016/j.ijggc.2014.11.010

Ávila-Neto, C. N., Dantas, S. C., Silva, F. A., Franco, T. V., Romanielo, L. L., Hori, C. E., & Assis, A. J. (2009). Hydrogen production from methane reforming: Thermodynamic assessment and autothermal reactor design. Journal of Natural Gas Science and Engineering, 1(6), 205–215. https://doi.org/10.1016/j.jngse.2009.12.003

Faheem, H. H., Tanveer, H. U., Abbas, S. Z., & Maqbool, F. (2021). Comparative study of conventional steam-methane-reforming (SMR) and auto-thermal-reforming (ATR) with their hybrid sorption enhanced (SE-SMR & SE-ATR) and environmentally benign process models for the hydrogen production. Fuel, 297(February), 120769. https://doi.org/10.1016/j.fuel.2021.120769

CHAPTER 6

HYDROGEN PROCESS DESIGN AND OPTIMISATION

6.1. Introduction

Hydrogen has emerged as a promising candidate in pursuing sustainable energy sources due to its versatility and potential to reduce greenhouse gas emissions. One of the critical processes for hydrogen production is steam reforming, which involves the reaction of hydrocarbons with steam to yield hydrogen and carbon dioxide. This chapter explores the optimisation of the steam reforming process, given the reduced search space developed in Chapter 4. The primary objective is to outline the optimisation model for the most viable reaction pathway, which, in this case, is steam reforming.

6.2. Steam reforming: A viable reaction pathway

Steam reforming has been identified as the most viable reaction pathway for hydrogen production through rigorous screening and reduced search space ranking. Steam reforming of hydrocarbons, such as methane, involves complex reactions that must be carefully controlled to achieve high hydrogen yield and purity. The viability of this reaction pathway stems from its maturity, scalability, and established technological infrastructure.

6.3. Steam reforming process design

The conventional steam reforming process flowsheet obtained in the previous chapter is used as a reference process; however, modified to introduce an option for the model

to choose a bypass or water gas shift reactor and implement a recycle stream. Figure 6.1 shows the conventional steam reforming process.

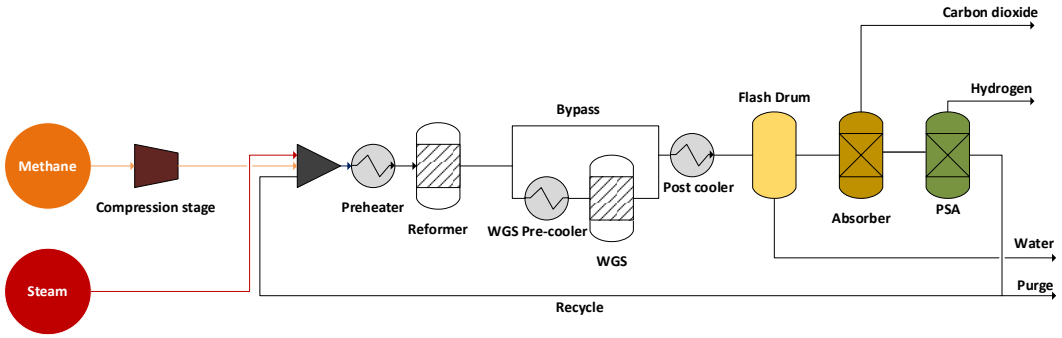

Figure 6.1: The modified conventional steam reforming process

6.4. Process design and optimisation model development

The optimisation of the steam reforming process involves minimising the costs involved in its production while considering operational constraints and sizing of the units. A comprehensive optimisation model is developed to achieve this, encompassing various variables, parameters, and constraints relevant to the steam reforming reaction.

As shown in Figure 6.1, methane and steam are the initial feedstocks that enter the process. The feed ratios are unknown, hence the need to optimize the process. The pressure of the process is kept at 10 bar, the pressure at which the steam comes into the process. The inlet temperature and pressure of methane are kept at 1 bar and 298 K; hence, the methane stream requires compression. The compressor is modeled using equation 6.1:

$$Power_i^{comp} = \sum_{i=methane}^{n} F_i^{comp} \left[(Pr)^{\left(\frac{\gamma}{\gamma-1}\right)} - 1\right]\left(\frac{\gamma}{\gamma-1}\right)\eta^{-1}R_g T_{feed} \qquad 6.1$$

where $Power_i^{comp}$ is the power of the compressor, F_i^{comp} is the flowrate of methane into the compressor, Pr is the pressure ratio, γ is the heat capacity ratio, η is the compressor efficiency, and the feed temperature of methane is represented by T_{feed}.

The compression stage has an unknown number of stages; therefore, Equation 6.2 calculates the total power required for compression, $Power_{total}^{comp}$. Equation 6.3 is a constraint that ensures the number of stages, ns, is between 1 and 3. The pressure ratio is calculated using Equation 6.4 and Equation 6.5, which necessitates keeping the pressure ratio between 1 and 3.

$$Power_{total}^{comp} = ns(Power_i^{comp}) \quad 6.2$$

$$1 \leq ns \leq 3 \quad 6.3$$

$$Pr = \frac{P_{out}}{P_{in}} \quad 6.4$$

$$1 \leq Pr \leq 3 \quad 6.5$$

Equations 6.6-6.9 calculate the cost of the compressors. Each compressor is expected to dissipate the same amount of power, given that there is no change in the flowrate. Also, the compression is from the exact temperature of 298 K; thus, the total cost of the compressors, Cbm_{total}^{comp} is calculated by multiplying the purchased cost, C_{po}^{comp} , by the number of stages. The operating costs for the compression stage is calculated using the cost of electricity multiplied by the power of the compressor and the expected hours of operation per year, H_t.

$$logcp_o^{comp} = 2.2897 + 1.3604 \log\left(Power_i^{comp}\right) - 0.1027 * \log\left(Power_i^{comp}\right)^2 \quad 6.6$$

$$C_{po}^{comp} = 10^{logcp_o^{comp}} \quad 6.7$$

$$Cbm_{total}^{comp} = C_{po}^{comp} * 2.8 * ns \quad 6.8$$

$$Op^{Comp} = E_{cost} * Power_i^{comp} * ns * H_t \quad 6.9$$

For the costing equations to be applicable, the constraint in Equation 6.10 is used to ensure that the power of the compressors is within limits.

$$450 \leq Power_i^{comp} \leq 3000 \quad 6.10$$

The compressed temperature, T_n^{out}, is calculated using Equation 6.11. This temperature should not exceed 473 K, as in equation 6.12.

$$T_n^{out} = T_{feed,n}(Pr)^{\left(\frac{\gamma-1}{\gamma}\right)} \quad 6.11$$

$$273\ K\ \leq T_n^{out} \leq 473\ K \quad 6.12$$

The cooling utility required for stagewise heat exchangers is calculated using Equation 6.13. which is given by the integral of the product of the moles in the steam (n) with the specific heat capacity of the component (C_p). The heat exchangers cool the gas to the feed temperature of 298 K to ensure that the temperature out of the compressors does not exceed 473 K. The area of the heat exchangers and cost are calculated using equations 6.16-6.20.

$$\hat{Q}_n^{hx} = \int_{To}^{Tn} nC_p dT \quad 6.13$$

$$Area_j^{intercooler} = \frac{\hat{Q}_n^{hx}}{U\Delta T} \quad 6.14$$

$$\Delta T = T_n - T_o \quad 6.15$$

$$HxlogC_p^0 = 4.8306 - 0.8509\log\left(Area_j^{intercooler}\right) + 0.3187[\log\left(Area_j^{intercooler}\right)]^2 \quad 6.16$$

$$C_p^0 = 10^{HxlogC_p^0} \quad 6.17$$

$$logF_p = 0.03881 - 0.11272\log(P) + 0.08183[\log(P)]^2 \quad 6.18$$

$$Hx_{Cbm}^{intercooler} = C_p^0\left(1.63 + \left(1.66 * 1.4 * F_p\right)\right) * (ns - 1) \quad 6.19$$

$$Op^{intercooler} = m_{coolant} * C_{coolant} * H_t * (ns - 1) \quad 6.20$$

The mass of the coolant, $m_{coolant}$ is calculated using Equation 6.21, where Q is the amount of cooling required, and ΔT is the change in the coolant temperature.

$$m_{coolant} = \frac{Q}{C_p \Delta T} \quad 6.21$$

The feed streams and the recycle are mixed, and the temperature of the mixture (T_{mix}) is calculated using Equation 6.22.

$$T_{mix} = \frac{\sum n_j C_{p,j} T_j^{out}}{\sum n_j C_{p,j}} \qquad \forall j \in J \quad 6.22$$

The preheater is modeled using equations 6.23-6.30.

$$\hat{Q}_n^{preheater} = \int_{Tmix}^{Tsmr} nC_p dT \quad 6.23$$

$$Area_j^{preheater} = \frac{\hat{Q}_n^{preheater}}{U\Delta T} \quad 6.24$$

$$\Delta T = T_{smr} - T_{mix} \quad 6.25$$

$$Hxlog C_{p,preheater}^0 = 4.8306 - 0.8509 \log\left(Area_j^{preheater}\right) + 0.3187[\log\left(Area_j^{preheater}\right)]^2 \quad 6.26$$

$$C_{p,preheater}^0 = 10^{Hxlog C_{p,preheater}^0} \quad 6.27$$

$$logF_{p,preheater} = 0.03881 - 0.11272 \log(P) + 0.08183[\log(P)]^2 \quad 6.28$$

$$Hx_{Cbm}^{preheater} = C_{p,preheater}^0 \left(1.63 + \left(1.66 * 1.4 * F_p\right)\right) \quad 6.29$$

$$Op^{preheater} = m_{heating\ medium} * C_{heating\ medium} * H_t \quad 6.30$$

The fresh feed to the reactor, $F_i^{fresh\ feed}$ consists of methane and steam, which are costed as in Equation 6.31. The cost of the raw material, raw_i is multiplied by the amount of fresh feed required for the process yearly. The feed to the reactor, $F_i^{reactor}$, is calculated using Equation 6.32 which adds the fresh feed and the recycled

components, $F_i^{recycle}$. The reformer is modeled using the following kinetics to size it and obtain the required volume (Hoang et al., 2005; Halabi et al., 2008; Taji et al., 2018).

$$Cost_i^{fresh\ feed} = raw_i * F_i^{fresh\ feed} * M_i * H_t \tag{6.31}$$

$$F_i^{reactor} = F_i^{fresh\ feed} + F_i^{recycle} \qquad \forall i \in I \tag{6.32}$$

$$K_1 = \exp\left(\frac{-26830}{T_s} + 30.114\right) \quad (bar^2) \tag{6.33}$$

$$K_2 = K_1 K_3 \quad (bar^2) \tag{6.34}$$

$$K_3 = \exp\left(\frac{4400}{T_s} - 4.036\right) \tag{6.35}$$

$$P_i^{partial} = y_i P \qquad \forall i \in I \tag{6.36}$$

$$\sum_{i=1} P_i^{partial} = P \tag{6.37}$$

$$R_1 = \frac{k_1}{p_{H_2}^{2.5}}\left(p_{CH_4} p_{H_2O} - \frac{p_{H_2}^3 p_{co}}{K_1}\right)\frac{1}{\Omega^2} \tag{6.38}$$

$$R_2 = \frac{k_1}{p_{H_2}^{3.5}}\left(p_{CH_4}p_{H_2O}^2 - \frac{p_{H_2}^4 p_{CO_2}}{K_2}\right)\frac{1}{\Omega^2} \quad 6.39$$

$$R_3 = \frac{k_1}{p_{H_2}}\left(p_{co}p_{H_2O} - \frac{p_{H_2}p_{CO_2}}{K_3}\right)\frac{1}{\Omega^2} \quad 6.40$$

$$\Omega = 1 + K_{co}p_{co} + K_{H_2}p_{H_2} + K_{H_2}p_{H_2} + K_{H_2O}\frac{p_{H_2O}}{p_{H_2}} \quad 6.41$$

$$k_j = k_{oj} \times \exp\left(\frac{-E_j}{RT}\right) \quad 6.42$$

$$r_{CH_4} = -\eta_1 R_1 - \eta_2 R_2 - \eta_4 R_4 \quad 6.43$$

$$r_{CO_2} = \eta_2 R_2 + \eta_3 R_3 \quad 6.44$$

$$r_{H_2O} = -\eta_1 R_1 - 2\eta_2 R_2 - \eta_3 R_3 \quad 6.45$$

$$r_{H_2} = 3\eta_1 R_1 + 4\eta_2 R_2 + \eta_3 R_3 \quad 6.46$$

$$r_{CO} = \eta_1 R_1 - \eta_3 R_3 \quad 6.47$$

$$\eta_1 = 0.07, \eta_2 = 0.06, \eta_3 = 0.7 \quad 6.48$$

The flux of flowrate along the weight of the catalyst in the reactor is calculated using the reactor design equation assuming a packed bed reactor. These fluxes are based on steam reforming governing reactions, as shown in Equations 6.49-6.51.

$$CH_4 + H_2O \leftrightarrow CO + 3H_2 \quad 6.49$$

$$CO + H_2O \leftrightarrow CO_2 + H_2 \quad 6.50$$

$$CH_4 + 2H_2O \leftrightarrow CO_2 + 4H_2 \quad 6.51$$

$$\frac{dF_{CH_4}}{dW} = r_{CH_4} \quad 6.52$$

$$\frac{dF_{CO_2}}{dW} = r_{CO_2} \quad 6.53$$

$$\frac{dF_{CO}}{dW} = r_{CO} \quad 6.54$$

$$\frac{dF_{H_2O}}{dW} = r_{H_2O} \quad 6.55$$

$$\frac{dF_{H_2}}{dW} = r_{H_2} \quad 6.56$$

To incorporate the differential equations into the algebraic expression-based modeling software, the differential Equations 6.52-6.56 are discretized. A combination of central finite difference (CFD) and the backward finite difference (BFD) method of accuracy order 2 is used to discretize the differential equation. Equation 6.57 presents the general form of the central finite difference discretization approximation for a first-order

derivative differential equation approximated to the accuracy of order 2. The CFD, in this case, is used to estimate the point $k=2$ on the reactor since the value $k=1$ is unknown. The general form of the first derivative with an order of accuracy 2 of a backward finite difference approximation is given by Equation 6.58. The BFD method was implemented for $k>2$ using the values from K=2. Equations 6.59-6.60 show how the flowrate of the reactor and the catalyst's weight are related to the general form. Equation 6.60 shows that the total weight of the catalyst is the product, $dW^{reactor,}$ and the number of subdivisions of the catalyst weight is given by *K-1*.

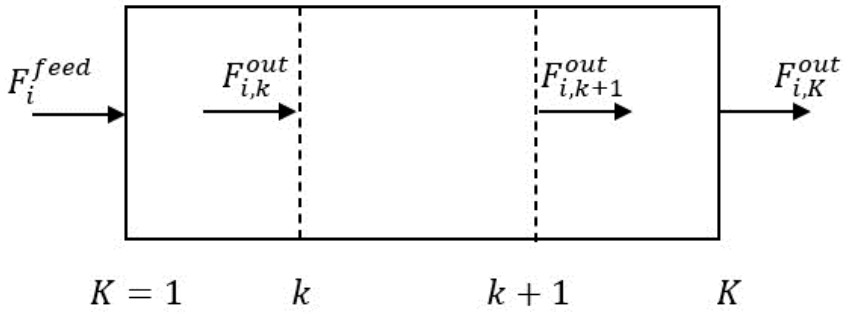

Figure 6.2: Schematic representation of the reactor

$$f' = \frac{f(x_{k+1}) - f(x_{k-1})}{2\Delta x} \qquad ;\Delta x = h \tag{6.57}$$

$$f' = \frac{\frac{1}{2}f(x_{k-2}) - 2f(x_{k-1}) + \frac{3}{2}f(x_k)}{h} \Rightarrow f' = \frac{f(x_{k-2}) - 4f(x_{k-1}) + 3f(x_k)}{2h} \tag{6.58}$$

$$f' \Rightarrow dF_i \qquad ; h \Rightarrow dW^{reactor} \tag{6.59}$$

$$dW^{reactor} = \frac{W^{reactor}}{K-1} \tag{6.60}$$

Discretising $\frac{dF_i}{dW^{reactor}}$ based on the CFD model, estimating the flow rates at *k=2* yields Equation 6.61.

$$\frac{F_{i,k+1}^{out} - F_{i,k-1}^{out}}{2dW^{reactor}} = \frac{(K-1)(F_{i,k+1}^{out} - F_{i,k-1}^{out})}{2W^{reactor}} \tag{6.61}$$

Applying BFD to discretize $\frac{dF_i}{dW^{reactor}}$ to compute the flowrates of the components at *k>2* results in Equation 6.62.

$$\frac{F_{i,k-2}^{out} - 4F_{i,k-1}^{out} + 3F_{i,k}^{out}}{2dW^{reactor}} = \frac{(K-1)(F_{i,k-2}^{out} - 4F_{i,k-1}^{out} + 3F_{i,k}^{out})}{2W^{reactor}} \tag{6.62}$$

The algebraic expressions presented in Equations 6.61 and 6.62 are substituted into Equations 6.52-6.56 to give Equations 6.63 and 6.64. Equations 6.63 and 6.64, therefore, compute the flowrates of component *i* at point *k* of the catalyst.

$$\frac{K-1}{2W^{reactor}}\left(F_{i,k+1}^{out} - F_{i,k-1}^{out}\right) = r_{i,k} \qquad \forall i \in I, k \in K, k = 2 \tag{6.63}$$

$$\frac{K-1}{2W^{reactor}}\left(F_{i,k-2}^{out} - 4F_{i,k-1}^{out} + 3F_{i,k}^{out}\right) = r_{i,k} \qquad \forall i \in I, k \in K, k > 2 \tag{6.64}$$

Carrying out an atomic species mass balance around the reactor area bound by *k=k* and *k=K*, as presented in Figure 6.2, yields Equation 6.65, which states that the product of

the individual atomic species, n_s and the flowrate of the molecules in which the atoms are found in the feed stream, $F_{i,k=1}^{out}$ are equal to those in the exit stream, $F_{i,k}^{out}$.

$$\sum_{s=1}^{S} n_s F_{i,k=1}^{out} = \sum_{s=1}^{S} n_s F_{i,k}^{out} \qquad \forall i \in I, k \in K, s \in S, S = \{C, H, O\} \tag{6.65}$$

The flowrate out of *k=1* is equal to the flowrate of the feed to the reactor, F_i^{feed}. The reaction rate of each component at *k=1* is equal to 0 because it is assumed that no reaction occurs at the entry point.

$$F_{i,k=1}^{out} = F_i^{feed} \qquad \forall i \in I, k \in K, k = 1 \tag{6.66}$$

$$r_{i,k=1} = 0 \qquad \forall i \in I, k \in K, k = 1 \tag{6.67}$$

The cost of the reactor is dependant on its the volume. Therefore, Equation 6.68 calculates the volume, $V^{reactor}$ utilizing the weight of the catalyst, $W^{reactor}$ and the bulk catalyst density, $\rho^{catalyst}$.

$$V^{reactor} = \frac{W^{reactor}}{\rho^{catalyst}} \tag{6.68}$$

The cost of the reactor is calculated using Equations 6.69-6.71.

$$SMRlogC_p^0 = 3.3496 + 0.7235\, log(V^{reactor}) + 0.0025[log\,(V^{reactor})]^2 \tag{6.69}$$

$$C_{p,smr}^{0} = 10^{SMRlogC_{p,smr}^{0}} \quad 6.70$$

$$SMR_{Cbm}^{reactor} = C_{p,smr}^{0} \times 4 \quad 6.71$$

If the bypass is not considered, the WGS route is taken. A cooler is added to cool the stream to the WGS reactor temperature. Binary variables are introduced to show the existence of the bypass or the WGS option. The existence of the bypass is represented by the binary variable, Ys, and the existence of WGS by the binary variable, Yw. Only one option exists, and the two cannot happen simultaneously. The following equations are used to model the WGS precooler:

$$\hat{Q}_{n}^{wgsprecooler} = \int_{Tsmr}^{Twgs} nC_{p}dT \quad 6.72$$

$$Area^{wgsprecooler} = \frac{\hat{Q}_{n}^{wgsprecooler}}{U\Delta T} \quad 6.73$$

$$\Delta T = T_{wgs} - T_{smr} \quad 6.74$$

$$HxlogC_{p,wgsprecooler}^{0} = 4.8306 - 0.8509\log(Area^{wgsprecooler}) + 0.3187[\log(Area^{wgsprecooler})]^{2} \quad 6.75$$

$$C_{p,wgsprecooler}^{0} = 10^{HxlogC_{p,wgsprecooler}^{0}} \quad 6.76$$

$$logF_{p,wgsprecooler} = 0.03881 - 0.11272\log(P) + 0.08183[\log(P)]^2 \quad 6.77$$

$$Hx_{Cbm}^{wgsprecooler} = C_{p,wgsprecooler}^{0}\left(1.63 + \left(1.66 * 1.4 * F_p\right)\right) \times Yw \quad 6.78$$

$$Op^{precooler} = m_{coolant} * C_{coolant} * H_t \quad 6.79$$

The feed to the reactor, $F_i^{WGS,in}$, is calculated using Equation 6.80, which is equal to the flowrate out of the reformer, $F_{i,k=K}^{out}$. The water gas shift reactor is modeled using kinetics to size it and obtain the required volume (Choi & Stenger, 2003; Sato et al., 2004; Ding & Chan, 2008).

$$F_i^{WGS,in} = F_{i,k=K}^{out} \qquad \forall i \in I, k \in K \quad 6.80$$

$$K_{eq} = \exp\left(\frac{4577.8}{T_{wgs}} - 4.33\right) \quad (bar^2) \quad 6.81$$

$$P_i^{partial,wgs} = y_i^{wgs} P \qquad \forall i \in I \quad 6.82$$

$$\sum_{i=1} P_i^{partial,wgs} = P \quad 6.83$$

$$R^{WGS} = k\left(\frac{p_{H_2O}^{WGS}p_{CO}^{WGS} - {p_{H_2}^{WGS}p_{CO_2}^{WGS}}/{K_{eq}}}{(1 + K_1^{WGS}p_{CO}^{WGS} + K_2^{WGS}p_{H_2O}^{WGS} + K_3^{WGS}p_{CO_2}^{WGS} + K_4^{WGS}p_{H_2}^{WGS})^2}\right) \quad 6.84$$

$$k = 748.824 \times \exp\left(\frac{-53821}{RT}\right) \quad 6.85$$

$$K_1^{WGS} = 2.222 \times exp\left(\frac{23616}{RT}\right) \quad 6.86$$

$$K_2^{WGS} = 2.006 \times 10^{-5} \times exp\left(\frac{-66104}{RT}\right) \quad 6.87$$

$$K_3^{WGS} = 0.036 \times exp\left(\frac{-9795}{RT}\right) \quad 6.88$$

$$K_4^{WGS} = 2.197 \times 10^{-5} \times exp\left(\frac{-63540}{RT}\right) \quad 6.89$$

$$r_{CO}^{WGS} = -R^{WGS} \quad 6.90$$

$$r_{CO_2}^{WGS} = R^{WGS} \quad 6.91$$

$$r_{H_2O}^{WGS} = -R^{WGS} \quad 6.92$$

$$r_{H_2}^{WGS} = R^{WGS} \tag{6.93}$$

The mass balance equations are shown in Equations 6.94-6.98.

$$\frac{dF_{CO_2}^{WGS}}{dW^{WGS}} = r_{CO_2}^{WGS} \tag{6.94}$$

$$\frac{dF_{CO}^{WGS}}{dW^{WGS}} = r_{CO}^{WGS} \tag{6.95}$$

$$\frac{dF_{H_2O}^{WGS}}{dW^{WGS}} = r_{H_2O}^{WGS} \tag{6.96}$$

$$\frac{dF_{H_2}^{WGS}}{dW^{WGS}} = r_{H_2}^{WGS} \tag{6.97}$$

$$\frac{dF_{CH_4}^{WGS}}{dW^{WGS}} = 0 \tag{6.98}$$

The same discretization process for the reformer is followed to yield Equations 6.99 and 6.100.

$$\frac{K-1}{2W^{WGS}}\left(F_{i,k+1}^{out,WGS} - F_{i,k-1}^{out,WGS}\right) = r_{i,k} \qquad \forall i \in I, k \in K, k = 2 \tag{6.99}$$

$$\frac{K-1}{2W^{WGS}}\left(F_{i,k-2}^{out,WGS} - 4F_{i,k-1}^{out,WGS} + 3F_{i,k}^{out,WGS}\right) = r_{i,k} \qquad \forall i \in I, k \in K, k > 2 \tag{6.100}$$

Carrying out an atomic species mass balance around the Water Gas Shift reactor area bound by *k=k* and *k=K*, as presented in Figure 6.2, yields Equation 6.101. Equation 6.101 states that the product of the individual atomic species, n_s and the flowrate of the molecules in which the atoms are found in the feed stream, $F_{i,k=1}^{out,WGS}$ are equal to those in the exit stream, $F_{i,k=K}^{out,WGS}$.

$$\sum_{s=1}^{S} n_s F_{i,k=1}^{out,WFS} = \sum_{s=1}^{S} n_s F_{i,k}^{out,WGS} \qquad \forall i \in I, k \in K, s \in S, = \{C, H, O\} \tag{6.101}$$

Similar to the cost of the WGS reactor, it depends on the volume. Therefore, Equation 6.102 calculates the volume $V^{WGSreactor}$ utilizing the weight of the catalyst, $W^{WGSreactor}$ and the bulk catalyst density, $\rho^{catalyst}$.

$$V^{WGSreactor} = \frac{W^{WGSreactor}}{\rho^{WGScatalyst}} \tag{6.102}$$

The cost of the WGS reactor is calculated using Equations 6.103-6.105.

$$WGSlogC_p^0 = 3.3496 + 0.7235\, log(V^{WGSreactor}) + 0.0025[log\ (V^{WGSreactor})]^2 \tag{6.103}$$

$$C_{p,WGS}^0 = 10^{WGSlogC_{p,WGS}^0} \tag{6.104}$$

$$WGS_{Cbm}^{reactor} = C_{p,WGS}^0 \times 4 \times Yw \tag{6.105}$$

The post cooler is modeled using the Equations 6.106-6.122. The temperature to be cooled, T_p can be the temperature of the reformer or the WGS temperature. Equations

6.107-6.115 show algebraic equations using the binary variables. The variable M is any positive large number. The mass balance around the post cooler is represented by equations 6.112-6.115. The mass balance utilizes binaries to ensure that the flow is from one source, as the bypass and the WGS cannot exist simultaneously.

$$\hat{Q}_n^{postcooler} = \int_{Tp}^{Tflash} nC_p dT \qquad 6.106$$

$$T_p \leq T_{smr} + (1 - Ys) * M \qquad 6.107$$

$$T_p \geq T_{smr} - (1 - Ys) * M \qquad 6.108$$

$$T_p \leq T_{wgs} + (1 - Yw) * M \qquad 6.109$$

$$T_p \geq T_{wgs} - (1 - Yw) * M \qquad 6.110$$

$$Yw + Ys = 1 \qquad 6.111$$

$$F_i^{Postcooler} \leq F_{i,k=K}^{out} + (1 - Ys) * M \qquad \forall i \in I, k \in K \qquad 6.112$$

$$F_i^{Postcooler} \geq F_{i,k=K}^{out} - (1 - Ys) * M \qquad \forall i \in I, k \in K \qquad 6.113$$

$$F_i^{Postcooler} \leq F_{i,k=K}^{out,WGS} + (1 - Yw) * M \qquad \forall i \in I, k \in K \qquad 6.114$$

$$F_i^{Postcooler} \geq F_{i,k=K}^{out,WGS} - (1 - Yw) * M \qquad \forall i \in I, k \in K \qquad 6.115$$

$$Area^{postcooler} = \frac{\hat{Q}_n^{postcooler}}{U\Delta T} \quad 6.116$$

$$\Delta T = T_p - T_{wgs} \quad 6.117$$

$$Hxlog C_{p,postcooler}^0 = 4.8306 - 0.8509\log(Area^{postcooler}) + 0.3187[\log(Area^{postcooler})]^2 \quad 6.118$$

$$C_{p,postcooler}^0 = 10^{Hxlog C_{p,postcooler}^0} \quad 6.119$$

$$logF_{p,postcooler} = 0.03881 - 0.11272\log(P) + 0.08183[\log(P)]^2 \quad 6.120$$

$$Hx_{Cbm}^{postcooler} = C_{p,postcooler}^0\left(1.63 + \left(1.66 * 1.4 * F_p\right)\right) \quad 6.121$$

$$Op^{postcooler} = m_{coolant} * C_{coolant} * H_t \quad 6.122$$

The flash separator removes water in a simple mass balance, letting the rest of the components pass through. Equations 6.123-6.128 are used to model the flash separator. The ratio of the length to the diameter of the flash separator is to be between 2.5 and 5. The liquid holdup time is 5 mins based on ½ volume vessel. The parameter *k*=0.0305 for vessels without mesh entrainers. The gas velocity, *u*, is calculated by multiplying k

with the ratio of the liquid density, ρ_l to the vapor density, ρ_v minus one. The actual gas velocity, u_{act} is 75 % of the calculated gas velocity.

$$u = k\sqrt{\frac{\rho_l}{\rho_v} - 1} m/s \qquad 6.123$$

$$u_{act} = 0.75u \qquad 6.124$$

$$2.5 \leq \frac{L}{D} \leq 5 \qquad 6.125$$

$$mass\ flow\ of\ vapor = \frac{u\rho_v \pi D^2}{4} \qquad 6.126$$

$$5\ \text{min}\ liquid\ flow = t * m_{H_2O} \qquad 6.127$$

$$V_{flash} = \frac{\pi L D^2}{4} \qquad 6.128$$

The cost of the flash is then calculated using Equations 6.129-6.132.

$$Flash log C_p^0 = 3.4974 - 0.4485 \log\left(V_{flash}\right) + 0.1074[\log\left(V_{flash}\right)]^2 \qquad 6.129$$

$$FlashC_p^0 = 10^{flashlogC_p^0} \quad 6.130$$

$$FlashlogF_{p,flash} = \frac{\frac{PD_{flash}}{2[850 - 0.6(P)} + 0.00315}{0.0063} \quad 6.131$$

$$Cbm_{flash} = FlashC_p^0 \left(2.25 + \left(1.82 * 1 * F_{p,flash}\right)\right) \quad 6.132$$

The absorber is used to remove CO_2 from the process. It is modelled using Equations 6.133-6.153. Since the flash removes the water, the absorber mass balances do not include water. The components that enter the absorber, $F_i^{abs,in}$ is equal to those that exit the absorber, $F_i^{abs,out}$ except for the CO_2. The efficiency, δ of the absorber, is assumed to be between 0.80 and 0.99.

$$F_i^{abs,in} = F_i^{abs,out} \qquad \forall i\{CO_2\} \quad 6.133$$

$$F_{CO_2}^{abs,out} = F_{CO_2}^{abs,in} - F_{CO_2} \quad 6.134$$

$$F_{CO_2} = \delta F_{CO_2}^{abs,in} \quad 6.135$$

$$0.80 \leq \delta \leq 0.99 \quad 6.136$$

The sizing of the absorber column is done by calculating the minimum number of stages, N_{min}. The N_{min} is dependent on the compositions of the overhead and bottoms

and the relative volatility using the Fenske Equation. The minimum reflux, R_{min} is dependent on the feed, *F*, and distillate, *D*, and relative volatility, α.

$$N_{min} = \frac{\ln\left(\frac{x}{(1-x)_{ovhd}} \Big/ \frac{x}{(1-x)_{bot}}\right)}{\ln \alpha} \quad 6.137$$

$$Number\ or\ stages = 2N_{min} \quad 6.138$$

$$R_{min} = \frac{F/D}{\alpha - 1} \quad 6.139$$

$$1.2 \leq R_{min} \leq 1.5 \quad 6.140$$

To calculate the relative volatility, α, vapor pressures are required. These are calculated using Antoine's equation, as shown in Equation 6.141.

$$\log(p^*) = A - \frac{B}{C + T} \quad 6.141$$

Due to the Antione constants being out of the required range of temperatures, the Clausius Clapeyron equation (Equation 6.142) is used to correct the vapor pressures. The relative volatility is then calculated as the ratio of *K* factors.

$$\mathrm{Ln}\left(\frac{p^*_{1,i}}{p^*_{2,i}}\right) = \frac{\Delta H_i}{R}\left(\frac{1}{T_2} - \frac{1}{T_1}\right) \quad 6.142$$

$$\alpha = \frac{K_i}{K_{ref}} \tag{6.143}$$

$$K_i = \frac{p_{2,i}^*}{P} \tag{6.144}$$

Using a safety factor of 10% on the number of trays, the actual number of stages, N_{actual}, is calculated using Equation 6.145. ε_{tray} is the efficiency of the tray, which is between 60 and 90 %.

$$N_{actual} = 1.1N_{min}/\varepsilon_{tray} \tag{6.145}$$

$$60\% \leq \varepsilon_{tray} \leq 90\% \tag{6.146}$$

The diameter of the absorber is calculated using Equation 6.147, where *v* is the vapor flow of CO_2, and *u* is the gas velocity of the absorber. The ratio of the absorber length to diameter is maintained between 2.5 and 5.

$$D_{abs} = (\frac{4v}{\pi u})^{0.5} \tag{6.147}$$

$$2.5 \leq \frac{L_{abs}}{D_{abs}} \leq 5 \tag{6.148}$$

The cost of the absorber is evaluated using equations 6.149-6.153. The costing utilizes the volume of the absorber, V_{abs}.

$$Abslog C_p^0 = 3.4974 - 0.4485\log(V_{abs}) + 0.1074[\log(V_{abs})]^2 \tag{6.149}$$

$$AbsC_p^0 = 10^{AbslogC_p^0} \quad 6.150$$

$$AbslogF_{p,abs} = \frac{\frac{PD_{abs}}{2[850 - 0.6(P)} + 0.00315}{0.0063} \quad 6.151$$

$$Cbm_{abs} = AbsC_p^0 \left(2.25 + \left(1.82 * 1 * F_{p,abs}\right)\right) \quad 6.152$$

$$Op^{abs} = F_{CO_2} * M_{CO_2} * C_{abs} * H_t \quad 6.153$$

The PSA unit is used to purify hydrogen. It requires 30 bars to carry out hydrogen adsorption, while it is desorbed at 1 bar. The low hydrogen content syngas is considered to maintain 30 bars at the exit of the PSA. Then, this flow is recycled to the reactor and/or purged to avoid methane buildup in the process. The pure hydrogen flow is not considered in the cost calculation. Equations 6.154-6.165 represent the mass balances, sizing, and PSA costing.

$$F_i^{PSA,out} = F_i^{PSA,in} \qquad \forall i \ \backslash\{H_2\} \quad 6.154$$

$$F_{H_2}^{PSA,out} = F_{H_2}^{PSA,in} - F_{H_2} \quad 6.155$$

$$F_{H_2}^{PSA,out} = 0.1F_{H_2}^{PSA,in} \quad 6.156$$

$$Power_{PSA} = \left(\frac{\gamma}{\gamma - 1}\right)\eta^{-1}R_g T_{PSA}\sum_{i=1}^{n} F_{ij}^{PSA}\left[(Pr)^{\left(\frac{\gamma}{\gamma-1}\right)} - 1\right] \quad 6.157$$

$$V_{PSA} = \hat{Q}_{gas} \times t_{cycle} \quad 6.158$$

$$2\ minutes \leq t_{cycle} \leq 10\ minutes \quad 6.159$$

$$2.5 = \frac{L_{PSA}}{D_{PSA}} \leq 5 \quad 6.160$$

$$PSAlogC_p^0 = 3.4974 - 0.4485\,log(V_{PSA}) + 0.1074[log\ (V_{PSA})]^2 \quad 6.161$$

$$PSAC_p^0 = 10^{PSAlogC_p^0} \quad 6.162$$

$$PSAlogF_{p,PSA} = \frac{\frac{PD_{PSA}}{2[850 - 0.6(P)} + 0.00315}{0.0063} \quad 6.163$$

$$Cbm_{PSA} = PSAC_p^0\left(2.25 + \left(1.82 * 1 * F_{p,PSA}\right)\right) \quad 6.164$$

$$Op^{Comp} = E_{cost} * Power_i^{PSA} * H_t \quad 6.165$$

Equation 6.166 and Equation 6.167 represent the purge and recycle stream mass balances. The amount of recycle is dependent on the recycle ratio, R_{cr}.

$$F_i^{recycle} = R_{cr} F_i^{PSA,out} \tag{6.166}$$

$$F_i^{purge} = (1 - R_{cr}) F_i^{PSA,out} \tag{6.167}$$

$$0.4 \leq R_{cr} \leq 0.9 \tag{6.168}$$

After this last alternative, hydrogen is obtained from the process. The timing of when the cost data are presented can vary, leading to the need to transform this cost information into a current and precise representation. When relying on historical records or published relationships for pricing details, it is crucial to have the capability to adjust these costs to accommodate evolving economic circumstances, such as inflation. This can be accomplished by employing the following formula:

$$C_2 = C_1 \left(\frac{I_2}{I_1}\right) \tag{6.169}$$

The total annualised cost (TAC) of the system is calculated using Equation 6.170

$$TAC = Capital\ cost \times AF + \sum_j Op^j + \sum_i raw_i \tag{6.170}$$

$$AF = \frac{IR(IR+1)^{years}}{(IR+1)^{years} - 1} \tag{6.171}$$

6.5. Objective function

The primary objective of the optimisation is to maximise the TAC. The objective function can be formulated as follows:

$$Min: TAC = Capital\ cost \times AF + \sum_{j} Op^{j} + \sum_{i} raw_{i} \qquad 6.172$$
$$subject\ to\ constraints$$

6.6. Heat integration

Pinch Analysis technology is applied to design minimum energy targets and minimize the utility required. The same procedure as in section 3.7 is followed.

6.7. Application of the process design and optimization model

The applicability of the model is demonstrated using the steam reforming process in Figure 6.1. The conditions of the feed streams are set to 1 kmol/s of methane, and the feed ratio varies between 1 and 6 for methane and steam. Steam enters the process at 10 bar, selected as the process pressure. The model determines the unit sizes, the feed ratio, and reactor conditions that minimize the TAC. The model considers the thermodynamic and kinetic parameters of the steam reforming reactions and the reactor design variables.

The model consists of 2222 equations and 1534 variables, with 10 binary variables and 1 integer variable. The GAMS modelling platform is used to implement the model and solve it using the ANTIGONE solver. The results obtained from the model are summarized in Table 6.1, which illustrates the key findings from the model that minimizes the TAC. The reactor is analyzed using key performance indicators of the steam reforming process. These performance indicators include:

1. **Hydrogen Yield:** The amount of hydrogen produced per unit of methane feed. It is a crucial parameter for evaluating the efficiency of the steam reforming process.

$$Y_{H_2} = \frac{F^{out}_{H_2,k=K}}{F^{out}_{CH_4,k=1} - F^{out}_{CH_4,k=K}} \qquad \forall k \in K \tag{6.173}$$

2. **Methane Conversion:** The percentage of methane that undergoes conversion to other products, including hydrogen and carbon monoxide.

$$X^{Overall}_{CH_4} = \frac{F^{Fresh\ feed}_{methane} - F^{purge}_{methane}}{F^{Fresh\ feed}_{methane}} \qquad \forall i \in I, k \in K \tag{6.174}$$

3. **Hydrogen Selectivity:** The efficiency of converting a specific reactant, like methane, into hydrogen while minimizing undesirable byproducts.

$$S_{H_2} = \frac{F^{out}_{H_2,k=K}}{F^{out}_{CO_2,k=K}} \qquad \forall k \in K \tag{6.175}$$

Table 6.1: Results Summary for the steam reforming process

Variables	Value
Hydrogen produced (kg/s)	3.54
Feed ratio (S/C)	3
Carbon dioxide absorbed (kg/s)	18.22
Carbon dioxide emitted (kg/s)	0.066
Methane conversion	
Single pass (%)	24
Overall (%)	48
Selectivity (mol H_2/molCO_2)	4.70
Yield (mol H_2/molCH_4)	4.14
Reformer conditions	
Temperature (K)	908
Pressure (bar)	10
Compression	
Total compression power (kW)	8126

Number of stages	3
Unit sizing	
Preheater area (m^2)	759
Reformer volume (m^3)	10.50
Post cooler area (m^2)	803
Flash drum volume (m^3)	303
Absorber volume (m^3)	5.83
PSA volume (m^3)	391
Binaries	
Ys	1
Yw	0
Net utility demands (Before heat integration)	
Heating demand (kW)	113304
Cooling demand (kW)	157333
Net utility demands (After heat integration)	
Heating demand (kW)	4630.60
Cooling demand (kW)	2277.80
Total Annualized Cost	
Before heat integration (million $/year)	255
After heat integration (million $/year)	214

The optimal steam-to-carbon feed ratio was found to be 3:1. A temperature of 908 K was found to be optimal for the process. The single-pass conversion of methane was observed before the recycle stream was introduced. The single pass conversion decreases from 30% to 24%. Generally, as the steam-to-carbon ratio increases, the conversion increases. However, the ratio decreases as the recycle stream is introduced because the concentration of methane increases.

On the other hand, the overall conversion of methane increases as more methane is retained in the process and less is removed from the process. The overall conversion of methane increases from 30% to 48% due to recycling. Given that the steam reforming process is endothermic, the low conversions are justified due to the low temperature of 908 K, which was optimal for decreasing the TAC. The optimal recycle ratio that minimizes the TAC is found to be 0.65.

A three-stage compression strategy emerged as the optimal configuration for minimizing total annualized costs for the process. This finding underscores the significance of careful optimization in process design and operational decisions, with the potential to lead the steam reforming process towards substantial cost savings and enhanced energy efficiency. As steam reforming processes continue to grapple with the challenges of cost control and sustainability, the implications of the finding provide a clear path for improved decision-making in stagewise compression processes, ultimately contributing to a more economically and environmentally sustainable future.

The model selected a flowsheet with no separate WGS reactor but rather just the reaction taking place in the steam reformer. The WGS reaction plays a critical role in enhancing the produced syngas' quality, purity, and environmental friendliness while allowing for better control and efficiency in hydrogen production. However, on a cost basis, having a stand-alone WGS reactor increases the capital and utility costs of the process. Traditionally, the water-gas shift reaction is executed in a separate reactor downstream of the steam reformer. This method incurs additional capital and operational expenses, including procuring and installing a distinct reactor, increased maintenance requirements, and additional space within the overall production facility. Moreover, the need for heat integration and management between the two reactors introduces complexities in process control and optimization, further elevating operational costs.

The absorber efficiency was calculated to be 99%. A highly efficient CO_2 absorber offers numerous benefits in industrial processes. It substantially reduces CO_2 emissions, aiding climate change mitigation and regulatory compliance. A high efficiency enhances process economics by reducing energy consumption, making carbon capture more economically viable. Less CO_2 is released into the atmosphere, thus making the process more environmentally friendly.

Pinch analysis assessed potential efficiency improvements in the process by optimizing utility usage. As presented in Table 6.1, comparing utility requirements before and after heat integration reveals significant opportunities for energy savings. 96% and 71%

savings were found for the heating and cooling demands, respectively. This optimization translates into reduced utility expenses, directly affecting overall process costs. Integrating various streams within the process creates a clear potential to minimize the expenditures associated with procuring external utilities, contributing to cost-effectiveness and improved sustainability. Pinch analysis unveils avenues to enhance process efficiency and economize resource utilization, positively impacting the bottom line.

The final flowsheet is then determined, as shown in Figure 6.3.

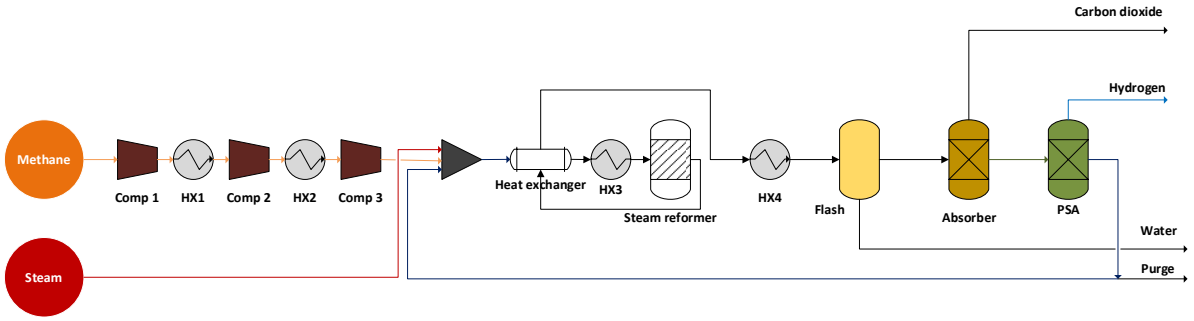

Figure 6.3: Final optimized steam reforming flowsheet

6.8. Conclusion

This chapter has taken a significant step towards optimizing the hydrogen production pathway, explicitly focusing on steam reforming. The developed optimization model, which considers many operational constraints and economic factors, is a valuable tool for enhancing the efficiency and cost-effectiveness of hydrogen production processes. The application of this model to a practical scenario with a methane feed of 1 kmol/s has yielded valuable insights. Notably, the findings suggest that an S/C feed ratio of 3:1 and a reactor temperature of 908 K are optimal conditions for minimizing the TAC. Furthermore, incorporating the WGS reaction within the steam reformer, rather than employing a standalone WGS reactor, emerges as a more cost-effective strategy. Stagewise compression with three stages has also been identified as the most optimal compression approach. These findings contribute to a deeper understanding of steam

reforming and offer practical recommendations for industry practitioners seeking to improve hydrogen production efficiency while minimizing costs.

6.9. References

Choi, Y., & Stenger, H. G. (2003). Water gas shift reaction kinetics and reactor modeling for fuel cell grade hydrogen. Journal of Power Sources, 124(2), 432–439. https://doi.org/10.1016/S0378-7753(03)00614-1

Ding, O. L., & Chan, S. H. (2008). Water-gas shift reaction - A 2-D modeling approach. International Journal of Hydrogen Energy, 33(16), 4325–4336. https://doi.org/10.1016/j.ijhydene.2008.05.087

Halabi, M. H., de Croon, M. H. J. M., van der Schaaf, J., Cobden, P. D., & Schouten, J. C. (2008). Modeling and analysis of autothermal reforming of methane to hydrogen in a fixed bed reformer. Chemical Engineering Journal, 137(3), 568–578. https://doi.org/10.1016/j.cej.2007.05.019

Hoang, D. L., Chan, S. H., & Ding, O. L. (2005). Kinetic and modelling study of methane steam reforming over sulfide nickel catalyst on a gamma alumina support. Chemical Engineering Journal, 112(1–3), 1–11. https://doi.org/10.1016/j.cej.2005.06.004

Sato, T., Kurosawa, S., Smith, R. L., Adschiri, T., & Arai, K. (2004). Water gas shift reaction kinetics under noncatalytic conditions in supercritical water. Journal of Supercritical Fluids, 29(1–2), 113–119. https://doi.org/10.1016/S0896-8446(03)00049-4

Taji, M., Farsi, M., & Keshavarz, P. (2018). Real time optimization of steam reforming of methane in an industrial hydrogen plant. International Journal of Hydrogen Energy, 43(29), 13110–13121. https://doi.org/10.1016/j.ijhydene.2018.05.094

CHAPTER 7

CONCLUSION

In conclusion, the dissertation introduces a systematic framework that effectively narrows the myriad possibilities for hydrogen production, reducing them from an initial 19 to a mere 3 plausible alternatives, marking an impressive 84% decrease in the search space. This comprehensive analysis method is constructed by establishing a superstructure, streamlined through the utilization of the Simultaneous Evaluation of Criteria and Alternatives (SECA) technique. The critical component involves the creation of a robust Reaction Pathway Database (RPD), which is meticulously assessed against well-defined criteria. The final rankings within this condensed search space are ascertained by employing a performance index, considering factors such as availability, cost implications, and environmental considerations.

Drawing upon the extensive data gathered and analyzed within the RPD, a clear frontrunner emerges as the most promising route for hydrogen production. Steam reforming is the most viable method among the numerous pathways explored. This exceptional viability is underpinned by the precise optimization of operational conditions, namely an operating temperature of 1230 K and a pressure of 10 bar. The choice of steam reforming as the preferred pathway is rooted in its exceptional performance across several critical parameters. First and foremost, it exhibits outstanding efficiency in hydrogen generation, making it a standout choice for large-scale industrial applications. The operating temperature of 1230 K and pressure of 10 bar create the ideal environment for the reforming reactions to occur with maximum yield and efficiency, resulting in a high hydrogen production rate.

Additionally, its adaptability and compatibility with carbon capture technology set steam reforming apart from alternative methods. Incorporating carbon capture technology within the steam reforming process adds a layer of environmental responsibility and sustainability that elevates its feasibility compared to other potential pathways. This enhancement is crucial in the contemporary drive towards reducing greenhouse gas emissions and mitigating climate change.

Furthermore, through rigorous optimization of the steam reforming pathway utilizing reaction kinetics, the optimal operating conditions are determined to be 908 K and 10 bar pressure, achieving an impressive 48% methane conversion rate. The optimal pre-reactor configuration is revealed to be a three-stage compressor unit operation, followed by a pre-heater step post-mixing the methane and steam fresh feed. The ideal feed steam-to-carbon ratio is determined to be 3:1, with an optimal recycle ratio of 0.65. Incorporating the water-gas shift (WGS) reaction within the steam reformer itself, rather than opting for the conventional approach of utilizing a standalone WGS reactor, emerges as a highly compelling and economically advantageous strategy. This innovative method ingeniously merges two vital steps of hydrogen production into a single streamlined process, yielding many benefits that significantly impact cost-effectiveness and operational efficiency. However, it is crucial to emphasize that the outcomes presented within this dissertation are inherently contingent upon the total annualized costs, which should be critically considered in real-world applications.

One of the notable strengths of this framework lies in its adaptability, as it follows a systematic, stepwise procedure inherently tied to the development of the RPD. This means the RPD can be easily modified to include alternative pathways, rendering this framework versatile beyond hydrogen production alone. Furthermore, the significant reduction in the exploration space for reaction pathways ensures more efficient resource allocation. It empowers decision-makers with knowledge of the most efficient and viable pathway early, pre-empting the need for extensive design and optimization processes, thereby saving valuable time and resources. This systematic approach holds substantial promise for enhancing hydrogen production and the efficiency of process

design and optimization in various domains. Integrating this systematic approach into local, national, and global contexts can drive advancements in hydrogen production, contribute to sustainability goals, and foster economic and technological progress.

APPENDICES

8.1. Appendix A: List of symbols

Symbol	Value represented	Symbol	Value represented
ΔH	Amount of heat evolved or absorbed in the reaction at constant pressure [kJ/mol]	$\Delta H_{rxn}(T)$	Enthalpy of the reaction at a specific temperature [kJ/mol]
G_{total}	Total Gibbs free energy to be minimized [kJ/mol]	$\Delta\widehat{H}_{i,phase\ change}$	Enthalpy requited for phase change [kJ/mol]
n_i	Number of moles [mol]	ξ	Extent of reaction
$\bar{G}_i$	Partial molar Gibbs free energy [kJ/mol]	$F_{ij}^{abs\ out}$	Flow out of the absorber for component j in process i [kmol/s]
μ_i	Chemical potential	$F_{ij}^{abs\ in}$	Flow into the absorber for component j in process i [kmol/s]
G_i^0	Standard Gibbs free energy [kJ/mol]	$F_{i,CO_2}^{abs\ out}$	Flow of CO_2 out of the absorber for component j in process i [kmol/s]
R	Universal gas constant [kJ/(mol K)]	$F_{i,CO_2}^{abs\ in}$	The flow of CO_2 into the absorber for process i [kmol/s]
T	Temperature [K]	F_{i,CO_2}	Amount of the absorbed CO_2 for CO_2 in

			process i [kmol/s]
P	The pressure of the system [bar]	F_{max}	Maximum allowable flow [kmol/s]
$n_{total,gas\ product}$	The total amount of moles in the mixture [mol]	$F_{ij}^{flash\ out}$	Flow out of the flash vessel for component j in process i [kmol/s]
a_{ij}	Number of gram atoms of the element	$F_{ij}^{flash\ in}$	Flow into the flash vessel for component j in process i [kmol/s]
b_j	Total number of atoms of the element	F_{i,H_2O}	Amount of water flashed in process i [kmol/s]
M	Number of elements present in the reacting mixture	$F_{H_2O}^{flash\ in}$	The flow of water into the flash vessel for process i [kmol/s]
ΔG_i^o	Standard Gibbs energy of formation	$F_{ij}^{PSA\ out}$	Flow out of the PSA for component j in process i [kmol/s]
ΔH_i^o	Standard enthalpy of formation [kJ/mol]	$F_{ij}^{PSA\ in}$	Flow into the PSA for component j in process i [kmol/s]
x_{ij}^N	Normalised performance value of the i-th alternative on the j-th criterion	$F_{i,H_2}^{PSA\ out}$	Flow of H_2 out of the PSAin process i [kmol/s]

w_j	Weight of the criterion	$F_{i,H_2}^{PSA\ in}$	Flow of H_2 into the PSAin process i [kmol/s]
σ_j^N	The standard deviation of each element	F_{i,H_2}	Amount of hydrogen absorbed in process i [kmol/s]
π_j^N	Degree of conflict between the *j*-th criterion and other criteria	raw_i	Total cost of raw materials in process i [$/kmol]
ε	A small positive parameter equal to 0.001 is a lower bound for criteria weights.	δ_{ij}	The cost of each component that is fed to process i [$/kmol]
β	Parameter used to merge the objective function and minimize the deviation from reference points	F_{ij}^0	The amount of feed required for each process [kmol/s]
P_i^{out}	Outlet pressure [bar]	t_h	Number of hours of the plant per year [hours/year]
P_i	Inlet pressure in [bar]	C_p^o	The purchased ambient cost at standard conditions [$]
ΔP_i	Change in pressure [bar]	A	Capacity of the unit
P_{max}	Maximum pressure possible [bar]	K_1, K_2 , and K_3	Purchased cost constants
$Power_i^{comp}$	Power of the compressor [kW]	F_p	Pressure factor
γ	Heat capacity ratio	C_1, C_2, and C_3	Pressure factor constants

η	Compressor efficiency	D	Diameter (m)
R_g	Universal gas constant	C_{BM}	Bare module costs of the unit operations [$]
T_{feed}	Inlet stream temperature [K]	F_{BM}	Bare module factor
F_{ij}^{comp}	Feed to the compressor [kmol/s]	B_1 and B_2	Bare module cost constants
T_n^{out}	Temperature out of the compressor [K]	F_M	Material factor
n	Number of moles [mol]	ΔT_{lm}	Logarithmic temperature difference [°C]
$\hat{Q}_n^{comp}$	Cooling required for the intercoolers [kW]	U	Overall heat transfer
$C_p/C_{p,j}$	Heat capacity of the components [kJ/K]	Q	Heat transferred [kW]
T_{mix}	Temperature of the mixture [K]	t_2	Cold fluid inlet temperature [°C]
$\hat{Q}_{hx}$	Heating required for the reactor [kW]	t_1	Cold fluid outlet temperature [°C]
$\bar{H}_{ij}^0$	Enthalpy flow of the inlet [kJ/mol]	T_1	Hot fluid outlet temperature [°C]
$\bar{H}_{ij}$	Enthalpy flow of the outlet [kJ/mol]	T_2	Hot fluid inlet temperature [°C]
F_{ij}^{out}	Flow out of the reactor [kmol/s]	Op_{abs}	Absorber operating costs [$]
$F_{methane}^0$	Initial methane feed [kmol/s]	Op_{ut}	Utility costs [$]
X_i	The ratio of component *j* exiting process *i* and the	Ut_i	Cost of each utility [$/kW]

	fresh feed of the limiting reagent		
TAC	Total Annualized Cost	ΔT	Temperature difference [°C]
Cap_i	Capital cost of process i [$]	C_{hot}	Heat capacity of the hot stream
AF	Annualizing factor	C_{cold}	Heat capacity of the cold stream
IR	Interest rate	ns	Number of stages
$LCOH$	Levelized Cost of Hydrogen [$/kg]	$Power_{total}^{comp}$	Total Power of the compression stage
$mass_{hydrogen\ produced}$	Mass of hydrogen produced [kg/year]	Pr	Pressure ratio
GWP	Global Warming Potential	E_{cost}	Cost of electricity
$Adj\ T$	Adjusted temperatures [°C]	H_t	Total hours per year
$C_{coolant}$	Cost of coolant [$/kg]	$F_i^{recycle}$	The amount recycled for component i [kmol/s]
T_{smr}	Temperature of the reformer [°C]	$F_i^{reactor}$	Feed to the reactor of component i [kmol/s]
$m_{heating\ medium}$	Mass of heating medium [kg/s]	y_i	The molar fraction of component i
$C_{heating\ medium}$	Cost of heating medium [$/kg]	p_i	Partial pressure of component i [bar]
$F_i^{fresh\ feed}$	Fresh feed to the process of component i [kmol/s]	r_i	Rate of disappearance or appearance of component i
η_i	Effectiveness factors	W	Weight of catalyst [kg]

R_n	Reaction rates [mol/kg catalyst s]	V	Volume of reactor (m^3)

8.2. Appendix B: Costing procedure (constants and graphs)

This appendix details the constants and graphs required for the costing procedure detailed in sections 3.6.2 and 6.4.

8.2.1.Purchased equipment cost constants

Table 8.1: Equipment cost data and applicable bounds

Equipment	Description	K_1	K_2	K_3	Min	Max
Compressors (kW)	Centrifugal, Axial & Reciprocating	2.2897	1.3604	-0.1027	450	3000
	Rotary	5.0355	-1.8002	0.8253	18	950
Heat Exchangers (m^2)	Scraped Wall	3.7803	0.8569	0.0349	2	20
	Teflon Tube	3.8062	0.8924	-0.1647	1	10
	Bayonet	4.2768	-0.0495	0.1431	10	1000
	Floating Head	4.8306	-0.8509	0.3187	10	1000
	Fixed Tube	4.3247	-0.3030	0.1634	10	1000
	U-Tube	4.1884	-0.2503	0.1974	10	1000
	Kettle Reboiler	4.4646	-0.5277	0.3955	10	100
	Double Pipe	3.3444	0.2745	-0.0472	1	10
	Multiple Pipe	2.7652	0.7282	0.0783	10	100
	Flat Plate	4.6656	-0.1557	0.1547	10	1000
	Spiral Plate	4.6561	-0.2947	0.2207	1	100
	Air Cooler	4.0336	0.2341	0.0497	10	10000
	Spiral Tube	3.9912	0.0668	0.2430	1	100
Packing (m^3)	Loose	2.4493	0.9744	0.0055	0.03	628
Process Vessels (m^3)	Horizontal	3.5565	0.3776	0.0905	0.1	628
	Vertical	3.4974	0.4483	0.1074	0.3	520
Pumps (kW)	Reciprocating	3.8696	0.3161	0.1220	0.1	200
	Positive Displacement	3.4771	0.1350	0.1438	1	100
	Centrifugal	3.3892	0.0536	0.1538	1	300
	Autoclave	4.5587	-0.7014	0.0020	1	15

Reactor (m^3)	Fermenter	4.1052	-0.4680	-0.0005	0.1	35
	Inoculum Tank	3.7957	-0.5407	0.0160	0.07	1
	Jacketed Agitated	4.1052	-0.4680	-0.0005	0.1	35
	Jacketed Non-agitated	3.3496	-0.2765	0.0025	5	45
	Mixer/Settler	4.7116	-0.5521	0.0004	0.04	60
Towers (m^3)	Tray and Packed	3.4974	0.44885	0.1074	0.3	520
Trays (m^2)	Sieve	2.9949	0.4465	0.3961	0.07	12.30
	Valve	3.3322	0.4838	0.3434	0.70	10.50
	Demisters	3.2353	0.4838	0.3434	0.70	10.50
Turbines (kW)	Axial Gas	2.7051	1.4398	-0.1776	100	4000
	Radial Gas/ Liquid Expanders	2.2476	1.4965	-0.1618	100	1500

8.2.2.Pressure factors for non-pressure-driven unit operations

Table 8.2:Pressure factors for process equipment

Equipment	Description	C_1	C_2	C_3	Range (barg)
Compressors	Centrifugal, Axial, Rotary and Reciprocating	0	0	0	-
Heat Exchangers	Scraped Wall	0	0	0	P < 40
		0.6072	-0.9120	0.3327	40 < P < 100
		13.1467	-12.6574	3.0705	100 < P < 400
	Teflon Tube	0	0	0	P < 15
	Bayonet, Fixed Tube Sheet, Floating Head, Kettle Reboiler, U-Tube (Shall & Tube)	0	0	0	P < 5
		0.03881	-0.11272	0.08183	5 < P < 140
	Bayonet, Fixed Tube Sheet, Floating Head, Kettle Reboiler, U-tube (Tube)	0	0	0	P < 5
		-0.00164	-0.00627	0.0123	5 < P < 40

	Double Pipe and Multiple Pipe	0	0	0	P < 40
		0.6072	-0.9120	0.3327	40 < P < 100
		13.1467	-12.6574	3.0705	100 < P < 300
	Flat Plate and Spiral Plate	0	0	0	P < 19
	Air Cooler	0	0	0	P < 10
		-0.1250	0.15361	-0.02861	10 < P < 100
	Spiral Tube (Shell & Tube)	0	0	0	P < 150
		-0.4045	0.1859	0	150 < P < 400
	Spiral Tube (Tube)	0	0	0	P < 150
		-0.2115	0.09717	0	150 < P < 400
Packing	Loose	0	0	0	-
Pumps	Reciprocating	0	0	0	P < 10
		-0.245382	0.259016	-0.01363	10 < P < 100
	Positive Displacement	0	0	0	P < 10
		-0.245382	0.259016	-0.01363	10 < P < 100
	Centrifugal	0	0	0	P < 10
		-0.3935	0.3957	-0.00226	10 < P < 100
Trays	Sieve, Valve, and Demisters	0	0	0	-
Turbines	Axial Gas, Radial Gas, Liquid Expanders	0	0	0	-

8.2.3.Bare module and material factors for heat exchangers, process vessels, and pumps

The following table details the identification numbers associated with each unit operation and is utilized in association with Figure 8.1.

Table 8.3: Identification numbers for material factors for heat exchangers, process vessels, and pumps

Identification Number	Equipment	Description	Material of Construction
1	Heat Exchanger	Double pipe, multiple pipe, fixed tube sheet, floating head, U-Tube, bayonet, kettle	CS-Shell/CS-Tube
2			CS-Shell/Cu-Tube
3			Cu-Shell/Cu-Tube
4			CS-Shell/SS-Tube
5			SS-Shell/SS-Tube
6		reboiler, scraped wall, and spiral tube	CS-Shell/Ni Alloy Tube
7			Ni Alloy Shell/Ni Alloy Tube
8			CS-Shell/Ti-Tube
9			Ti-Shell/Ti-Tube
10		Air Cooler	CS Tube
11			Al Tube
12			SS Tube
13		Flat Plate and Spiral Plate	CS (in contact with fluid)
14			Cu (in contact with fluid)
15			SS (in contact with fluid)
16			Ni Alloy (in contact with fluid)
17			Ti (in contact with fluid)
18	Process Vessels	Horizontal and Vertical (Including Towers)	CS
19			SS Clad
20			SS
21			Ni Alloy Clad
22			Ni Alloy
23			Ti Clad
24			Ti
25		Reciprocating	Cast Iron
26			Carbon Steel
27			Cu Alloy
28			SS
29			Ni Alloy
30			Ti

31	Pumps	Positive Displacement	Cast Iron
32			Carbon Steel
33			Cu Alloy
34			SS
35			Ni Alloy
36			Ti
37		Centrifugal	Cast Iron
38			Carbon Steel
39			SS
40			Ni Alloy

Figure 8.1 utilizes the identification numbers in Figure, with each number being associated with its material factor based on the type of equipment in question and the material from which it is constructed.

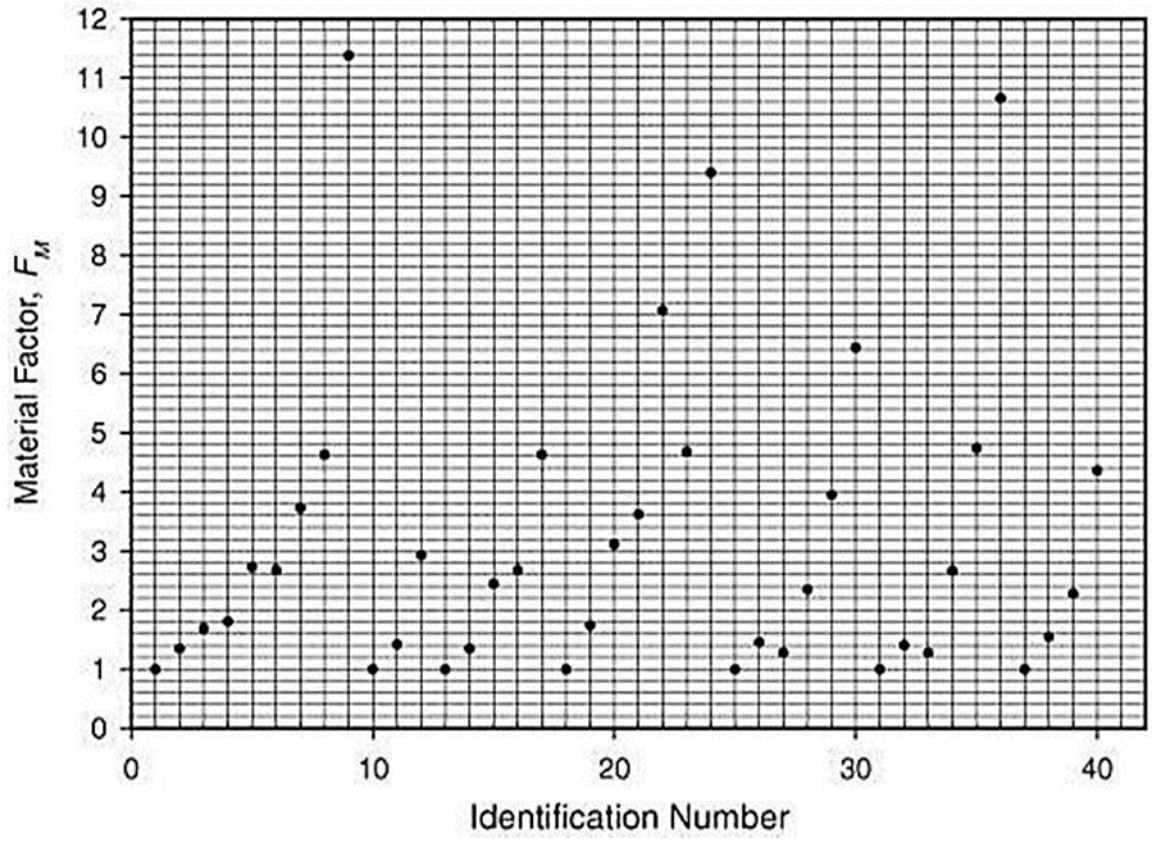

Figure 8.1: Material factors for the equipment in Table 8.3

Table 8.4 shows the bare module cost factors for the equipment.

Table 8.4:Constants for bare module factors

Equipment	Description	B_1	B_2
Heat Exchanger	Double pipe, multiple pipes, scraped wall, and spiral tube	1.74	1.55
	Fixed tube sheet, floating head, U-tube, bayonet, kettle reboiler and Teflon tube	1.63	1.66
	Air cooler, spiral plate, and flat plate	0.96	1.21
Process Vessels	Horizontal	1.49	1.52
	Vertical (including towers)	2.25	1.82
Pumps	Reciprocating, Positive Displacement, and Centrifugal	1.89	1.35

The bare module factor for the remaining process equipment is shown in Table 8.5.

Table 8.5: Identification numbers for material factors for the rest of the unit operations

Identification Number	Equipment	Description	Material of Construction
1	Compressors	Centrifugal	CS
2			SS
3			Ni Alloy
4		Axial	CS
5			SS
6			Ni Alloy
7		Rotary	CS
8			SS
9			Ni Alloy
10		Reciprocating	CS
11			SS
12			Ni Alloy
57	Power Recovery Equipment	Turbines	CS
58			SS
59			Ni Alloy
60	Trays and Demister Pads	Sieve and Valve Trays	CS
61			SS
62			Ni Alloy
63		Demister Pads	SS
64			Fluorocarbon
65			Ni Alloy
66	Tower Packing	Packing	Metal (304SS)
67			Polyethylene
68			Ceramic

The material factors associated with each identification number given in Table 8.5 are shown in Figure 8.2.

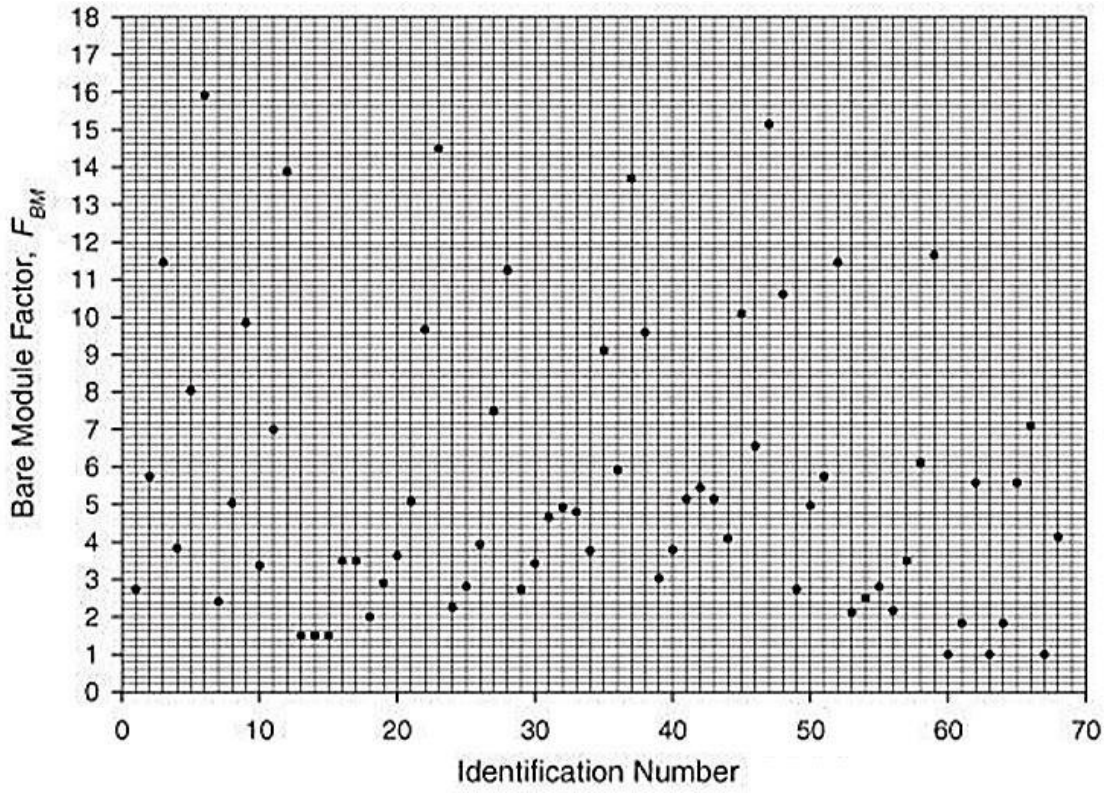

Figure 8.2: Material factors for the equipment in Table 8.5

8.3. Appendix C: MATLAB code for heat integration

This appendix details the MATLAB code utilized for heat integration adapted from Tewari et al. (2015).

```
%part-1
clear;% clear the workspace
clc;% clear the command window
hi=input('enter the hot fluid stream inlet temperature in
column=\n');%inlet of hot fluid streams
hi=input('enter the  hot fluid stream outlet temperature in
column=\n');%outlet of hot fluid streams
ci=input('enter the cold fluid stream inlet temperature in
column=\n');%inlet of cold fluid streams
ci=input('enter the cold fluid stream outlet temperature in
column=\n');%outlet of cold fluid streams
%Q(heat transfer) or C(heat capacity) which is given,it take it
QC=input(' enter the values of heat capacity or heat
transfer(1=Q[qh,qc](heat transfer))&(2=C[shh,shc](HeatCapacity)) 1/2= \n');
if (QC==1);
qh=input('enter the hot fluid stream heat transfer in column=\n');%heat
transfer in hot fluid streams
[nnd1,nnd2]=size(qh);
for i=1:nnd1
if (qh(i)<0)
qh(i)=-qh(i);
else
qh(i)=qh(i);
end
end
shh=qh./(hi-ho);%calculating the heat capacity of hot fluid streams
qc=input ('enter the cold fluid stream heat transfer in column=\n');%heat
transfer in cold fluid streams
shc=qc./(co-ci);%calculating the heat capacity of cold fluid streams
else(QC==2);
shh=input ('enter hot fluid stream heat capacity in column=\n');%heat
capacity of hot fluid streams
shc=input ('enter cold fluid stream heat capacity in column=\n');%heat
capacity of cold fluid streams
end;
sh=[shh;shc];%%combine heat capacity of hot and cold fluid streams
%part 2
dt=input('dt=')% entering the value of delta T minimum
hs=[hi ho];%combining the  inlet & outlet hot streams
ha=[hs-dt];%adjusted hot streams temperatures
cs=[ci co];%combining inlet & outlet hot streams
ca=cs;%adjusted hot stream temperature(no change in cold stream)
[hp1,hp2]=size(ha);%determining the size of Matrix
[hp3,hp4]=size(ca);%determining the size of Matrix
hp=hp1+hp3;%total hot and cold stream
at=[ha;ca];%combine adjusted hot & cold streams temperatures
```

```
shat=[sh at];
%combining the heat capacities & the adjusted hot & cold streams
temperatures
t=[at(:)];
%adjusted hot & cold streams temperatures in one column
at1s=sort(t,'descend');
%sorting the adjusted hot & cold streams temperatures in
%descending order
[sortedValue_t ,t_ranked] = sort(t,'descend');
%sorting of adjusted temperature in descending order in one column
%& give a rank row wise
[~, ~, forwardrank] = unique(t);
%give a unique ranking in ascending order
rank = max(forwardrank) - forwardrank + 1;
%Matrix operation for ranking in descending order
rr = reshape(rank,(length(rank)/2),2);%reshape the rank
c =[shat rr];
%all values arrange in table form contain heat capacity,
%adjusted temperature and rank
%part-3
h=[sh;sh];%matrix operation
n=max(rank);%largest element of rank
[sum1,sum2]=size(rank);%determine the size of Matrix
[sum3,sum4]=size(c);%determine the size of Matrix
for j=1:n-1
x=0;%initializing the value for row
c1=0;%initializing the value for hot stream
c3=0;%initializing the value for cold stream
for i1=1:sum1
if(rank(i1,1) == j)
temp= t(i1,1);
elseif (rank(i1,1) == j+1)
f=t(i1,1);
end;
end;
%this loop stores a value of temperature corresponding
%rank in temp & f in ascending order
for i=1:sum3
x=x+1;%for increment
if(c(i,2) < c(i,3))%check inlet adjusted temperature is less than
%the outlet adjusted temperature
if (( c(i,2)>=f && c(i,3)<=temp) || (c(i,2)<=f && c(i,3)>=temp))
if (((x>=1 && x<=hp1) || (x>=(hp+1) && x<=(hp+hp1))))
%check range in hot stream
c1=c1+h(i,1);
else
c3=c3+h(x,1);
end ;
end;%check the range temperature in every row and stores the value of
%hot stream in c1 and cold stream in c3
else
if (( c(i,2)>=temp && c(i,3)<=f) || (c(i,2)<=temp && c(i,3)>=f))
if (((x>=1 && x<=hp1) || (x>=(hp+1) && x<=(hp+hp1))))
```

```
%check range in hot stream
c1=c1+h(i,1);
else
c3=c3+h(x,1);
end ;
end ;
%check the range temperature in every row and stores the value of
%hot stream in c1 and cold stream in c3
end
end
c3=-c3;
dh(j)=(c1+c3)*(temp-f);%formula for calculate heat transfer in Matrix form
H=dh';%transpose of matrix
end
%part-4
m=0;%initilize the value of q
for k=1:n-1
m=m+H(k,1);
d(k)=m;
dd=d';
end
%sum the values of all temperature intervals assume initially heating
%load is 0
kt=min(dd);%to find least element in dd
if (kt<0)%check kt is negative
kt4=-kt;
for f=1:n-1
kt4=kt4+H(f,1);
g(f)=kt4;
gg=g';
end
%sum the values of all temperature intervals assume initially heating
%load is kt4
[pko1,pko2]=size(gg);%determine the size of matrix
for w=1:pko1
if (gg(w,1)>=(-1e-8) && gg(w,1)<=(1e-8))
%find the element in gg tends to zero
kt3=w+1;
end
end
for y=1:sum1
if (rank(y,1)==kt3)%find the element in rank which is equal to kt3
kt1=y;%element no. which equal to kt3
coldpinch=t(kt1,1)
hotpinch=coldpinch+dt
minheatingload=-kt
mincoolingload=gg(pko1,1)
break;
end;
end;%got the value of cold pinch,hot pinch,minimum heating load,
%minimum cooling load
elseif (kt>0)
fprintf('no pinch exists')
```

```
else
[pko3,pko4]=size(H);%determine the size of matrix
for w=2:pko3
if (dd(w,1)>=(-1e-8) && dd(w,1)<=(1e-8))
%find the element in dd tends to zero
kt3=w+1;
end
end
for y=1:sum1
if (rank(y,1)==kt3)%find the element in rank which is equal to kt3
kt1=y;%element no. which equal to kt3
coldpinch=t(kt1,1)
hotpinch=coldpinch+dt
minheatingload=-kt
mincoolingload=dd(pko3,1)
break;
end;
end;%got the value of cold pinch,hot pinch,minimum heating load,
%minimum cooling load
end
%Output of the program: The above code runs in MATLAB and the achieved
output involves:
%coldpinch = A, hotpinch = B, minheatingload = C, mincoolingload = D, where
A, B, C, and D are
%the calculated variables from the code.
```